

A general scheme for modeling gamma-ray burst prompt emission

Pawan Kumar & Erin McMahon

Astronomy Department, University of Texas, Austin, TX 78712

ABSTRACT

We describe a general method for modeling gamma-ray burst prompt emission, and determine the range of magnetic field strength, electron energy, Lorentz factor of the source, and the distance of the source from the central explosion that is needed to account for the prompt γ -ray emission of a typical long duration burst. We find that for the burst to be produced via the synchrotron process unphysical conditions are required – the distance of the source from the center of the explosion (R_γ) must be larger than $\sim 10^{17}$ cm and the source Lorentz factor $\gtrsim 10^3$; for such a high Lorentz factor the deceleration radius (R_d) is less than R_γ even if the number density of particles in the surrounding medium is as small as $\sim 0.1 \text{ cm}^{-3}$. The result, $R_\gamma > R_d$, is in contradiction with the early x-ray and optical afterglow data that show that γ -rays precede the afterglow flux that is produced by a decelerating forward shock. This problem for the synchrotron process applies to all long-GRBs other than those that have the low energy spectrum precisely $\nu^{-1/2}$. In order for the synchrotron process to be a viable mechanism for long-bursts, the energy of electrons radiating in the γ -ray band needs to be continuously replenished by some acceleration mechanism during much of the observed spike in GRB lightcurve – this is not possible if GRB prompt radiation is produced in shocks (at least the kind that has been usually considered for GRBs) where particles are accelerated at the shock front and not as they travel down-stream and emit γ -rays, but *might* work in some different scenarios such as magnetic outflows.

The synchrotron-self-Compton (SSC) process fares much better. There is a large solution space for a typical GRB prompt emission to be produced via the SSC process. The prompt optical emission accompanying the burst is found to be very bright ($\lesssim 14$ mag; for $z \sim 2$) in the SSC model, which exceeds the observed flux (or upper limit) for most GRBs. The prompt optical is predicted to be even brighter for the sub-class of bursts that have the spectrum $f_\nu \propto \nu^\alpha$ with $\alpha \sim 1$ below the peak of νf_ν . Surprisingly, there are no SSC solutions for bursts that have $\alpha \sim 1/3$; these bursts might require continuous or repeated acceleration of electrons or some physics beyond the simplified, although generic, SSC model considered in this work. Continuous acceleration of electrons can also significantly reduce the optical flux that would otherwise accompany γ -rays in the SSC model.

Subject headings: gamma rays: bursts, theory, method: analytical – radiation mechanisms: non-thermal

1. Introduction

The last 10 years have seen a rapid advance in our understanding of gamma-ray bursts, due mainly to the study of GRB afterglows. We now know that at least some of the long duration GRBs (that last for more than about 5s) are produced in the collapse of massive (young) stars (Galama et al. 1998; Stanek et al. 2003; Hjorth et al. 2003; Kawabata et al. 2003; Malesani et al. 2004; Della Valle et al. 2003; Pian et al. 2006; Della Valle et al. 2006) as proposed by Woosley (1993) and Paczynski (1998), and short duration bursts are associated with old stellar populations and are a likely product of merging neutron-star binaries (Paczynski 1991; Narayan et al. 1992; Gehrels et al. 2005; Fox et al. 2005; Berger et al. 2005; Gorosabel et al. 2006; Nakar 2007); for recent reviews please see Piran (2005); Mészáros (2002); Woosley & Bloom (2006); Zhang (2007). We also have good estimates of the total energy and beaming for these explosions as well as the property of the medium within about 1 pc of the explosion (Rhoads 1999; Sari, Piran & Halpern, 1999; Frail et al 2001; Panaitescu & Kumar, 2001). However, our understanding of how the prompt γ -ray emission is generated, and the mechanism for energy transport from the central engine (via magnetic field or kinetic energy of protons-neutrons and/or electron-positron pairs) remains highly uncertain.

The goal of this paper is to provide a nearly model independent way of modeling the prompt γ -ray emission with synchrotron or synchrotron-self-Compton (SSC) processes. We determine the basic properties of the γ -ray source from the data, and then determine how these can be interpreted in currently popular models such as the internal/external shock model.

In the next section we provide the basic idea and details of the technique we use to model γ -ray emission (the idea in its early form can be found in Kumar et al. 2006), and in §3 & §4 we describe the synchrotron and SSC results, respectively.

2. Modeling γ -ray emission: basic idea and technical formalism

The starting point for our modeling of the prompt γ -ray emission in GRBs is the assumption that the radiation is produced via the synchrotron or synchrotron-self-Compton processes¹ in a source moving relativistically outward from the inner engine. Figure 1 provides a cartoon description of our model. For a simple GRB light-curve (LC) consisting of a single peak we determine the average source properties corresponding to the time when the observed light curve peaks, and for a multi-peak GRB LC our calculation applies to individual pulses or spikes in the lightcurve.

The source property can be uniquely described by the following set of 5 parameters: the

¹Mechanisms such as the inverse-Compton scattering of “photospheric” emission from a hot fireball (cf. Lazzati et al. 2000; Broderick, 2005) are not modeled by the approach we have adopted. And if it were to turn out that the GRB prompt emission is produced by such a mechanism then the work presented here is of little relevance.

magnetic field strength (B) in Gauss, the number of radiating particles (N) i.e., electrons and positrons, the optical depth of the source to Thomson scattering (τ), the Lorentz factor of the source with respect to the rest frame of the GRB host galaxy (Γ), and the minimum electron energy² γ_i at the location where particles are accelerated (all the variables we use in this paper are defined in table 1 for easy reference). In addition, the particle distribution above γ_i is taken to be a power-law function: $dn/d\gamma \propto \gamma^{-p}$. Particles cool as a result of radiative losses and with time, or as they travel away from the acceleration site, and the distribution function becomes steeper than the index p at some energy where radiative losses become important. We calculate the modified distribution self-consistently as discussed below. We constrain this 5D parameter space with at least 4 observed quantities – the νf_ν peak frequency ν_γ , the spectral index below ν_γ , the flux f_γ at ν_γ , the decay time of a single pulse in a GRB LC t_γ ; p , the power law index, is constrained by the high energy spectral index, for $\nu > \nu_\gamma$.

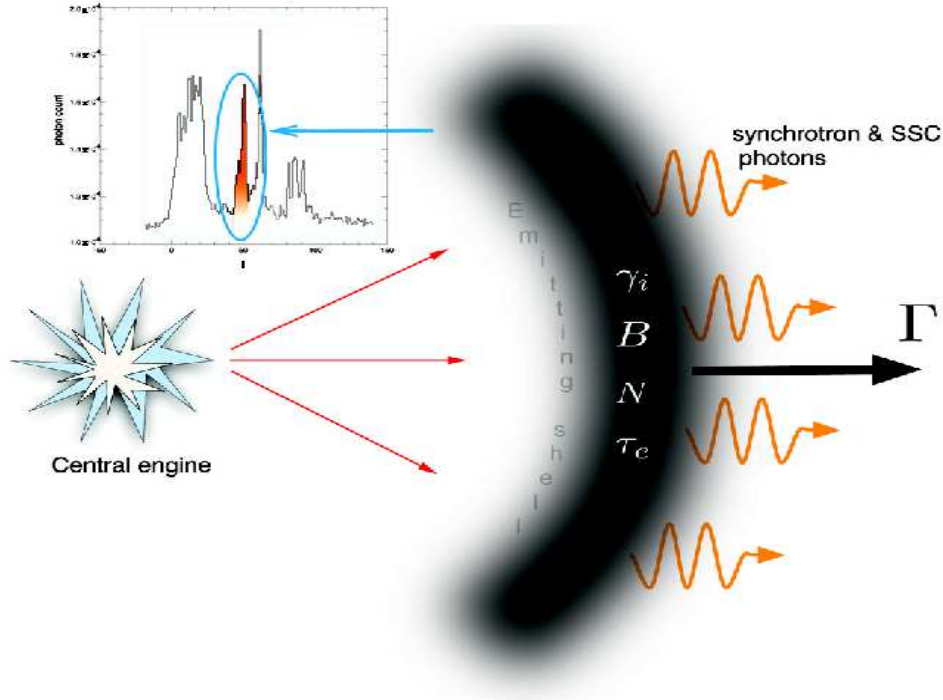


Fig. 1.— A schematic representation of our model. Assuming that radiation is synchrotron and inverse Compton, the γ -ray source properties can be described by five parameters ($\gamma_i, \Gamma, B, N, \tau$) that determine the observed flux at one instance in time. We take this time to be the peak of a pulse in a GRB lightcurve. All of the calculations presented in this work apply to one single pulse in a typical GRB prompt lightcurve, as shown in the top left corner.

²The electron energy is $\gamma_i m_e c^2$, however, for convenience we suppress the factor $m_e c^2$.

Table 1. Definition of variables

| | |
|---------------|--|
| γ_i | minimum electron LF in source comoving frame |
| Γ | bulk LF of the source |
| B | magnetic field strength, in Gauss, in source comoving frame |
| τ | optical depth to Thomson scattering |
| N | number of radiating electrons(isotropic equivalent) |
| α | The spectral index below the peak of νf_ν i.e. $f_\nu \propto \nu^\alpha$ |
| γ_a | LF of electrons emitting synchrotron at ν_a |
| γ_c | LF of electrons emitting synchrotron at ν_c |
| Γ_{sh} | LF of the shocked gas wrt the unshocked gas |
| ν_γ | observed peak frequency of GRB νf_ν spectrum ($\nu_{\gamma 5} \equiv \nu_\gamma/10^5 \text{ eV}$) |
| ν_i | synchrotron injection frequency in observer frame ($\nu_{i 5} \equiv \nu_i/10^5 \text{ eV}$) |
| ν_c | synchrotron cooling frequency in observer frame ($\nu_{c 5} \equiv \nu_c/10^5 \text{ eV}$) |
| ν_a | synchrotron self absorption frequency in observer frame |
| ν_a^{ic} | SSC self absorption frequency, below which the f_ν^{ic} spectral index is +1 |
| A_* | external medium wind parameter, $n = (A/m_p)r^{-2}$; $A_* \equiv A/5 \times 10^{11} \text{ g cm}^{-1}$ |
| d_{L28} | luminosity distance in units of 10^{28} cm |
| E_\pm | kinetic energy of electrons and positrons (lab frame; isotropic equivalent) |
| E_B | energy in magnetic field (lab frame; isotropic equivalent) |
| E_{53} | isotropic equivalent of outflow energy in units of 10^{53} ergs |
| $f_{B/ke}$ | E_B/E_\pm – ratio of magnetic to e^\pm energy |
| f_R | synchrotron prompt optical flux (in R band, at 2 eV) |
| f_x | synchrotron prompt x-ray flux, at 1 keV |
| f_γ | observed flux (in mJy) at ν_γ |
| f_{ν_p} | synchrotron flux at peak – $\min(\nu_i, \nu_c)$ |
| n_0 | density of circum-burst medium |
| n_e | comoving electron density in unshocked shell |
| p | power law index of electron energy distribution |
| R_γ | distance from center-of-explosion at which the radiation is produced |
| R_d | deceleration radius |
| t_γ | duration of one pulse in GRB light-curve (observer frame) |
| t_a | the time available for electrons to cool before being re-accelerated |
| Y | Compton parameter |
| z | redshift |
| η_i | γ_i/γ_c |
| η_a | γ_a/γ_i |

A relativistic moving source of finite angular size θ_j (as seen by an observer at the center of explosion) can be treated as spherically symmetric as long as $\Gamma^{-1} < \theta_j$. The angular size determined from afterglow modeling suggests that θ_j is larger than about two degrees for all bursts for which we have good data (Frail et al. 2001; Panaitescu & Kumar, 2001) and a number of lines of argument and evidence suggests that Γ is greater than about 100 (cf. Piran 1992; Lithwick & Sari, 2001). Therefore, we can treat the source for prompt γ -ray emission as spherically symmetric, and the numerical values we quote in this paper are all isotropic equivalent quantities; for instance N is the total number of radiating particles in the source assuming the source to be spherically symmetric.

2.1. Synchrotron and inverse-Compton radiations: basic equations

The synchrotron injection frequency, ν_i , corresponding to electron minimum energy γ_i , is

$$\nu_i = \frac{qB\gamma_i^2\Gamma}{2\pi m_e c(1+z)}, \quad (1)$$

(eg. Rybicki & Lightman, 1979; Wijers & Galama, 1999), where q is electron charge, m_e the electron mass, c the speed of light, and z is the burst redshift. The synchrotron cooling frequency, ν_c , the characteristic frequency at which electrons cooling on a time scale t_a (observer frame) radiate, is

$$\nu_c = \frac{18\pi q m_e c(1+z)}{\sigma_T^2 B^3 \Gamma t_a^2 (1+Y)^2}. \quad (2)$$

where σ_T is the Thomson scattering cross-section, and Y the Compton parameter.

For most of the calculations in this work we assume that electrons are accelerated only once, and the time scale for acceleration is taken to be much less than the duration of a pulse in the GRB light-curve (t_γ). One time acceleration is, for instance, believed to apply to shocks where electrons are accelerated at the shock front (by crossing the front back and forth multiple times) and not while they travel downstream; the picture is likely very different in magnetic reconnection/dissipation. To capture some of the effects of multiple-times particle acceleration in time period of a pulse duration in GRB LC we introduce a time scale, t_a , which is the average time in between two successive episodes of particle acceleration or the time available for electrons to cool in between acceleration; for one shot acceleration $t_a = t_\gamma$, and in the opposite limit of continuous acceleration $t_a = 0$ when the rate of energy gain is balanced by radiative loss rate. The electron distribution function resulting from the acceleration process is taken to be $dn/d\gamma_e \propto \gamma_e^{-p}$. The distribution function in the source as a whole is different due to the radiative cooling of electrons with time. The electron distribution function averaged over the source is described by two characteristic energies viz. γ_i and γ_c ; $\gamma_c m_e c^2$ is the energy of electrons that cool on time scale t_a . The electron distribution for $\gamma_e > \max(\gamma_i, \gamma_c)$ is proportional to γ_e^{-p-1} , and the distribution between γ_c and γ_i (for $\gamma_c < \gamma_i$) is proportional to γ_e^{-2} . Electrons cool via synchrotron and inverse-Compton losses. The rate of loss of energy is affected by the synchrotron self-absorption frequency ν_a — electrons with characteristic

synchrotron frequency below ν_a lose energy only via the inverse-Compton scattering process. We calculate γ_c and ν_a by solving a coupled set of equations as described in McMahon et al. (2006).

The synchrotron flux at the peak of the f_ν spectrum, at $\min[\nu_i, \nu_c]$, is given by

$$f_{\nu_p} = \frac{\sqrt{3}q^3 B N \Gamma}{4\pi d_L^2 m_e c^2}, \quad (3)$$

where d_L is the luminosity distance to the source. The effect of synchrotron self absorption is not included in the above expression for f_{ν_p} , and therefore the observed flux, in general, would be different from f_{ν_p} . The flux at other frequencies are calculated as described in Sari, Piran and Narayan (1998).

The inverse-Compton flux (in observer frame) at frequency ν , $f^{ic}(\nu)$, is calculated using the following equation (cf. Rybicki & Lightman, 1979)

$$f^{ic}(\nu) = \frac{3}{4}\sigma_T \delta r \int \frac{d\nu_s}{\nu_s} \frac{\nu}{\nu_s} f(\nu_s) \int_{\gamma_1}^{\infty} d\gamma_e \frac{dn}{\gamma_e^2 d\gamma_e} F\left(\frac{\nu}{4\gamma_e^2 \nu_s}\right), \quad (4)$$

where $f(\nu_s)$ is the synchrotron flux per unit frequency in the observer frame, δr is the radial extent of the source (comoving frame) which is related to the optical depth τ (one of the five parameters we use to characterize the source), the function $F(x)$ is

$$F(x) = 2x \ln x + x + 1 - 2x^2, \quad \text{for } 0 < x < 1, \quad (5)$$

and γ_1 is the minimum LF for electron distribution. We include the Klein-Nishina correction to the above expression when $\nu_s \gamma_e / \Gamma > m_e c^2$.

The expression for the Compton Y parameter is

$$Y = \sigma_T \int dr' \int d\gamma_e \gamma_e^2 \frac{dn_e}{d\gamma_e} = \frac{4}{3}\tau \left(\frac{p-1}{p-2}\right) \gamma_i^2 \times \begin{cases} (\nu_c/\nu_i)^{\frac{1}{2}} & \gamma_c \ll \gamma_i & p > 2 \\ (\nu_c/\nu_i)^{3-p} (3-p)^{-1} & \gamma_i \ll \gamma_c & 2 < p < 3 \\ (p-3)^{-1} & \gamma_i \ll \gamma_c & p > 3 \\ p(p-1)^{-1} & \gamma_i \sim \gamma_c & p > 2 \end{cases}, \quad (6)$$

where the r' -integral is over the comoving radial width of the source. For ease of future use we rewrite the above expression for Y as $Y = 4\tau \gamma_i^2 \xi / 3$ where

$$\xi \equiv \left(\frac{p-1}{p-2}\right) \times \begin{cases} (\nu_c/\nu_i)^{\frac{1}{2}} & \gamma_c \ll \gamma_i & p > 2 \\ (\nu_c/\nu_i)^{3-p} (3-p)^{-1} & \gamma_i \ll \gamma_c & 2 < p < 3 \\ (p-3)^{-1} & \gamma_i \ll \gamma_c & p > 3 \\ p(p-1)^{-1} & \gamma_i \sim \gamma_c & p > 2. \end{cases} \quad (7)$$

In our 5D parameter space search, we limit the Compton Y-parameter for a synchrotron solution to be less than 10 and for an inverse-Compton solution $Y \lesssim 100$. The rationale for the constraint on the Y-parameter is that we want an efficiency of $\gtrsim 10\%$ in the γ -ray energy band of ~ 10 –400 keV;

observations suggest this efficiency for a typical long duration burst from a comparison of energy in the γ -ray radiation and the kinetic energy of the ejecta determined from the afterglow observations (Panaitescu & Kumar, 2002).

We can calculate the distance of the source from the center of explosion with 2 of the 5 parameters, N and τ :

$$R_\gamma = \left(\frac{N\sigma_T}{4\pi\tau} \right)^{1/2}. \quad (8)$$

2.2. Relation between R_γ and pulse-width

We consider a γ -ray source of a finite lifetime, at a distance R_γ from the central explosion, that is responsible for generating one pulse in the observed GRB prompt lightcurve. Electrons in the source are heated during some time interval, set by the central engine variability/activity time, and subsequently the source undergoes adiabatic expansion. The width of an observed GRB pulse is determined by a number of different factors – the central engine variability time, the adiabatic expansion and cooling time, and the curvature time – which are described below.

1. **Central engine variability time:** *sets the observed GRB pulse width if the variability time is larger than $\sim R_\gamma/2c\Gamma^2$ and if the distance where γ -ray photons are generated does not increase with time; in this case GRB pulse duration is independent of R_γ . However, when the source is turned off the γ -ray flux would decline on a timescale of $R_\gamma/2c\Gamma^2$, the adiabatic expansion time scale; for all the calculations in this work we use the light-curve decline time although for simplicity we continue to refer to it as pulse width.*
2. **Curvature timescale:** *is the time interval between arrival of photons with angular separation of Γ^{-1} as seen by an observer at the center of explosion. It is the minimum time scale for a γ -ray pulse width, as long as the outflow from the GRB has an angular size larger than Γ^{-1} , and is equal to $R_\gamma/(c\Gamma^2)$.*
3. **Adiabatic expansion time scale** – *this is the timescale for electrons/protons to cool because of expansion of the source. As the distance of the source from the center doubles its volume increases by a factor $\gtrsim 4$, and electron/proton energy drops by a factor 2. This timescale in the observer frame is $\sim R_\gamma/(c\Gamma^2)$.*

We note that if electrons are heated by coupling with protons, then the time scale for electrons to cool down can be larger than $R_\gamma/(c\Gamma^2)$; e^\pm cooling time in this case can be as large as $R_\gamma/(c\Gamma^2) \times (\text{proton energy}/\text{electron energy})$ provided that protons transfer energy to electrons for this time duration, and the energy transfer rate balances the loss of energy for electrons to adiabatic and radiative coolings. However, the coupling between p^+ s and e^\pm s is unlikely to increase the pulse width by a large factor ($\gtrsim 5$) unless the energy in electrons is much smaller

than in p^+ s, but in that case the efficiency of γ -ray generation would be small which is not supported by observations.

4. **Radiative cooling timescale.** For $\nu_c > \nu_i$ the radiative cooling time scale is larger than the adiabatic time scale and in that case GRB pulse width is equal to the adiabatic or curvature time. For $\nu_c < \nu_i$ electrons cool on a smaller time scale, and once electron heating stops, the lightcurve falls off on the curvature timescale. We note that the observed pulse duration cannot be larger than $R_\gamma/(2c\Gamma^2)$ which corresponds to an elapsed time of R_γ/c in the center of explosion frame, and during this time the source has moved to R_γ from the center.

Thus we see that the observed decay time for a pulse in GRB LC, produced by a relativistic source, is

$$t_\gamma \approx \frac{R_\gamma(1+z)}{2c\Gamma^2}, \quad (9)$$

when the GRB redshift is z .

2.3. Energy etc.

The total energy in the source consists of the kinetic energy of electrons and positrons (E_\pm) and the magnetic field (E_B):

$$E_\pm = N(p-1)\gamma_i m_e c^2 \Gamma / (p-2), \quad E_B = R_\gamma^3 B^2 / 6. \quad (10)$$

Note that $(p-1)\gamma_i m_e c^2 / (p-2)$ is the average energy per electron/positron in the source comoving frame at the acceleration site, and in the calculation of E_B we took the comoving radial thickness of the source to be R_γ/Γ which is roughly what one expects for a causally connected source where the signal speed is close to the speed of light.

We do not make any assumptions regarding the energy in protons since protons do not contribute to the observed γ -ray radiation. This has the effect that the parameter space we determine is larger than it would be if protons carried a substantial amount of energy since the energy available to e^\pm would be smaller than the upper limit of 10^{55} erg (isotropic equivalent) we impose in our search for solutions in the 5D parameter space.

For a γ -ray source that arises from shock heated gas, the minimum electron energy behind the shock front, γ_i (one of the five parameters we use), can be related to the Lorentz factor of the shocked gas wrt the unshocked gas, Γ_{sh} . The minimum Γ_{sh} needed to produce γ_i is

$$\Gamma_{sh} = \left[\frac{m_e(p-1)}{m_p(p-2)} \right] 2\gamma_i, \quad (11)$$

where m_p (m_e) is proton (electron) mass. The factor 2 in the above expression is for the case where there is an energy equipartition between electrons and protons and there are no e^\pm pairs in the

plasma; Γ_{sh} will be larger if there are pairs or if electrons have less energy than protons.³

2.4. The basic technique for finding source properties

We determine the properties of the γ -ray source for a GRB by finding the region in the 5-D parameter space $(\gamma_i, \Gamma, B, N, \tau)$ that satisfies the following set of observational constraints: 1) the frequency at the peak of the νf_ν spectrum (ν_γ); 2) the peak flux at ν_γ ; 3) the spectral index above ν_γ – which constrains electron index p – and the index below ν_γ ; 4) the burst duration – for a GRB with a single pulse in the LC – or the duration of an individual pulse (t_γ) for GRBs with complicated LC; 5) optical and x-ray prompt flux or limit if available. The flux at a given observer time reflects the property of the source averaged over equal-arrival-time volume, therefore, the observed peak flux depends on the evolution of the source and this introduces uncertainty in the flux calculation by a factor of about two. For this reason we only require the theoretical flux to match the observed value to within a factor of ~ 2 .

We now use this technique to find the 5D solution space and source property for GRBs produced via synchrotron (§3) and SSC (§4).

3. Synchrotron solutions

We consider in this section the parameter space of solutions when the observed γ -rays are produced via the synchrotron process⁴. First, we determine approximate solutions by analytically solving a system of equations for our 5 parameters $(\gamma_i, \Gamma, B, N, \tau)$ for the generic synchrotron case. The solutions for each parameter are expressed in terms of the Compton Y parameter and three observed quantities: the frequency ν_γ where νf_ν peaks, the γ -ray flux at this frequency (f_γ ; in mJy), and the duration of a pulse in GRB LC (t_γ); Y is a convenient and useful parameter because its value is expected to lie in a limited range, e.g. $Y \lesssim 1$ for the synchrotron solutions & $1 \lesssim Y \lesssim 10$ for the SSC process. Having the general synchrotron solutions in hand, we then apply the analytical results to the low energy spectral index cases of $\alpha = 1/3$, $\alpha = -1/2$ and $\alpha = -(p-1)/2$, compare

³If there are “cold” protons and electrons in the shocked gas, i.e. only a fraction of particles in the shocked gas are accelerated, and electrons have more than $m_p c^2 \Gamma_{sh}$ energy, we would in that case overestimate Γ_{sh} . However, in this work we do not consider that there is a cold component to the γ -ray source since such a component would not radiate and affect observations and the solutions in the 5-D parameter space. Therefore, such a cold component, if present, would have little effect on all of the major results in this work; the only quantity affected by the cold component is the value for Γ_{sh} which is a peripheral quantity and not part of the central flow of the logic in this paper.

⁴ It has been suggested that another radiation process, called jitter, might be responsible for γ -ray generation for those bursts that have low energy spectrum $f_\nu \propto \nu$ (Medvedev, 2000). We show in appendix B that whenever jitter radiation dominates the observed flux to produce a $f_\nu \propto \nu$ spectrum the Compton- Y parameter is extremely large – $Y \gtrsim 10^6$ – and most of the energy of the explosion comes out in ~ 100 GeV SSC photons.

the analytical and numerical results, and draw conclusions as to the process by which γ -rays are generated in GRBs; the spectral index α is defined by $f_\nu \propto \nu^\alpha$ for $\nu < \nu_\gamma$.

The 5 equations that we solve are those for the observer frame synchrotron injection frequency ν_i (1), the cooling frequency ν_c (2), the pulse duration (t_γ) (8 & 9), synchrotron flux f_{ν_p} in mJy at $\nu_p \equiv \min(\nu_i, \nu_c)$ (3), and the Compton Y parameter (6):

$$\nu_{i5} = 1.1 \times 10^{-13} B \gamma_i^2 \Gamma (1+z)^{-1} \quad (12)$$

$$\nu_{c5} = 6.6 \times 10^4 (1+z) B^{-3} \Gamma^{-1} t_a^{-2} (1+Y)^{-2} \quad (13)$$

$$\tau \approx 1.5 \times 10^8 N_{55} (1+z)^2 \Gamma^{-4} t_\gamma^{-2} \quad (14)$$

$$f_{\nu_p} = 110 B \Gamma N_{55} d_{L28}^{-2} (1+z) \text{ mJy} \quad (15)$$

where $\nu_{i5} \equiv \nu_i/10^5 \text{ eV}$, $\nu_{c5} \equiv \nu_c/10^5 \text{ eV}$, and $N_{55} \equiv N/10^{55}$.

To solve Equations 12-15 & 6, we first eliminate N_{55} from equation (15) using equation (14), then eliminate τ using equation (6) to find

$$B \Gamma^5 \gamma_i^{-2} \approx 1.9 \times 10^6 f_{\nu_p} d_{L28}^2 (1+z) t_\gamma^{-2} Y^{-1} \xi. \quad (16)$$

Next, combining (16) & (12) we get

$$\gamma_i^{-4} \Gamma^4 \approx 2.1 \times 10^{-7} \nu_{i5}^{-1} f_{\nu_p} d_{L28}^2 Y^{-1} \xi t_\gamma^{-2}. \quad (17)$$

Multiplying the square root of equations (12) and (13) together, we have

$$B \gamma_i^{-1} \approx 8.5 \times 10^{-5} t_a^{-1} \nu_{c5}^{-\frac{1}{2}} \nu_{i5}^{-\frac{1}{2}} (1+Y)^{-1}. \quad (18)$$

We can eliminate γ_i from equations (17) and (18) by dividing equation (17) by (18) to the fourth power:

$$\Gamma^4 B^{-4} \approx 4.0 \times 10^9 \nu_{i5} \nu_{c5}^2 f_{\nu_p} d_{L28}^2 Y^{-1} (1+Y)^4 \xi t_a^4 t_\gamma^{-2} \quad (19)$$

And finally, if we multiply equation (19) by the fourth power of (16) and divide by the square of (17) we find the solution for Γ to be

$$\Gamma \approx 10^3 \nu_{i5}^{\frac{3}{16}} \nu_{c5}^{\frac{1}{8}} f_{\nu_p}^{\frac{3}{16}} t_\gamma^{-\frac{3}{8}} t_a^{\frac{1}{4}} Y^{-\frac{3}{16}} (1+Y)^{\frac{1}{4}} \xi^{\frac{3}{16}} d_{L28}^{\frac{3}{8}} (1+z)^{\frac{1}{4}}. \quad (20)$$

Using Γ , we can solve for γ_i , B , and τ :

$$\gamma_i \approx 4.7 \times 10^4 \nu_{i5}^{\frac{7}{16}} \nu_{c5}^{\frac{1}{8}} f_{\nu_p}^{-\frac{1}{16}} t_\gamma^{\frac{1}{8}} t_a^{\frac{1}{4}} Y^{\frac{1}{16}} (1+Y)^{\frac{1}{4}} \xi^{-\frac{1}{16}} d_{L28}^{-\frac{1}{8}} (1+z)^{\frac{1}{4}} \quad (21)$$

$$B \approx 4.0 \nu_{i5}^{-\frac{1}{16}} \nu_{c5}^{-\frac{3}{8}} f_{\nu_p}^{-\frac{1}{16}} t_\gamma^{\frac{1}{8}} t_a^{-\frac{3}{4}} Y^{\frac{1}{16}} (1+Y)^{-\frac{3}{4}} \xi^{-\frac{1}{16}} d_{L28}^{-\frac{1}{8}} (1+z)^{\frac{1}{4}} \text{ Gauss} \quad (22)$$

$$\tau \approx 3.3 \times 10^{-10} \nu_{i5}^{-\frac{7}{8}} \nu_{c5}^{-\frac{1}{4}} f_{\nu_p}^{\frac{1}{8}} t_\gamma^{-\frac{1}{4}} t_a^{-\frac{1}{2}} Y^{\frac{7}{8}} (1+Y)^{-\frac{1}{2}} \xi^{-\frac{7}{8}} d_{L28}^{\frac{1}{4}} (1+z)^{-\frac{1}{2}}. \quad (23)$$

Equations (20)–(23) provide approximate solutions for $(\gamma_i, \Gamma, B, N, \tau)$ when the synchrotron process produces the observed γ -ray radiation; more accurate solutions for these parameters are obtained by numerical calculations and the results are shown in Figures 2–8. These general solutions can be used to investigate different cases of low energy spectral indices (α) by adopting appropriate values for ν_{i5} and ν_{c5} . The full dependences on these two frequencies are not completely shown here – each case of α has a different functional dependence on ξ , and ξ is a function of ν_i and ν_c .

Note that f_{ν_p} is not the observed flux at ν_γ , the peak of γ -ray spectrum, but is the flux at $\min(\nu_i, \nu_c) \equiv \nu_p$, and the effect of synchrotron-self-absorption, if any, at ν_p has been ignored. Since the dependence of the parameters Γ , γ_i etc. on f_{ν_p} is very weak (eqs. 20–23), we do not worry about the difference between f_{ν_p} & f_γ at this point, even though f_{ν_p} can be much greater than f_γ (the flux at ν_γ); ν_γ is the peak of νf_ν – for $p < 3$, $\nu_\gamma = \max[\nu_i, \nu_c]$ & for $p > 3$ $\nu_\gamma = \min[\nu_i, \nu_c]$.

Using the parameter solutions, we can derive the distance of the γ -ray source from the center of explosion (R_γ), and the energy in the magnetic field and electrons. The radius $R_\gamma = 2c\Gamma^2 t_\gamma(1+z)^{-1}$ is found to be

$$R_\gamma \approx 6.0 \times 10^{16} \nu_{i5}^{\frac{3}{8}} \nu_{c5}^{\frac{1}{4}} f_{\nu_p}^{\frac{3}{8}} t_\gamma^{\frac{1}{4}} t_a^{\frac{1}{2}} Y^{-\frac{3}{8}} (1+Y)^{\frac{1}{2}} \xi^{\frac{3}{8}} d_{L28}^{\frac{3}{4}} (1+z)^{-\frac{1}{2}} \text{ cm} \quad (24)$$

and should be compared to the deceleration radius (R_d) of the GRB outflow in both a homogeneous external medium with particle number density n_0 , and a wind external medium where the particle number density is given by $(A/m_p)r^{-2}$ (these are two special cases of a power law density stratification – the density varying as r^{-s} – corresponding to $s = 0$ & $s = 2$)

$$R_d = \begin{cases} 1.2 \times 10^{17} E_{53}^{\frac{1}{3}} n_0^{-\frac{1}{3}} \Gamma_2^{-\frac{2}{3}} & \text{cm} \quad s = 0 \\ 1.8 \times 10^{15} E_{53} A_*^{-1} \Gamma_2^{-2} & \text{cm} \quad s = 2 \end{cases} \quad (25)$$

where E_{53} is the isotropic equivalent energy in GRB-ejecta in units of 10^{53} ergs, $\Gamma_2 = \Gamma/100$, and $A_* = A/(5 \times 10^{11} \text{ g cm}^{-1})$. Substituting in the solution for Γ , we find R_d to be

$$R_d \approx \begin{cases} 2.6 \times 10^{16} E_{53}^{\frac{1}{3}} n_0^{-\frac{1}{3}} \nu_{i5}^{-\frac{1}{8}} \nu_{c5}^{-\frac{1}{12}} f_{\nu_p}^{-\frac{1}{8}} t_\gamma^{\frac{1}{4}} t_a^{-\frac{1}{6}} Y^{\frac{1}{8}} (1+Y)^{-\frac{1}{6}} \xi^{-\frac{1}{8}} d_{L28}^{-\frac{1}{4}} (1+z)^{-\frac{1}{6}} & \text{cm} \quad s = 0 \\ 1.8 \times 10^{13} E_{53} A_*^{-1} \nu_{i5}^{-\frac{3}{8}} \nu_{c5}^{-\frac{1}{4}} f_{\nu_p}^{-\frac{3}{8}} t_\gamma^{\frac{3}{4}} t_a^{-\frac{1}{2}} Y^{\frac{3}{8}} (1+Y)^{-\frac{1}{2}} \xi^{-\frac{3}{8}} d_{L28}^{-\frac{3}{4}} (1+z)^{-\frac{1}{2}} & \text{cm} \quad s = 2 \end{cases} \quad (26)$$

The magnetic and e^\pm energies, given by equation (10), are found to be

$$E_B \approx 5.8 \times 10^{50} \nu_{i5} f_{\nu_p} t_\gamma Y^{-1} \xi d_{L28}^2 (1+z)^{-1} \text{ ergs} \quad (27)$$

and

$$E_\pm \approx 8.5 \times 10^{50} \left(\frac{p-1}{p-2} \right) \nu_{i5}^{\frac{1}{2}} \nu_{c5}^{\frac{1}{2}} f_{\nu_p} t_a (1+Y) d_{L28}^2 (1+z)^{-1} \text{ ergs.} \quad (28)$$

Since the dependence of the above two quantities on f_{ν_p} is linear, we should replace f_{ν_p} with f_γ , the flux observed at ν_γ . This will be done in the following sections, since the expression for f_γ depends on α .

We can relate the solution-subspace we find to parameters for the shock model for GRBs; if electrons are accelerated in a relativistic shock then the LF of shock front (Γ_{sh}) wrt to the unshocked material is related to γ_i (one of the 5 parameters) and is given by equation (11)

$$\Gamma_{sh} \approx 50 \epsilon_e^{-1} \left(\frac{p-1}{p-2} \right) \nu_{i5}^{\frac{7}{16}} \nu_{c5}^{\frac{1}{8}} f_{\nu_p}^{-\frac{1}{16}} t_{\gamma}^{\frac{1}{8}} t_a^{\frac{1}{4}} Y^{\frac{1}{16}} (1+Y)^{\frac{1}{4}} \xi^{-\frac{1}{16}} d_{L28}^{-\frac{1}{8}} (1+z)^{\frac{1}{4}}, \quad (29)$$

where ϵ_e is the ratio of energy in electrons and the total thermal energy in the γ -ray source.

We now apply the results obtained in this section to each possible synchrotron low energy spectral index α .

3.1. Synchrotron solutions when the low energy spectrum is $\nu^{-\frac{(p-1)}{2}}$

We use equation (7) to eliminate ξ from the analytical solutions given by equations 20–23 for the $\gamma_i \ll \gamma_c$ & $2 < p < 3$ case, and substitute $\nu_{\gamma_5} = \nu_{c5}$ & $f_{\nu_p} = f_{\gamma}(\nu_{\gamma_5}/\nu_{i5})^{\frac{(p-1)}{2}}$, to find that synchrotron solutions for $\alpha = -\frac{(p-1)}{2}$ are:

$$\Gamma \approx 10^3 \nu_{\gamma_5}^{\frac{19-3p}{32}} f_{\gamma}^{\frac{3}{16}} t_{\gamma}^{-\frac{3}{8}} \nu_{i5}^{\frac{3p-9}{32}} t_a^{\frac{1}{4}} Y^{-\frac{3}{16}} (1+Y)^{\frac{1}{4}} (1+z)^{\frac{1}{4}} d_{L28}^{\frac{3}{8}} A_{1p}^{\frac{3}{16}} \quad (30)$$

$$\gamma_i \approx 4.7 \times 10^4 \nu_{\gamma_5}^{\frac{p-1}{32}} f_{\gamma}^{-\frac{1}{16}} t_{\gamma}^{\frac{1}{8}} \nu_{i5}^{\frac{19-p}{32}} t_a^{\frac{1}{4}} Y^{\frac{1}{16}} (1+Y)^{\frac{1}{4}} (1+z)^{\frac{1}{4}} d_{L28}^{-\frac{1}{8}} A_{1p}^{-\frac{1}{16}} \quad (31)$$

$$B \approx 4.0 \nu_{\gamma_5}^{\frac{p-17}{32}} f_{\gamma}^{-\frac{1}{16}} t_{\gamma}^{\frac{1}{8}} \nu_{i5}^{\frac{3-p}{32}} t_a^{-\frac{3}{4}} Y^{\frac{1}{16}} (1+Y)^{-\frac{3}{4}} (1+z)^{\frac{1}{4}} d_{L28}^{-\frac{1}{8}} A_{1p}^{-\frac{1}{16}} \text{ Gauss} \quad (32)$$

$$\tau \approx 3.3 \times 10^{-10} \nu_{\gamma_5}^{\frac{15p-47}{16}} f_{\gamma}^{\frac{1}{8}} t_{\gamma}^{-\frac{1}{4}} \nu_{i5}^{\frac{29-15p}{16}} t_a^{-\frac{1}{2}} Y^{\frac{7}{8}} (1+Y)^{-\frac{1}{2}} (1+z)^{-\frac{1}{2}} d_{L28}^{\frac{1}{4}} A_{1p}^{-\frac{7}{8}} \quad (33)$$

where

$$A_{1p} \equiv \frac{(p-1)}{(p-2)(3-p)}, \quad (34)$$

and we should emphasize that t_{γ} is **not** the burst duration – it is the width of a single spike in the GRB prompt-lightcurve.

For a typical long duration GRB with $f_{\gamma} = 1\text{mJy}$, $\nu_{\gamma} = 100\text{keV}$, $t_{\gamma} = 0.1\text{s}$, $z = 1$, $d_{L28} = 2$, and $t_a \sim t_{\gamma}$ – henceforth we will refer to a GRB with these observed parameters as *GRB-†* – the 5-parameters of the γ -ray source ($\gamma_i, \Gamma, B, N, \tau$) are obtained from equations 30–33 and are given by

$$\Gamma \gtrsim 3.2 \times 10^3 Y^{-\frac{3}{16}} (1+Y)^{\frac{1}{4}} \quad (35)$$

$$\gamma_i \lesssim 6.0 \times 10^3 Y^{\frac{1}{16}} (1+Y)^{\frac{1}{4}} \quad (36)$$

$$B \lesssim 16 Y^{\frac{1}{16}} (1+Y)^{-\frac{3}{4}} \text{ Gauss} \quad (37)$$

$$\tau \gtrsim 4.7 \times 10^{-9} Y^{\frac{7}{8}} (1+Y)^{-\frac{1}{2}}. \quad (38)$$

In deriving these inequalities we took $p = 2.5$, $\nu_c = \nu_{\gamma} = 100 \text{ keV}$, and $\nu_{i5} < 0.1$.

The dependence of Γ , γ_i , B & τ on Y is weak, so the coefficients in above expressions are reasonable estimates for the γ -ray source basic physical parameters for *GRB- \natural* . We see that the γ -ray source LF, Γ , is required to be rather large – $\Gamma \gtrsim 3 \times 10^3$ – if the radiation is to be produced via the synchrotron process. This large Γ is not consistent with afterglow modeling, which gives a value of a few hundred or less (Panaitescu & Kumar, 2002). Furthermore, as shown below, the distance of γ -ray source from the center of explosion turns out to be larger than the deceleration radius for this large Γ value, unless n_0 is very small. This suggests that the synchrotron solution is internally inconsistent; after the deceleration radius Γ is a function of N , γ_i and n_0 and is no longer an independent parameter as considered in these derivations. The possibility that $R_\gamma > R_d$ is also ruled out by early optical afterglow data – eg. GRBs 050801, 050820A, 060124, 060418, 060607A, 060614, 060714 – that show that γ -rays precede a rising afterglow flux that is produced by a decelerating forward shock. Moreover, if $R_\gamma \gtrsim R_d$, then in this case of a decelerating source we should see an increasing GRB pulse duration with time, which is not observed.

The distance of the γ -ray source from the center of explosion, $R_\gamma \approx 2ct_\gamma\Gamma^2/(1+z)$, is calculated using eq. (30), and is given by

$$R_\gamma \approx 6.0 \times 10^{16} \nu_{\gamma 5}^{\frac{19-3p}{16}} f_\gamma^{\frac{3}{8}} t_\gamma^{\frac{1}{4}} \nu_{i5}^{\frac{3p-9}{16}} t_a^{\frac{1}{2}} Y^{-\frac{3}{8}} (1+Y)^{\frac{1}{2}} (1+z)^{-\frac{1}{2}} d_{L28}^{\frac{3}{4}} A_{1p}^{\frac{3}{8}} \text{ cm} \quad (39)$$

or $R_\gamma \sim 3 \times 10^{16} Y^{-\frac{3}{8}} (1+Y)^{\frac{1}{2}} \text{ cm}$ for *GRB- \natural* .

We now compare these analytical estimates to the numerically computed solution space for synchrotron radiation. A numerical search of the allowed region of the 5-D parameter space that satisfies the observational constraints (ν_γ , f_γ & t_γ ; the same constraints that we used in the derivation of analytical expressions), confirms that for synchrotron solutions $R_\gamma \gtrsim 10^{16} \text{ cm}$, $\Gamma \gtrsim 10^3$, and $10 \lesssim \gamma_i \lesssim 10^4$ (see fig. 2). We have considered a wide range of values of peak frequency (ν_γ), γ -ray flux at the peak, and pulse duration, to see if we can find some viable synchrotron solutions for any GRBs with $\alpha = -(p-1)/2$. These solutions are shown in Figure 2. We find that by decreasing any of the observable parameters R_γ decreases, but the dependence is weak in agreement with the scaling given in equation (39). Furthermore, a decrease in t_γ reduces Γ as expected from equation (30), but even for $t_\gamma = 10 \text{ ms}$, Γ is still $\gtrsim 10^3$.

We next calculate the deceleration radius and compare it with R_γ to ensure $R_\gamma < R_d$ for self consistent solutions. The deceleration radius for GRB-ejecta is calculated using eq. (26) and is given by

$$R_d \approx \begin{cases} 2.6 \times 10^{16} E_{53}^{\frac{1}{3}} n_0^{-\frac{1}{3}} \nu_{\gamma 5}^{\frac{3p-19}{48}} f_\gamma^{-\frac{1}{8}} t_\gamma^{\frac{1}{4}} \nu_{i5}^{\frac{3-p}{16}} t_a^{-\frac{1}{6}} Y^{\frac{1}{8}} (1+Y)^{-\frac{1}{6}} (1+z)^{-\frac{1}{6}} d_{L28}^{-\frac{1}{4}} A_{1p}^{-\frac{1}{8}} \text{ cm} & s=0 \\ 1.8 \times 10^{13} E_{53} A_*^{-1} \nu_{\gamma 5}^{\frac{3p-19}{16}} f_\gamma^{-\frac{3}{8}} t_\gamma^{\frac{3}{4}} \nu_{i5}^{\frac{9-3p}{16}} t_a^{-\frac{1}{2}} Y^{\frac{3}{8}} (1+Y)^{-\frac{1}{2}} (1+z)^{-\frac{1}{2}} d_{L28}^{-\frac{3}{4}} A_{1p}^{-\frac{3}{8}} \text{ cm} & s=2 \end{cases} \quad (40)$$

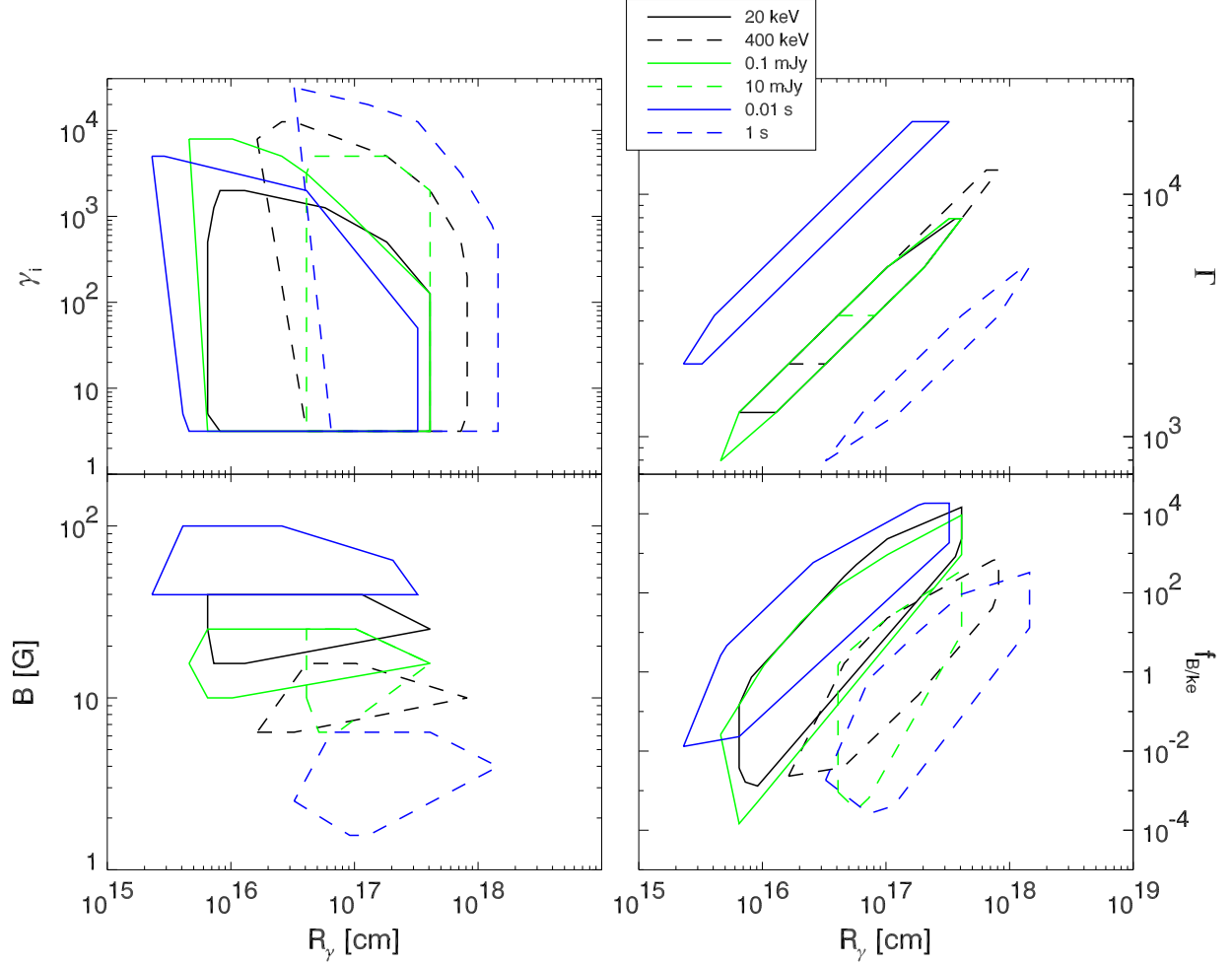


Fig. 2.— Results of numerical calculation for the allowed synchrotron solution space when the spectrum below the peak of νf_ν , at ν_γ , is: $f_\nu \propto \nu^{-(p-1)/2}$ for $\nu < \nu_\gamma$. A point in the 5-D parameter space $(\gamma_i, \Gamma, B, N, \tau)$ is considered an allowed solution for the observed GRB parameters $(\nu_\gamma, f_\gamma, t_\gamma, \alpha)$ provided that ν_γ is within a factor 2 of the observed value, the pulse duration (t_γ) & flux at ν_γ (f_γ) are within a factor 1.5 & 3 of the observed value respectively; the larger tolerance on flux is due to larger error in flux calculation. The x-axis shows the distance of the γ -ray source from the center of the explosion. The top left panel is γ_i – the minimum LF of electrons in source comoving frame at the site where they are accelerated (electron distribution function for $\gamma_e > \gamma_i$ is: $dn_e/d\gamma_e \propto \gamma_e^{-2.5}$ i.e. $p = 2.5$). The top right panel shows the bulk LF of the source, the bottom left panel shows the comoving magnetic field in Gauss, and the bottom right panel shows the ratio of energy in the magnetic field and electrons. For all of the numerical calculations we took the burst redshift $z = 1$. Legend shows several different cases of GRBs corresponding to different observed values for ν_γ , f_γ , and t_γ . Only one observational parameter – that noted in the legend – is changed at a time, all the remaining parameters are left unchanged; the base value for the parameters is the same as we took for *GRB-4*, i.e. $\nu_\gamma = 100$ keV, $f_\gamma = 1$ mJy, $t_\gamma = 0.1$ s, and $t_a = t_\gamma$. For instance, for the 20 keV case, denoted by the solid black line, $\nu_\gamma = 20$ keV, and f_γ & t_γ are same as for *GRB-4* i.e. 1 mJy and 0.1 s respectively.

and the ratio of R_γ and R_d is:

$$\frac{R_\gamma}{R_d} \approx \begin{cases} 2.3 E_{53}^{-\frac{1}{3}} n_0^{\frac{1}{3}} \nu_{\gamma 5}^{\frac{19-3p}{12}} f_\gamma^{\frac{1}{2}} \nu_{i5}^{\frac{p-3}{4}} t_a^{\frac{2}{3}} Y^{-\frac{1}{2}} (1+Y)^{\frac{2}{3}} (1+z)^{-\frac{1}{3}} d_{L28} A_{1p}^{\frac{1}{2}} & s=0 \\ 3.3 \times 10^3 E_{53}^{-1} A_* \nu_{\gamma 5}^{\frac{19-3p}{8}} f_\gamma^{\frac{3}{4}} t_\gamma^{-\frac{1}{2}} \nu_{i5}^{\frac{3p-9}{8}} t_a Y^{-\frac{3}{4}} (1+Y) d_{L28}^{\frac{3}{2}} A_{1p}^{\frac{3}{4}} & s=2 \end{cases} \quad (41)$$

Substituting in the observable parameters for *GRB-1* into the above equation and solving for n_0 & A_* such that $R_\gamma/R_d < 1$, we find

$$n_0 < 0.057 E_{53} t_a^{-2} Y^{\frac{3}{2}} (1+Y)^{-2} \text{ cm}^{-3} \quad s=0 \quad (42)$$

$$A_* < 5.5 \times 10^{-5} E_{53} t_a^{-1} Y^{\frac{3}{4}} (1+Y)^{-1} \quad s=2 \quad (43)$$

Note that n_0 & A_* must be very small to ensure that $R_\gamma < R_d$, especially for $Y < 1$ expected of synchrotron solutions. Figure (3) shows the results of numerical calculations which confirms these analytical estimates. Moreover, if we want $R_\gamma/R_d \lesssim 0.5$, in order to have a clear separation between internal and external shocks, then $n_0 \lesssim 10^{-2} \text{ cm}^{-3}$. Therefore, self-consistent synchrotron solutions with $R_\gamma \lesssim R_d$ require very low density for the circumstellar medium compared with $n_0 \sim 1 \text{ cm}^{-3}$ obtained from afterglow modeling (Panaitescu & Kumar 2001). The limit on n_0 can be increased by decreasing t_a (see eq. 42). Numerical result for the upper limit on n_0 when $t_a = t_\gamma/100$ is shown in fig. 3. It confirms the analytical result that $n_0 \sim 1 \text{ cm}^{-3}$ can give $R_\gamma < R_d$ provided that $t_a \ll t_\gamma$. It should be noted that for systems involving shock heating of particles we expect $t_a \sim t_\gamma$ because electrons are accelerated at the shock front and there is no subsequent acceleration as particles travel downstream; in magnetic reconnections or dissipation it is natural to expect $t_a \ll t_\gamma$.

We now estimate the ratio of energy in e^\pm and magnetic field to find out if it is much less than unity or not when $t_a < t_\gamma$ (a small value for E_\pm/E_B results in low efficiency for γ -ray generation). The ratio E_\pm/E_B can be calculated using eqs. (27) & (28) and is given by

$$\frac{E_\pm}{E_B} \approx 1.5(3-p) \left(\frac{\nu_{\gamma 5}}{\nu_{i5}} \right)^{p-\frac{5}{2}} \left[\frac{t_a}{t_\gamma} \right] Y(1+Y), \quad (44)$$

for $2 < p < 3$ (numerical calculations take $p = 2.5$). For the solution space corresponding to $\alpha = -(p-1)/2$, $0.1 \lesssim \nu_\gamma/\nu_i \lesssim 10^5$ and so $E_\pm > E_B$ even when $t_a/t_\gamma \sim 10^{-2}$. Therefore, small t_a/t_γ solutions are fine from the point of radiative efficiency; the above equation needs to be modified, when $t_a \ll t_\gamma$, to include the total energy input in electrons during a GRB pulse width of t_γ , which will further improve the radiative efficiency when t_a/t_γ is very small.

The reason that these synchrotron solutions have large R_γ is not hard to understand. It requires a certain minimum number of electrons to produce the observed flux of $f_\gamma \sim 1 \text{ mJy}$ at $\nu_\gamma \sim 100 \text{ keV}$: $N \sim 10^{53}/(B\Gamma)$ – see eq. 15. And in order to keep the Compton-Y parameter, $Y \sim \tau\gamma_i\gamma_c$, less ~ 10 — otherwise most of the energy will come out in IC-scattered photons at $\nu \gg 1 \text{ MeV}$ — we must have large R_γ for the source. The solution offered by $t_a \ll t_\gamma$ is also easy to

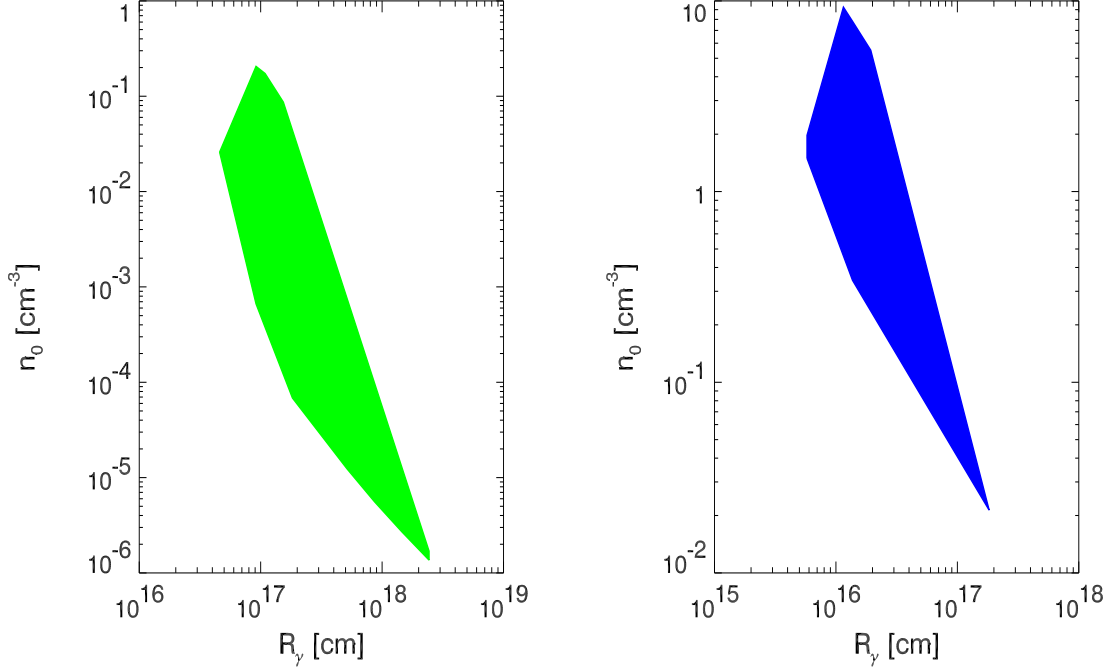


Fig. 3.— *Left panel:* the upper limit to the ISM density (n_0) for synchrotron solutions with $\alpha = -(p-1)/2$ for a burst with $\nu_\gamma = 100$ keV, $f_\gamma = 1$ mJy, $t_\gamma = 1$ s & $t_a = t_\gamma$. *Right panel:* same as the left panel except that $t_a = t_\gamma/100$. Note that by decreasing the amount of time electrons have to radiate away their energy before being re-accelerated (t_a) increases the $\max(n_0)$ roughly as t_a^{-1} . The n_0 upper limit decreases when any of the GRB parameters (ν_γ , f_γ , t_γ) is increased; $n_0 \propto f_\gamma^{-1}$.

understand. Frequent re-acceleration of charge particles makes it possible to have larger magnetic field while keeping $\nu_c \gtrsim 100$ keV. This decreases the number of particles required to produce the observed flux f_γ , and that in turn makes it possible to have a smaller R_γ .

We conclude that the synchrotron process in a shock heated medium cannot account for the prompt γ -ray emission of long-duration GRBs with low energy spectrum $f_\nu \propto \nu^{-\frac{p-1}{2}}$. However, synchrotron solutions appear to be viable when $t_a \ll t_\gamma$, i.e. when electrons are accelerated repeatedly, as might occur when magnetic field is dissipated and the energy is deposited in e^\pm .

3.2. Synchrotron solution when the low energy spectrum is $\nu^{\frac{1}{3}}$

This is a special case of $\alpha = -(p-1)/2$ analyzed in the previous subsection (§3.1) when $\gamma_i \sim \gamma_c$; the solutions are a subset of those found in §3.1. The analytical solutions for this case, obtained

by substituting $\xi = \frac{p}{(p-2)}$ (see eq. 7), $\nu_{i5} \sim \nu_{c5} = \nu_{\gamma5}$, and $f_\gamma \sim f_{\nu_p}$, into equations 20–23 are

$$\Gamma \approx 10^3 \nu_{\gamma5}^{\frac{5}{16}} f_\gamma^{\frac{3}{16}} t_\gamma^{-\frac{3}{8}} t_a^{\frac{1}{4}} Y^{-\frac{3}{16}} (1+Y)^{\frac{1}{4}} (1+z)^{\frac{1}{4}} d_{L28}^{\frac{3}{8}} \left[\frac{p}{p-2} \right]^{\frac{3}{16}} \quad (45)$$

$$\gamma_i \approx 4.7 \times 10^4 \nu_{\gamma5}^{\frac{9}{16}} f_\gamma^{-\frac{1}{16}} t_\gamma^{\frac{1}{8}} t_a^{\frac{1}{4}} Y^{\frac{1}{16}} (1+Y)^{\frac{1}{4}} (1+z)^{\frac{1}{4}} d_{L28}^{-\frac{1}{8}} \left[\frac{p}{p-2} \right]^{-\frac{1}{16}} \quad (46)$$

$$B \approx 4.0 \nu_{\gamma5}^{-\frac{7}{16}} f_\gamma^{-\frac{1}{16}} t_\gamma^{\frac{1}{8}} t_a^{-\frac{3}{4}} Y^{\frac{1}{16}} (1+Y)^{-\frac{3}{4}} (1+z)^{\frac{1}{4}} d_{L28}^{-\frac{1}{8}} \left[\frac{p}{p-2} \right]^{-\frac{1}{16}} \text{ Gauss} \quad (47)$$

$$\tau \approx 3.3 \times 10^{-10} \nu_{\gamma5}^{-\frac{9}{8}} f_\gamma^{\frac{1}{8}} t_\gamma^{-\frac{1}{4}} t_a^{-\frac{1}{2}} Y^{\frac{7}{8}} (1+Y)^{-\frac{1}{2}} (1+z)^{-\frac{1}{2}} d_{L28}^{\frac{1}{4}} \left[\frac{p}{p-2} \right]^{-\frac{7}{8}}. \quad (48)$$

Substituting $f_\gamma = 1 \text{ mJy}$, $\nu_{\gamma5} = 1$, $t_\gamma = 0.1 \text{ s}$ (the observed parameters for *GRB-1*), & $t_a \sim t_\gamma$, in these equations, we find

$$\Gamma \sim 2.5 \times 10^3 Y^{-\frac{3}{16}} (1+Y)^{\frac{1}{4}} \quad (49)$$

$$\gamma_i \sim 2 \times 10^4 Y^{\frac{1}{16}} (1+Y)^{\frac{1}{4}} \quad (50)$$

$$B \sim 18 Y^{\frac{1}{16}} (1+Y)^{-\frac{3}{4}} \text{ Gauss} \quad (51)$$

$$\tau \sim 6.3 \times 10^{-10} Y^{\frac{7}{8}} (1+Y)^{-\frac{1}{2}} \quad (52)$$

and indeed, the solutions are a subset of the $\alpha = -(p-1)/2$ solution space – these have smaller τ and larger Γ & γ_i . The distance of the source from the center of the explosion is:

$$R_\gamma \approx 6.0 \times 10^{16} \nu_{\gamma5}^{\frac{5}{8}} f_\gamma^{\frac{3}{8}} t_\gamma^{\frac{1}{4}} t_a^{\frac{1}{2}} Y^{-\frac{3}{8}} (1+Y)^{\frac{1}{2}} (1+z)^{-\frac{1}{2}} d_{L28}^{\frac{3}{4}} \left[\frac{p}{p-2} \right]^{\frac{3}{8}} \text{ cm} \quad (53)$$

or $R_\gamma \sim 2 \times 10^{16} Y^{-\frac{3}{8}} (1+Y)^{\frac{1}{2}} \text{ cm}$ for *GRB-1*. This case has the same problems as $\alpha = -(p-1)/2$ case discussed in §3.1 i.e., large R_γ and Γ , and requiring extremely small external density in order that $R_\gamma \lesssim R_d$. Also, the conclusions drawn in §3.1 regarding $t_a/t_\gamma \ll 1$ offering a way out of this problem apply here as well.

The numerical calculation of the hypersurface in 5-D parameter space allowed by GRB observations – ν_γ , f_γ & t_γ – for *GRB-1* finds $\gamma_i \gtrsim 10^4$, $\Gamma \gtrsim 10^3$, $200 \lesssim \gamma_i/\Gamma \lesssim 700$, source radius (R_γ) $10^{16} - 10^{18} \text{ cm}$, and B between 1 and 10^2 Gauss for the entire solution space (see fig. 4) – which is in very good agreement with analytical estimates. For a wide range of values for the three observable parameters we find the GRB source to be located between $\sim 10^{15} \text{ cm}$ & 10^{18} cm , $\gamma_i \gtrsim 3 \times 10^3$, and $\Gamma \gtrsim 10^3$ (fig. 4). In order that $R_\gamma/R_d < 1$, the density of the surrounding medium (n_0) is required to be less than $\sim 0.1 \text{ cm}^{-3}$ which is much smaller than the value inferred from late time afterglow modeling for long duration GRBs. The density requirement is relaxed if $t_a \ll t_\gamma$ (see fig. 5).

In conclusion, the synchrotron process, in a shock heated medium, has serious problems accounting for prompt γ -ray emission for those bursts that have spectrum below the peak frequency

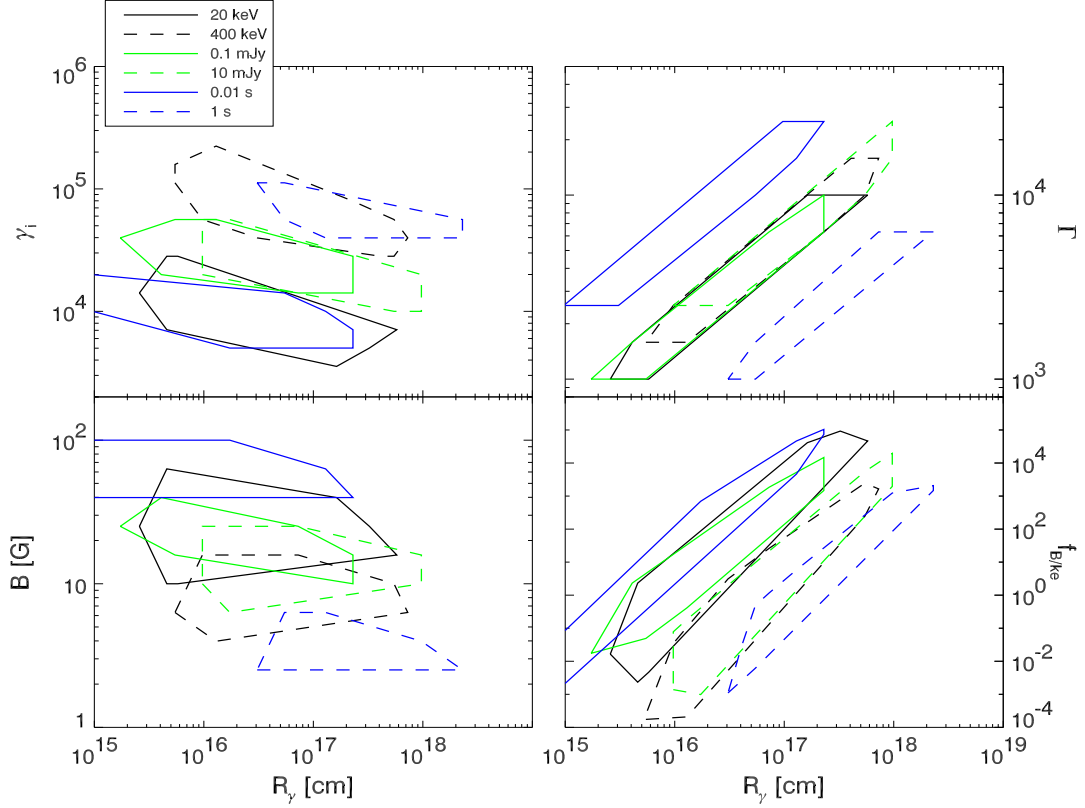


Fig. 4.— Synchrotron solution space when the spectrum below ν_γ , the peak of νf_ν , is $f_\nu \propto \nu^{1/3}$, i.e. $\alpha = 1/3$. See Figure 2 caption for details.

(ν_γ) scaling as $f_\nu \propto \nu^{1/3}$ or $\nu^{-(p-1)/2}$. A possible resolution is provided if electrons are more or less continuously accelerated while they are radiating γ -ray photons during the entire time period of a spike in the observed GRB lightcurve; in other words $t_a \ll t_\gamma$. It should be pointed that $t_a \sim t_\gamma$ in shocks whereas continuous acceleration might be possible in regions of magnetic reconnection/dissipation.

3.3. Synchrotron solution when the low energy spectrum is $\nu^{-1/2}$

Substituting $f_{\nu_p} = f_\gamma (\nu_{i5}/\nu_{c5})^{1/2}$, $\nu_{\gamma5} = \nu_{i5}$, and ξ from equation (7) for the case where $\nu_c < \nu_i$, into eqs. 20–23 we find the allowed part of the 5-D parameter space when the spectrum below ν_γ is $f_\nu \propto \nu^{-1/2}$

$$\Gamma \approx 10^3 \nu_{\gamma5}^{3/16} f_\gamma^{3/16} t_\gamma^{-3/8} \nu_{c5}^{1/8} t_a^{1/4} Y^{-3/16} (1+Y)^{1/4} (1+z)^{1/4} d_{L28}^{3/8} A_{2p}^{3/16} \quad (54)$$

$$\gamma_i \approx 4.7 \times 10^4 \nu_{\gamma5}^{7/16} f_\gamma^{-1/16} t_\gamma^{1/8} \nu_{c5}^{1/8} t_a^{1/4} Y^{1/16} (1+Y)^{1/4} (1+z)^{1/4} d_{L28}^{-1/8} A_{2p}^{-1/16} \quad (55)$$

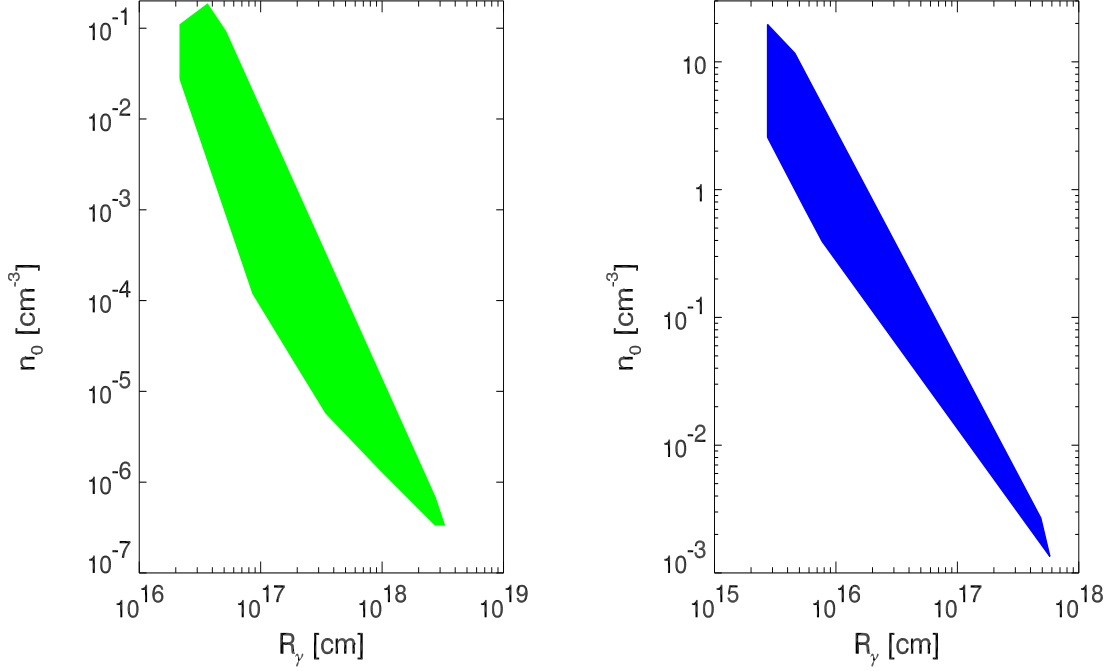


Fig. 5.— *Left panel:* the maximum density of the circum-burst-medium so that $R_\gamma < R_d$ for synchrotron solutions with $\alpha = 1/3$ and for a burst with $\nu_\gamma = 100$ keV, $f_\gamma = 1$ mJy, $t_\gamma = 1$ s & $t_a = t_\gamma$. *Right panel:* is same as the left panel except that $t_a = t_\gamma/100$; note that by decreasing the amount of time electrons have to radiate away their energy before being re-accelerated (t_a) increases the upper limit for n_0 roughly as t_a^{-1} . The n_0 upper limit is weakly dependent on ν_γ , and decreases with increasing t_γ & f_γ being most sensitive to $f_\gamma - \max(n_0) \propto f_\gamma$.

$$B \approx 4.0 \nu_{\gamma 5}^{-\frac{1}{16}} f_\gamma^{-\frac{1}{16}} t_\gamma^{\frac{1}{8}} \nu_{c5}^{-\frac{3}{8}} t_a^{-\frac{3}{4}} Y^{\frac{1}{16}} (1+Y)^{-\frac{3}{4}} (1+z)^{\frac{1}{4}} d_{L28}^{-\frac{1}{8}} A_{2p}^{-\frac{1}{16}} \quad \text{Gauss} \quad (56)$$

$$\tau \approx 3.3 \times 10^{-10} \nu_{\gamma 5}^{-\frac{3}{8}} f_\gamma^{\frac{1}{8}} t_\gamma^{-\frac{1}{4}} \nu_{c5}^{-\frac{3}{4}} t_a^{-\frac{1}{2}} Y^{\frac{7}{8}} (1+Y)^{-\frac{1}{2}} (1+z)^{-\frac{1}{2}} d_{L28}^{\frac{1}{4}} A_{2p}^{-\frac{7}{8}}, \quad (57)$$

where

$$A_{2p} \equiv \frac{p-1}{p-2}. \quad (58)$$

For *GRB-4* — $t_\gamma = 0.1$ s, $\nu_\gamma = 100$ keV, $f_\gamma = 1$ mJy & $t_a = t_\gamma$ — and taking $\nu_{c5} < 10^{-4}$ (in agreement with the numerical calculation) we find $\Gamma \lesssim 720 Y^{-\frac{3}{16}}$, $\gamma_i \lesssim 6.7 \times 10^4$, & $B \gtrsim 590 (1+Y)^{-\frac{3}{4}}$ Gauss. In contrast to the previous two cases considered in §3.1 & §3.2, $\Gamma < 1000$ in this case. We find the γ -ray source distance, R_γ , to be

$$R_\gamma \approx 6.0 \times 10^{16} \nu_{\gamma 5}^{\frac{3}{8}} f_\gamma^{\frac{3}{8}} t_\gamma^{\frac{1}{4}} \nu_{c5}^{\frac{1}{4}} t_a^{\frac{1}{2}} Y^{-\frac{3}{8}} (1+Y)^{\frac{1}{2}} (1+z)^{-\frac{1}{2}} d_{L28}^{\frac{3}{4}} A_{2p}^{\frac{3}{8}} \text{ cm} \quad (59)$$

which is $R_\gamma \sim 2 \times 10^{15} Y^{-\frac{3}{8}} (1+Y)^{\frac{1}{2}}$ cm for *GRB- \ddagger* . We compare this radius to the deceleration radius, R_d , which is obtained from eq. (26) and is given by

$$R_d \approx \begin{cases} 2.6 \times 10^{16} E_{53}^{\frac{1}{3}} n_0^{-\frac{1}{3}} \nu_{\gamma 5}^{-\frac{1}{8}} f_\gamma^{-\frac{1}{8}} t_\gamma^{\frac{1}{4}} \nu_{c5}^{-\frac{1}{12}} t_a^{-\frac{1}{6}} Y^{\frac{1}{8}} (1+Y)^{-\frac{1}{6}} (1+z)^{-\frac{1}{6}} d_{L28}^{-\frac{1}{4}} A_{2p}^{-\frac{1}{8}} \text{ cm} & s = 0 \\ 1.8 \times 10^{13} E_{53} A_*^{-1} \nu_{\gamma 5}^{-\frac{3}{8}} f_\gamma^{-\frac{3}{8}} t_\gamma^{\frac{3}{4}} \nu_{c5}^{-\frac{1}{4}} t_a^{-\frac{1}{2}} Y^{\frac{3}{8}} (1+Y)^{-\frac{1}{2}} (1+z)^{\frac{1}{2}} d_{L28}^{-\frac{3}{4}} A_{2p}^{-\frac{3}{8}} \text{ cm} & s = 2 \end{cases} \quad (60)$$

and for the ratio $R_\gamma/R_d < 1$, we find that $n_0 \lesssim 8 E_{53} Y^{\frac{3}{2}} (1+Y)^{-2} \text{ cm}^{-3}$ and $A_* < 0.014 E_{53} Y^{\frac{3}{4}} (1+Y)^{-1}$ if $\nu_{c5} \sim 0.1$; the limits on n_0 & A_* are much higher for $\nu_{c5} \ll 0.1$ and poses no problem for synchrotron solutions in a shock heated source.

If the synchrotron solutions were to arise in a shock heated medium, we can calculate the LF of the shock front wrt the unshocked fluid, Γ_{sh} , using equation 11:

$$\Gamma_{sh} \approx 26 \epsilon_e^{-1} \nu_{\gamma 5}^{\frac{7}{16}} f_\gamma^{-\frac{1}{16}} t_\gamma^{\frac{1}{8}} \nu_{c5}^{\frac{1}{8}} t_a^{\frac{1}{4}} Y^{\frac{1}{16}} (1+Y)^{\frac{1}{4}} (1+z)^{\frac{1}{4}} d_{L28}^{-\frac{1}{8}} A_{2p}^{\frac{15}{16}}. \quad (61)$$

or $\Gamma_{sh} \lesssim 32 Y^{\frac{1}{16}} (1+Y)^{\frac{1}{4}}$ for *GRB- \ddagger* assuming that electrons receive half of the shock energy and that there are no e^\pm pairs. Note that as long as $\nu_{\gamma 5} \sim 1$, Γ_{sh} is pretty high (~ 20), and it is insensitive to ν_{c5} (and the other quantities). In order to produce $\Gamma_{sh} \sim 20$ in internal shocks, we need the relative LF of the two colliding shells $\Gamma_{rel} \sim 2\Gamma_{sh}^2 (n_1/n_2)^{\frac{1}{2}}$ (Panaitescu & Kumar 2004; Sari & Piran 1995), where n_1 and n_2 are the comoving densities of the two colliding shells (see appendix A for a discussion of how we calculate Γ_{rel}). For $\Gamma_{rel} \lesssim 5$, so that the ratio of the LFs of the colliding shells is not larger than 10, $n_1/n_2 \lesssim \sim 10^{-5}$ is required (see appendix A); $\Gamma_{rel} > 5$ is an unlikely situation to be realized in nature.

We calculate the total energy in electrons (E_\pm) and magnetic field (E_B) to determine the efficiency for synchrotron radiation — if there is a lot more energy in magnetic field than that in the electrons, the efficiency for γ -ray radiation would be small. The magnetic and electron energies for the case of $\nu^{-1/2}$ spectrum are obtained from equation (10) and the solutions for B , Γ , γ_i and R_γ derived above, and are given by –

$$E_B = B^2 R_\gamma^3 / 6 \approx 6.0 \times 10^{50} \nu_{\gamma 5} f_\gamma t_\gamma Y^{-1} (1+z)^{-1} d_{L28}^2 A_{2p} \text{ ergs}, \quad (62)$$

and

$$E_\pm = N(p-1) m_e c^2 \gamma_i \Gamma / (p-2) \approx 8.7 \times 10^{50} \nu_{\gamma 5} f_\gamma t_a (1+Y) (1+z)^{-1} d_{L28}^2 A_{2p} \text{ ergs}. \quad (63)$$

The ratio E_B/E_\pm is

$$f_{B/ke} \equiv \frac{E_B}{E_\pm} \approx 0.68 t_\gamma t_a^{-1} Y^{-1} (1+Y)^{-1}. \quad (64)$$

For $t_a \ll t_\gamma$ the above expression for the ratio $f_{B/ke}$ would need to be modified to include the total energy deposited in e^\pm s as a result of multiple acceleration episodes during a GRB pulse time period of t_γ ; for $t_\gamma/t_a \sim 1$ the expression for $f_{B/ke}$ reduces to the familiar form that depends only on the Compton- Y . For $Y \ll 1$ most of the energy is in the magnetic field and for these solutions the radiative efficiency to produce a GRB is very small.

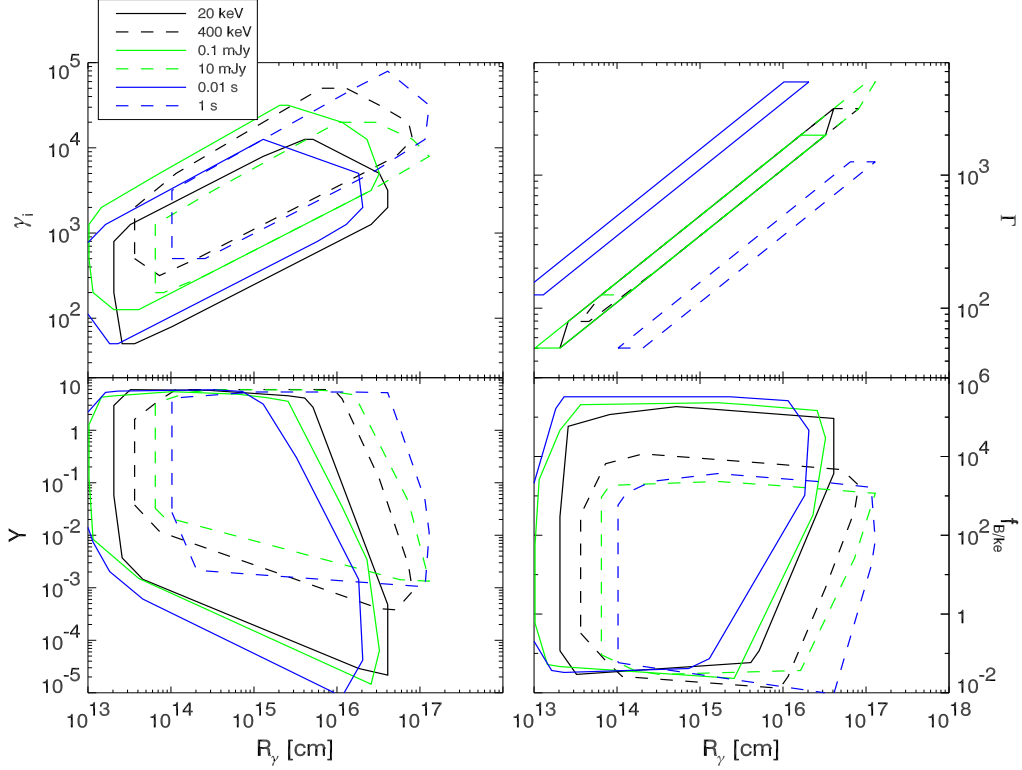


Fig. 6.— Synchrotron solution space when the spectrum below the peak of νf_ν is $f_\nu \propto \nu^{-1/2}$ for $\nu < \nu_\gamma$. γ_i , Γ , Y , and $f_{B/ke}$ are plotted against the distance of the source from the center of explosion (R_γ). The solution spaces for several different values of ν_γ , f_γ , and GRB pulse duration (t_γ) are shown in the four panels. Please see the Figure 2 caption for details.

We numerically search the 5-D parameter space subject to the three observational constraints $(\nu_\gamma, f_\gamma, t_\gamma)$ and find solutions with $10^{13} \text{ cm} < R_\gamma < 10^{17} \text{ cm}$, $10 \text{ Gauss} < B < 10^7 \text{ Gauss}$, $100 < \gamma_i < 3 \times 10^4$, $80 < \Gamma < 3000$, and $10^{-3} < Y < 7$ (see fig. 6) — all in good agreement with analytical estimates presented above. We find $2 < \Gamma_{sh} < 100$ and $10^{-2} < f_{B/ke} < 10^4$. So it would seem that we have solutions with $f_{B/ke} \sim 1$ and Γ_{sh} of order a few — however it turns out that for $f_{B/ke} \lesssim 10$, $\Gamma_{sh} \gtrsim 5$. For $\Gamma_{sh} \gtrsim 5$, $10^{-5} < \frac{n_1}{n_2} < 0.1$, and the ratio of the LFs of two colliding shells, Γ_{rel} , to produce this Γ_{sh} is greater than 20 (see fig. 7) — fluctuations in the LF of the outflow with Γ_{rel} on the order of a few are typically expected in internal shocks.

Numerical solutions for the allowed part of the 5-D space for a range of observable parameters are shown in Figure 6. An increase in ν_γ leads to a slight increase of γ_i and R_γ whereas Γ is quite insensitive to it. These behaviors are consistent with our analytical calculations (eqs. 54–57). The decrease of $f_{B/ke}$ with ν_γ (fig. 6) is due to an increase of Y . An increase of f_γ has little effect on γ_i (for the allowed solution space), Γ & Y increase a little, and $f_{B/ke}$ decreases; these parameters have a very weak dependence on f_γ (see eqs. 54–57). And finally, when t_γ is increased, γ_i and

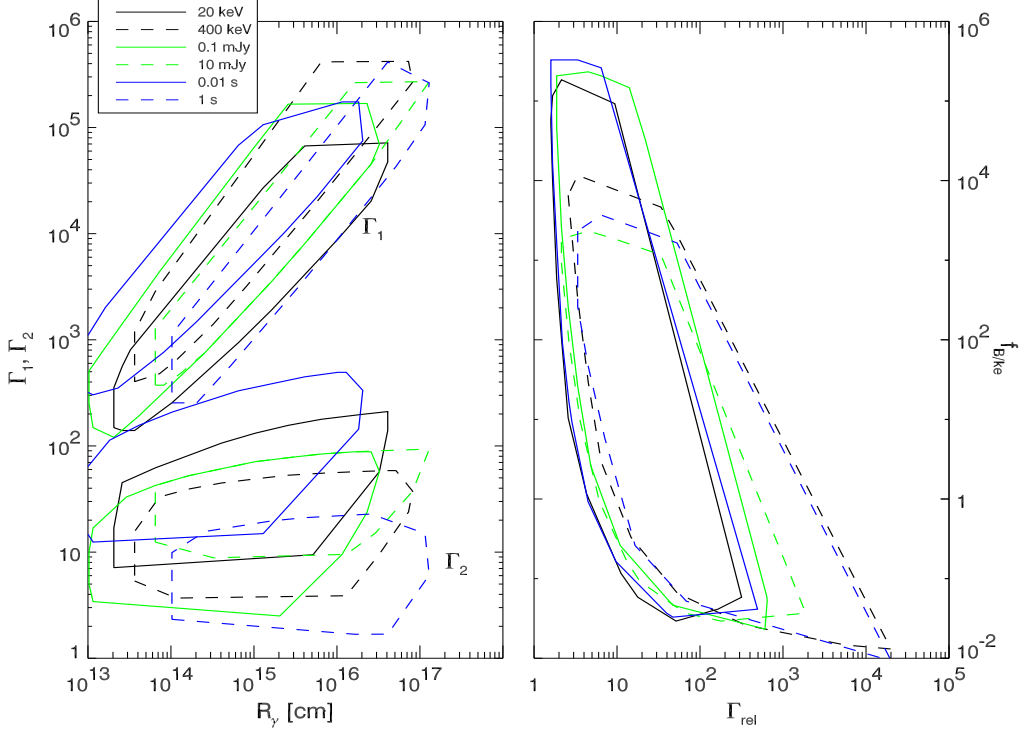


Fig. 7.— This figure, unlike all the previous ones, shows *model dependent* results. For each point in the allowed region of the 5-D parameter space, corresponding to synchrotron solutions for $\alpha = -1/2$ and for given ν_γ , f_γ & t_γ , we calculate parameters for the popular internal shock model for GRBs (see appendix A for details). The *left panel* shows the LFs Γ_1 & Γ_2 of the two colliding shells in the internal shock model as a function of R_γ , the distance from the center where the shells collide. The *right panel* shows $\Gamma_{rel} = \Gamma_1 \Gamma_2 (1 - v_1 v_2)$ vs. $f_{B/ke}$ (the ratio of energy in magnetic field and electrons). Different ν_γ , f_γ and t_γ cases are displayed as described in Figure 2. Note that Γ_{rel} is correlated with $f_{B/ke}$; for high Γ_{rel} , $f_{B/ke}$ is small (< 1), and for low Γ_{rel} , $f_{B/ke} \gg 1$. Low Γ_{rel} & $f_{B/ke} \gg 1$ solutions might correspond to a highly magnetized outflow.

Y increase, and Γ and $f_{B/ke}$ decrease. This is again in agreement with the analytical estimates – $\gamma_i \propto t_\gamma^{-\frac{1}{2}}$. The large decrease in Γ with t_γ is due to an increase of Y with t_γ – $\Gamma \propto t_\gamma^{-\frac{1}{8}} Y^{-\frac{3}{16}}$.

We have looked at the variation of Γ_{sh} , Γ_{rel} and $f_{B/ke}$ with ν_γ , f_γ & t_γ . The results are shown in Figure 7. The minimum value of Γ_{rel} has a weak dependence on ν_γ , f_γ , and t_γ ; Γ_{rel} is between 5 and 20 for $f_{B/ke} \lesssim 10$; $\Gamma_{rel} \sim 5$ solutions are only present when $t_\gamma \lesssim 0.01s$, $f_\gamma \lesssim 0.1$ mJy, or $\nu_\gamma < 20$ keV (note that we only alter one of the three at a time, i.e. for $t_\gamma \sim 0.01s$, $\nu_\gamma \sim 100$ keV and $f_\gamma \sim 1$ mJy). Γ_{rel} may be small enough, then, that the synchrotron mechanism can produce GRBs with $\nu^{-\frac{1}{2}}$ spectra if it has very short pulse duration, small peak frequency, or small flux.

3.3.1. X-ray flux during the GRB when $\alpha = -\frac{1}{2}$

So far, we have only considered prompt γ -ray emission due to the synchrotron process. We now calculate emission in other wavelengths, particularly the X-ray and optical, that should accompany γ -ray photons. In this subsection, and in §3.3.2, we relate the solutions we found in §3.3 to the internal shock model for GRBs (Rees & Meszaros, 1994; see Piran, 1999, for complete references) according to which shells of material ejected in the explosion undergo collisions and the resulting shocks convert part of the kinetic energy of the outflow to radiation. Throughout this section we assume that the γ -ray emission is produced in shell ‘1’ which is taken to be the faster of the two shells. The results are essentially identical if we assume that the GRB is produced in the outer, slower, shell, which we shall refer to as shell ‘2’. The x-ray flux from shell ‘1’, however, is independent of the internal shock model, and is expected to accompany the prompt synchrotron $\nu^{-\frac{1}{2}}$ γ -ray emission.

The x-ray and optical flux from shell ‘1’ lie on the $\nu^{-1/2}$ extrapolation of the γ -ray flux and therefore it is straightforward to calculate these using f_γ and the information that $\nu_c \lesssim 2\text{eV}$ & $\nu_a \lesssim 5\text{eV}$ for the entire solution sub-space of the 5-D parameter space. The calculation of emission from shell ‘2’ is more involved and also a bit uncertain. We provide here (and in §3.3.2) a lower limit to the x-ray and optical flux from shell ‘2’ for each point in the 5-D space that satisfies the three observational constraints $(\nu_\gamma, f_\gamma, t_\gamma)$. The calculation of flux from shell ‘2’ requires the knowledge of the LF of the shock front moving into this shell as well as the ratio of densities (n_1/n_2) . The calculation for these quantities is described in appendix A. The synchrotron injection frequency in shell ‘2’, ν_{i_2} , is smaller than that in shell 1 by a factor of $(\Gamma_{s_2} - 1)^2 / (\Gamma_{s_1} - 1)^2$; Γ_{s_1} & Γ_{s_2} are shock front LFs into shell ‘1’ & ‘2’ wrt unshocked gas in shells ‘1’ & ‘2’ respectively. This factor is approximately $\simeq \frac{n_1}{n_2}$ for $\Gamma_{s_1}, \Gamma_{s_2} \gg 1$, but the approximation breaks down for $\frac{n_1}{n_2} \lesssim 10^{-2}$ (see Figure 15) since the shock in shell ‘2’ becomes mildly relativistic (we note that this approximation is not used in our numerical calculations). The peak flux of the synchrotron spectrum at $\nu = \min(\nu_{i_2}, \nu_{c_2})$ in shell ‘2’, $f_{\nu_{p_2}}$, is larger than $f_{\nu_{p_1}}$ by a factor of $\left(\frac{n_2}{n_1}\right)^{\frac{1}{2}}$. The magnetic field is assumed to be the same in the two shells, and therefore the difference between the cooling frequencies in the shells is due to different Y -parameters; since synchrotron dominates over SSC here by design, the difference between ν_{c_2} and ν_{c_1} ends up being very small. The shell ‘2’ synchrotron self absorption frequency, ν_{a_2} is larger than that in shell 1 by a factor of $\left(\frac{n_1}{n_2}\right)^{0.2}$, or a factor of a few.

The 1 keV synchrotron and SSC flux from shells ‘1’ and ‘2’ for *GRB-4* is shown in the top left panel of Figure 8. The shell ‘2’ synchrotron flux contributes the most to the prompt x-ray flux, and the shell 1 synchrotron flux contributes a slightly smaller amount. SSC flux from either shell is negligible. There is a weak dependence of x-ray flux on Γ_{rel} . The shell ‘1’ synchrotron flux at 1 keV is about 10 mJy. This is simply the extrapolation of the 100 keV flux back to 1 keV, with a spectral index of $-\frac{1}{2}$ or $\left(\frac{1}{100}\right)^{-\frac{1}{2}} 1\text{mJy} \sim 10\text{mJy}$ for *GRB-4*.

Shell ‘2’ synchrotron x-ray flux ranges from 1 to 100 mJy. We expect the flux from shell ‘2’ at

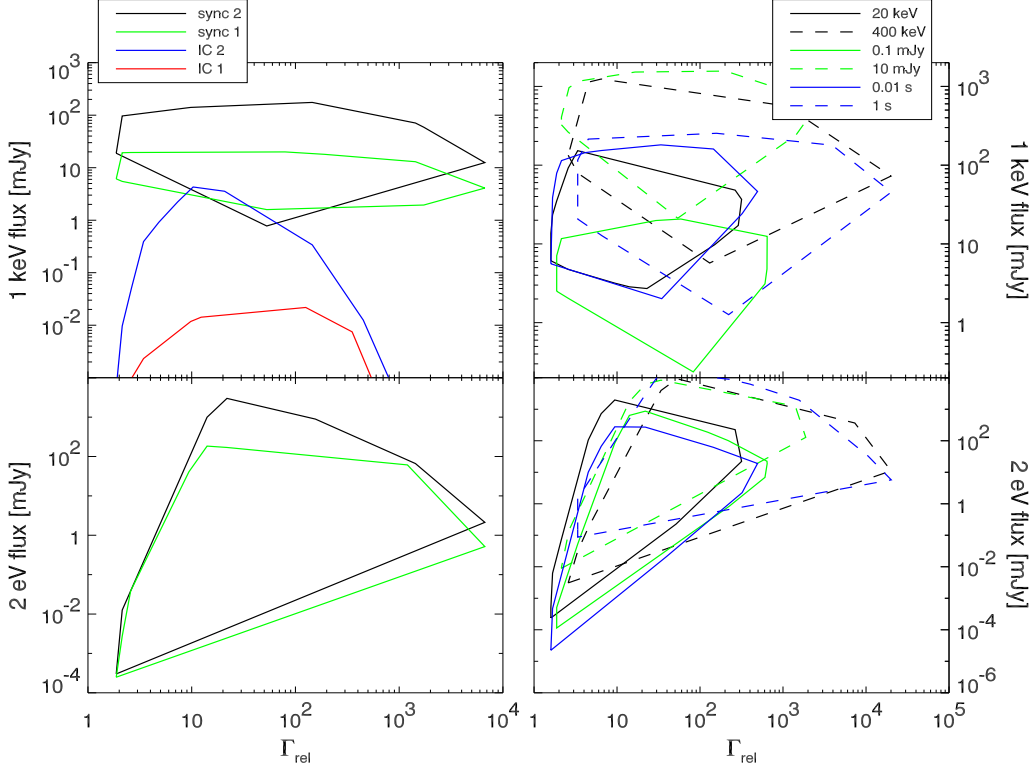


Fig. 8.— Prompt x-ray [1 keV] and optical [2 eV] flux associated with points in the solution sub-space of 5-D parameter space when cast in terms of the internal shock model or two colliding shells; the solutions are for synchrotron radiation with low energy spectrum $f_\nu \propto \nu^{-\frac{1}{2}}$. Top left: contributions of SSC and synchrotron to x-ray flux at 1 keV from shells ‘1’ and ‘2’ (see legend) for *GRB-1*. Top right: sum of all contributions is shown for the cases that have been described in Figure 2. Bottom left: contributions of synchrotron emission from shells ‘1’ and ‘2’ to the optical flux; IC contributions are negligible from either shell. Bottom right: sum of all contributions in the optical, for the same cases as the top right panel. The results shown here assume that the γ -ray flux is produced in shell ‘1’; production of the GRB in shell ‘2’ does not change the results significantly.

1 keV to be

$$f_{2x} \sim f_\gamma \frac{f_{\nu_{p2}}}{f_{\nu_{p1}}} \left(\frac{1\text{keV}}{\nu_{i2}} \right)^{-\frac{p}{2}} \left(\frac{\nu_{i2}}{100\text{keV}} \right)^{-\frac{1}{2}} \sim f_\gamma \left(\frac{n_1}{n_2} \right)^{\frac{1}{4}} \left(\frac{1\text{keV}}{\nu_\gamma} \right)^{-\frac{5}{4}} \text{ mJy} \quad (65)$$

using the above arguments and assuming that $\nu_{i2} < 1$ keV (valid when $\frac{n_1}{n_2} \lesssim 0.01$ – satisfied by roughly half of the solution points in the 5-D space), $\nu_{c1} \sim \nu_{c2}$, and $p = 2.5$. From this equation, we estimate that the flux at 1 keV should be between ~ 20 and 300 mJy (for $f_{1\gamma} = 1$ mJy and $\nu_\gamma \sim 100$ keV) – in agreement with the numerical results in Figure 8.

The shell ‘2’ SSC flux at 1 keV ranges from 10^{-5} to almost 10 mJy. The SSC peak frequency ($\sim \nu_{i2} \gamma_{i2}^2$) ranges from about 100 eV to very high values, so over a large part of the solution space,

the expected SSC flux at 1 keV in comparison to the synchrotron 100 keV flux from shell ‘1’ is (assuming that $\nu_{i2} > \nu_{c2}$)

$$\frac{f_{2x}^{ic}}{f_\gamma} \approx \frac{f_{\nu_{p2}} \tau_2}{f_{\nu_{p1}}} \left(\frac{1 \text{keV}}{\gamma_{c2}^2 \nu_{c2}} \right)^{-\frac{1}{2}} \left(\frac{\nu_{c1}}{100 \text{keV}} \right)^{-\frac{1}{2}} \sim 10 \left(\frac{n_2}{n_1} \right) \tau_1 \gamma_{c2} \quad (66)$$

which, after substituting in the solutions for τ and γ_c , is

$$f_{2x}^{ic} \approx 1.5 \times 10^{-4} \left(\frac{n_2}{n_1} \right) \nu_{\gamma 5}^{-\frac{7}{16}} f_\gamma^{\frac{17}{16}} t_\gamma^{-\frac{1}{8}} \nu_{c5}^{-\frac{1}{8}} t_a^{-\frac{1}{4}} Y^{\frac{15}{16}} (1+Y)^{-\frac{1}{4}} (1+z)^{-\frac{1}{4}} d_{L28}^{\frac{1}{8}} A_{2p}^{-\frac{15}{16}} \text{ mJy}; \quad (67)$$

with $Y \sim 1$ and $1 < n_2/n_1 < 10^5$, the range for the x-ray flux obtained from the above equation is in agreement with the numerical solutions.

The sum of synchrotron and SSC contributions to flux at 1 keV from both shells for various values of ν_γ , f_γ , and t_γ are shown in the upper right hand panel of Figure 8. The 1 keV flux ranges from 0.1 to a few thousand mJy, and is most sensitive to f_γ and ν_γ – in agreement with equation (65), $f_{2x} \propto f_\gamma \nu_\gamma^{\frac{5}{4}}$, since synchrotron emission dominates.

The early 0.2-10 keV x-ray flux as observed by the Swift x-ray telescope ranges from 10^{-12} to 10^{-8} ergs cm $^{-2}$ s $^{-1}$,⁵ which corresponds to 1 keV flux of about 10^{-4} to a few mJy (assuming $\nu^{-\frac{1}{2}}$ in the x-ray band). These observations are made at roughly 100s after the GRB trigger. The x-ray light curve from the γ -ray source should peak at about the same time as the GRB light curve. After the peak, assuming that the outflow opening angle is greater than $1/\Gamma$, the emission should be dominated by off-axis emission and the light curve should fall off as $t^{-2+\beta}$ (Kumar & Panaitescu 2000), which in this case is $t^{-2.5}$ since $f_\nu \propto \nu^{-1/2}$. Extrapolating the observed 1 keV flux of $\sim 10^{-4}$ –1 mJy backwards in time from 100s to 10s, we find the x-ray flux during the GRB to be consistent with values shown in the upper right panel of Figure 8.

3.3.2. Prompt optical emission when the GRB index $\alpha = -\frac{1}{2}$

In the bottom left panel of Figure 8, the R band (2 eV) flux from shell ‘1’ and ‘2’ are plotted against Γ_{rel} . Optical flux from the γ -ray source can be pretty bright during the burst for these solutions ranging from 10^{-3} and 100 mJy (24th to 11th magnitude in the R band). The synchrotron flux is smaller for smaller Γ_{rel} solutions. The SSC makes negligible contribution to the optical flux compared to the synchrotron process, because $\nu_a \gamma_c^2$ is well above the optical.

If we extrapolate the shell ‘1’ 100 keV flux back to 2 eV using the spectral index $\alpha = -\frac{1}{2}$, we expect $f_{1R} \sim 225 \nu_{\gamma 5}^{1/2} f_\gamma \sim 225 \text{mJy}$ for *GRB-150918A* whereas for most of the solution space the optical flux for shell ‘1’ falls below 10 mJy (fig. 8 bottom left panel) — this is because the synchrotron self

⁵[urlhttp://swift.gsfc.nasa.gov/cgi-bin/swift/grb_table/grb_table.py](http://swift.gsfc.nasa.gov/cgi-bin/swift/grb_table/grb_table.py)

absorption frequency is larger than the R-band frequency by a factor ~ 10 or more. The range of shell ‘2’ R-band flux is higher than shell ‘1’ by a factor of $\frac{f_{\nu p_2}}{f_{\nu p_1}} \sim \sqrt{\frac{n_2}{n_1}} \sim 30$.

In the bottom right panel of Figure 8, we show the affect of varying ν_γ , f_γ , and t_γ on the prompt optical flux; the total flux – obtained by adding the contributions for the two colliding shells – ranges from 10^{-4} to 10^3 mJy, or R magnitude of 26 to 9. The optical flux increases with ν_γ , f_γ , and t_γ – longer GRB pulses with higher peak frequency and/or flux tend to be brighter in the optical band. Synchrotron self absorption is larger at smaller Γ_{rel} , and that makes the optical flux smallest at the minimum of Γ_{rel} . There are $\Gamma_{rel} \sim 5$ solutions with $f_{B/ke} \sim 1$, that have small enough optical flux to be in accord with the observed upper limits, especially for smaller ν_γ , f_γ , and t_γ . Although $\nu_a > 2$ eV for much of the solution space, the optical light curve should peak at the same time as the GRB light curve, since $\nu_c < 2$ eV. After the peak, the light curve should fall off – if dominated by off-axis emission – as $t^{-2.5}$.

3.4. Synchrotron solutions for $f_\nu \propto \nu^{-\frac{p}{2}}$

If the observed spectral index is steep and consistent with $\nu^{-\frac{p}{2}}$ and no break is detected in the observed energy band of 15-150 keV, for instance, then this is a special case of either $\nu^{-\frac{1}{2}}$ or $\nu^{-\frac{(p-1)}{2}}$ low energy spectrum discussed in §3.1 & 3.3 – with $\nu_{\gamma 5} = \max(\nu_{\gamma 5}, \nu_{c 5}) \lesssim 0.15$. The allowed solution space for this situation should be close to the $\nu_\gamma = 20$ keV case in Figures 2 and 6; Specifically, $\gamma_i \lesssim 10^3$, $\Gamma > 100$, and $2 \lesssim \Gamma_{rel} \lesssim 200$.

4. Synchrotron-self-Compton – SSC – solutions

In this section, we present solutions for the prompt γ -ray emission to be produced via the synchrotron-self-inverse-Compton radiation or the SSC process. The basic approach is same as in section 3. We determine the hypersurface in the 5-D parameter space $(\gamma_i, \Gamma, B, N, \tau)$ that has SSC emission consistent with the three observational constraints ν_γ , f_γ & t_γ . Since different cases of low energy spectral index have different ordering for the characteristic synchrotron frequencies (ν_i, ν_c, ν_a) , we do not consider a general SSC solution, but describe analytical and numerical solutions for the positive low energy spectral index case i.e., $f_\nu \propto \nu^\alpha$ with $\alpha > 0$ for $\nu < \nu_\gamma$, and the negative index case i.e., $\alpha < 0$, separately in several subsections below.

4.1. SSC solutions: Positive low energy spectral index

This section is broken up in two subsections. One dealing with the special case of $f_\nu \propto \nu^{1/3}$ is discussed below. All the other cases of $\alpha > 1/3$ are discussed in §4.1.2.

4.1.1. SSC solutions: $\alpha \approx +1/3$

The SSC spectrum (νf_ν^{ic}) peaks at $\nu_\gamma \sim 4 \max(\nu_i, \nu_c) \max(\gamma_i, \gamma_c)^2$; where ν_i & ν_c are the injection and cooling frequencies of the underlying synchrotron radiation, γ_i is the minimum LF of electrons in the source comoving frame and γ_c is the LF of electrons that cool on time scale t_a available since last accelerated. For the spectrum below ν_γ to be $\sim \nu^{1/3}$, we must have $\gamma_i \sim \gamma_c$, and in that case $\nu_\gamma \sim 4\nu_i \gamma_i^2$. The IC flux at ν_γ is $f_\gamma \sim f_{\nu_p} \tau$ (f_{ν_p} is the synchrotron flux at ν_i). The equations for pulse duration t_γ and Compton-Y are same as in §3. The equations for $\nu_i \sim \nu_c$, the peak IC frequency ν_γ , the IC flux f_γ at ν_γ , and the Compton Y-parameter are given below –

$$B^2 \Gamma \gamma_i \approx 7.7 \times 10^8 (1+z) t_a^{-1} (1+Y)^{-1} \quad (68)$$

$$B \gamma_i^4 \Gamma \approx 2.3 \times 10^{12} \nu_{\gamma 5} (1+z) \quad (69)$$

$$B \Gamma^5 \tau^2 \approx 1.6 \times 10^6 f_\gamma t_\gamma^{-2} (1+z) d_{L28}^2 \quad (70)$$

$$\tau \gamma_i^2 \approx \frac{3}{4} Y \left(\frac{p-1}{p-2} \right)^{-1} \quad (71)$$

We first eliminate τ from equation (70) using (71) to get

$$B \Gamma^5 \gamma_i^{-4} \approx 2.8 \times 10^6 f_\gamma t_\gamma^{-2} (1+z) d_{L28}^2 Y^{-2} \left(\frac{p-1}{p-2} \right)^2. \quad (72)$$

Next, we divide equations (68) and (69) to eliminate Γ :

$$B \gamma_i^{-3} \approx 3.3 \times 10^{-4} t_a^{-1} (1+Y)^{-1} \nu_{\gamma 5}^{-1}, \quad (73)$$

divide equations (69) and (72) to eliminate B :

$$\gamma_i^8 \Gamma^{-4} \approx 8.2 \times 10^5 \nu_{\gamma 5} f_\gamma^{-1} t_\gamma^2 d_{L28}^{-2} Y^2 \left(\frac{p-1}{p-2} \right)^{-2}, \quad (74)$$

and combine equations (68) and (72) to obtain:

$$B \Gamma \approx 4.6 \times 10^4 t_a^{-\frac{4}{9}} (1+Y)^{-\frac{4}{9}} f_\gamma^{\frac{1}{9}} t^{-\frac{2}{9}} (1+z)^{\frac{5}{9}} d_{L28}^{\frac{2}{9}} Y^{-\frac{2}{9}} \left(\frac{p-1}{p-2} \right)^{\frac{2}{9}}. \quad (75)$$

Equations (73) and (75) give

$$\Gamma \gamma_i^3 \approx 1.4 \times 10^8 \nu_{\gamma 5} t_a^{\frac{5}{9}} (1+Y)^{\frac{5}{9}} f_\gamma^{\frac{1}{9}} t^{-\frac{2}{9}} (1+z)^{\frac{5}{9}} d_{L28}^{\frac{2}{9}} Y^{-\frac{2}{9}} \left(\frac{p-1}{p-2} \right)^{\frac{2}{9}}, \quad (76)$$

and substituting this into equation (74), we find the solution for γ_i to be

$$\gamma_i \approx 84 \nu_{\gamma 5}^{\frac{1}{4}} f_\gamma^{-\frac{1}{36}} t^{\frac{1}{18}} t_a^{\frac{1}{9}} Y^{\frac{1}{18}} (1+Y)^{\frac{1}{9}} d_{L28}^{-\frac{1}{18}} (1+z)^{\frac{1}{9}} A_{2p}^{-\frac{1}{18}}. \quad (77)$$

Note that the electron LF γ_i has a very weak dependence on the observed quantities as well as the Compton- Y parameter, and therefore $\gamma_i \sim 80$ for the entire SSC solution space. By plugging equation (77) back into equations (73), (74), and (71), we find the remaining parameters

$$B \approx 200 \nu_{\gamma_5}^{-\frac{1}{4}} f_{\gamma}^{-\frac{1}{12}} t_{\gamma}^{\frac{1}{6}} t_a^{-\frac{2}{3}} Y^{\frac{1}{6}} (1+Y)^{-\frac{2}{3}} d_{L28}^{-\frac{1}{6}} (1+z)^{\frac{1}{3}} A_{2p}^{-\frac{1}{6}} \text{ Gauss} \quad (78)$$

$$\Gamma \approx 240 \nu_{\gamma_5}^{\frac{1}{4}} f_{\gamma}^{\frac{7}{36}} t_{\gamma}^{-\frac{7}{18}} t_a^{\frac{2}{9}} Y^{-\frac{7}{18}} (1+Y)^{\frac{2}{9}} d_{L28}^{\frac{7}{18}} (1+z)^{\frac{2}{9}} A_{2p}^{\frac{7}{18}} \quad (79)$$

$$\tau \approx 1.1 \times 10^{-4} \nu_{\gamma_5}^{-1/2} f_{\gamma}^{\frac{1}{18}} t_{\gamma}^{-\frac{1}{9}} t_a^{-\frac{2}{9}} Y^{\frac{8}{9}} (1+Y)^{-\frac{2}{9}} d_{L28}^{\frac{1}{9}} (1+z)^{-\frac{2}{9}} A_{2p}^{-\frac{8}{9}}. \quad (80)$$

All of these parameters are weakly dependent on the three observable quantities viz. ν_{γ_5} , f_{γ} & t_{γ} . Substituting the *observed* values for *GRB-1*, i.e. $\nu_{\gamma_5} = 1$, $f_{\gamma} = 1$ mJy, and $t_a \sim t_{\gamma} = 0.1$ s, $z = 1$, & taking $p=3.2$, we find that $\gamma_i \sim 58 Y^{\frac{1}{18}} (1+Y)^{\frac{1}{9}}$, $B \sim 1.1 \times 10^3 Y^{\frac{1}{6}} (1+Y)^{-\frac{2}{3}} \text{ Gauss}$, $\Gamma \sim 110 Y^{-\frac{7}{18}} (1+Y)^{\frac{2}{9}}$, and $\tau \sim 1.3 \times 10^{-4} Y^{\frac{8}{9}} (1+Y)^{-\frac{2}{9}}$.

The distance of the γ -ray source from the center of the explosion, R_{γ} , is given by

$$R_{\gamma} \approx 3.3 \times 10^{15} \nu_{\gamma_5}^{\frac{1}{2}} f_{\gamma}^{\frac{7}{18}} t_{\gamma}^{\frac{2}{9}} t_a^{\frac{4}{9}} Y^{-\frac{7}{9}} (1+Y)^{\frac{4}{9}} (1+z)^{-\frac{5}{9}} d_{L28}^{\frac{7}{9}} A_{2p}^{\frac{7}{9}} \text{ cm}, \quad (81)$$

or $R_{\gamma} \sim 1.3 \times 10^{15} Y^{-\frac{7}{9}} (1+Y)^{\frac{4}{9}} \text{ cm}$ for *GRB-1*. This distance is smaller than the deceleration radius for a homogeneous or a wind external medium, unlike the situation when γ -rays are produced via the synchrotron process (see §3).

One constraint that we have not yet considered is that the SSC self absorption frequency, $\nu_a^{ic} \sim 4\nu_a \gamma_i^2$, must be smaller than ~ 20 keV otherwise the low energy spectral index, obtained by Band function fit to the BATSE or *Swift*/BAT data, would be steeper than $\alpha = 1/3$ we are considering in this subsection. The expression for ν_a^{ic} , valid for $\nu_a < \nu_i, \nu_c$, is

$$\nu_a^{ic} \sim \frac{1.7 \times 10^{-14} \gamma_i^2 \Gamma^{\frac{6}{5}}}{(1+z)} \left(\frac{f_p' \nu_i^{-\frac{1}{3}}}{2\gamma_i m_e} \right)^{\frac{3}{5}} \quad (82)$$

where $f_p' \equiv \sqrt{3} q^3 B \tau / \sigma_T m_e c^2$ is the comoving synchrotron flux. Substituting for γ_i , Γ , B & τ using equations 77–80 we find

$$\nu_a^{ic} \sim 2.2 \times 10^5 \nu_{\gamma_5}^{\frac{1}{10}} f_{\gamma}^{\frac{1}{6}} t_{\gamma}^{-\frac{1}{3}} t_a^{-\frac{1}{15}} Y^{\frac{4}{15}} (1+Y)^{-\frac{1}{15}} (1+z)^{-\frac{2}{3}} d_{L28}^{\frac{1}{3}} A_{2p}^{-\frac{4}{15}} \text{ eV} \quad (83)$$

which is very insensitive to *all* of the observed quantities and for a wide range of observables $\nu_a^{ic} \sim 100$ keV which is too large to produce an SSC spectrum with $f_{\nu}^{ic} \propto \nu^{\frac{1}{3}}$ below the peak.

We now try relaxing one of the constraints we had imposed to simplify the analytical calculation i.e., $\gamma_i \sim \gamma_c$. This approximation was guided by the observational result that the observed spectrum for $\nu > \nu_{\gamma}$ is almost always $\sim \nu^{-1.5}$ for GRBs with $\alpha \sim 1/3$. This result suggests $\gamma_i \sim \gamma_c$ provided that $p \approx 3$. However, if the electron distribution is steeper, $p \sim 4$, then ν_c can be much greater than ν_i , and a high energy spectrum of $\nu^{-(p-1)/2} \sim \nu^{-1.5}$ would be consistent with observations. We now

investigate this possibility and determine if letting $\nu_c > \nu_i$ would allow for a smaller ν_a^{ic} and hence $\alpha = 1/3$ solutions. Note that the opposite arrangement of frequencies ($\nu_c < \nu_i$) is uninteresting, since the low energy index is $-1/2$ in this case.

For $\nu_c > \nu_i$ equation (68) is modified to read

$$\gamma_i B^2 \Gamma = \frac{7.7 \times 10^8 (1+z)}{\eta_i t_a (1+Y)} \quad (84)$$

where $\eta_i \equiv \gamma_c/\gamma_i$. We also need to use the appropriate expression for Y when $\gamma_c \gg \gamma_i$ and $p > 3$ (see eq. 6)

$$Y = \frac{4}{3} \frac{(p-1)}{(p-2)(p-3)} \tau \gamma_i^2, \quad (85)$$

which apart from a factor $(p-3)$ is same as equation (71). We solve the above two equations together with eqs. (70) & (71) to find that $\nu_a^{ic} \propto \eta_i^{-\frac{1}{15}}$; so ν_a^{ic} does not decrease by much even if we take γ_c to be larger than γ_i by many orders of magnitude, and therefore there are no SSC solutions with low energy spectrum of $\nu^{1/3}$ between ~ 15 keV and 200 keV.

The above analytical calculation is based on a number of approximations for the SSC spectrum and flux. We check the validity of analytical results using numerical calculations and by searching the 5-D parameter space for SSC solutions with low energy spectral index $\alpha \approx 1/3$. It turns out that numerically also we find no solutions — ν_a^{ic} is indeed too high to produce a GRB with a low energy spectrum of $\nu^{1/3}$ in the ~ 15 –200 keV band.

The only other possibility is that the $\alpha \approx 1/3$ index is transitory, i.e. the spectrum is changing continuously from $\alpha \approx 1$ at $\nu \sim 20$ keV to $\alpha \approx -1$ at $\nu = \nu_\gamma$ and that $\alpha \sim 1/3$ is realized at some intermediate frequency. This might, however, pose a problem for those GRBs with $\nu_\gamma \gtrsim 100$ keV, since the spectrum would be steeper than $\nu^{1/3}$ near 15 keV and therefore a Band function fit to the spectrum will yield $\alpha > 1/3$.

4.1.2. SSC solutions: Spectral index $1/3 < \alpha \leq 1$

The analytical solution for this case is similar to the SSC $\alpha = 1/3$ case analyzed in §4.1.1. We take $\gamma_i \sim \gamma_c$ in order that the high energy spectrum is $\propto \nu^{-p/2} \sim \nu^{-1.5}$. The equations we solve are for ν_γ , f_γ , Compton-Y, and $\gamma_i \sim \gamma_c$:

$$B^2 \Gamma \gamma_i \approx 7.7 \times 10^8 (1+z) t_a^{-1} (1+Y)^{-1} \quad (86)$$

$$B \gamma_i^4 \Gamma \approx 2.3 \times 10^{12} \nu_{\gamma 5} (1+z) \eta_a^{-2} \quad (87)$$

$$B \Gamma^5 \tau^2 \approx 1.6 \times 10^6 f_\gamma t_\gamma^{-2} (1+z) d_{L28}^2 \eta_a^p \quad (88)$$

$$\tau \gamma_i^2 \approx \frac{3}{4} Y \left(\frac{p-1}{p-2} \right)^{-1} \quad (89)$$

where $\eta_a \equiv \gamma_a/\gamma_i \gtrsim 1$ since $\nu_a \gtrsim \nu_c, \nu_i$. The above equations are solved in the exact same way that we solved them in section 4.1.1, and we find that the solutions are:

$$\gamma_i \approx 84 \nu_{\gamma_5}^{\frac{1}{4}} f_{\gamma}^{-\frac{1}{36}} t_{\gamma}^{\frac{1}{18}} t_a^{\frac{2}{9}} Y^{\frac{1}{18}} (1+Y)^{\frac{1}{9}} d_{L28}^{-\frac{1}{18}} (1+z)^{\frac{1}{9}} A_{2p}^{-\frac{1}{18}} \eta_a^{-\frac{-(p+18)}{36}} \quad (90)$$

$$B \approx 200 \nu_{\gamma_5}^{-\frac{1}{4}} f_{\gamma}^{-\frac{1}{12}} t_{\gamma}^{\frac{1}{6}} t_a^{-\frac{2}{3}} Y^{\frac{1}{6}} (1+Y)^{-\frac{2}{3}} d_{L28}^{-\frac{1}{6}} (1+z)^{\frac{1}{3}} A_{2p}^{-\frac{1}{6}} \eta_a^{\frac{6-p}{12}} \text{ Gauss} \quad (91)$$

$$\Gamma \approx 240 \nu_{\gamma_5}^{\frac{1}{4}} f_{\gamma}^{\frac{7}{36}} t_{\gamma}^{-\frac{7}{18}} t_a^{\frac{2}{9}} Y^{-\frac{7}{18}} (1+Y)^{\frac{2}{9}} d_{L28}^{\frac{7}{18}} (1+z)^{\frac{2}{9}} A_{2p}^{\frac{7}{18}} \eta_a^{\frac{7p-18}{36}} \quad (92)$$

$$\tau \approx 1.1 \times 10^{-4} \nu_{\gamma_5}^{-\frac{1}{2}} f_{\gamma}^{\frac{1}{18}} t_{\gamma}^{-\frac{1}{9}} t_a^{-\frac{2}{9}} Y^{\frac{8}{9}} (1+Y)^{-\frac{2}{9}} d_{L28}^{\frac{1}{9}} (1+z)^{-\frac{2}{9}} A_{2p}^{-\frac{8}{9}} \eta_a^{\frac{p+18}{18}}. \quad (93)$$

For $p = 3.2$, $t_a \sim t_{\gamma}$, $\eta_a \gtrsim 1$, and parameters corresponding to *GRB-1* we find from the above equations that $\Gamma \gtrsim 110 Y^{-\frac{7}{18}}$, $\gamma_i \lesssim 100$, and $\tau \gtrsim 1.3 \times 10^{-4} Y^{\frac{8}{9}} (1+Y)^{-\frac{2}{9}}$. These analytical results are roughly consistent with numerical determination of the allowed region in 5-D parameter space (see fig. 9); we also find $\eta_a \approx 1$ numerically.

The distance of the γ -ray source from the center of the explosion is shown in fig. (9) for various GRB parameters and is greater than $\sim 10^{14}$ cm for $Y \lesssim 10$. The ratio of magnetic to electron energy is small – $f_{B/ke} < 0.1$ for the entire solution space (fig. 9) since $Y \gtrsim 1$.

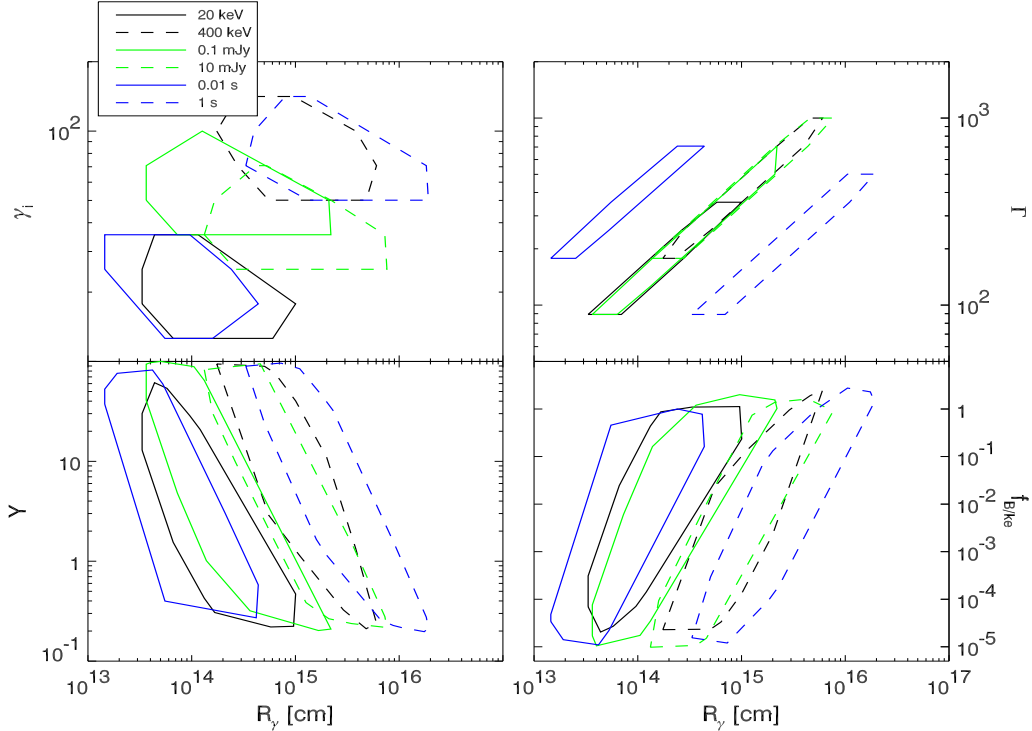


Fig. 9.— The SSC solution space when the low energy spectrum is $f_{\nu}^{ic} \propto \nu^{\alpha}$, for $\nu < \nu_{\gamma}$, with $1/3 < \alpha \leq 1$. The different cases in legend are as described in Figure 2.

The SSC solutions we have found can be related to the internal shock model. The relative

LF of collision between shells – obtained from γ_i (see eq. 11 and appendix A) – is found to be between 2 and 10, which is significantly less than what we were finding for synchrotron solutions. The LFs of shells before collision (assuming that γ -rays are produced in the inner, faster, shell) is $300 \lesssim \Gamma_1 \lesssim 5000$ and $100 \lesssim \Gamma_2 \lesssim 1000$; the ratio $\Gamma_1/\Gamma_2 > 2$ and the efficiency for producing γ -rays is $\gtrsim 10\%$ for the allowed 5-D parameter space for SSC. The bulk LF of post-shock gas $100 < \Gamma < 1000$ is compatible with late time afterglow modeling.

We now calculate the x-ray and optical emissions accompanying the γ -ray pulse.

4.1.2a. X-ray emission for $1/3 < \alpha \leq 1$ SSC solutions

The 1 keV prompt emission from SSC and synchrotron processes is shown in the top two panels of figure 10. The contributions of SSC & synchrotron to 1 keV flux is shown separately in the top left panel for *GRB- \dagger* , and the sum of the two for a variety of GRB parameters can be found in the top right panel.

The x-ray flux can be estimated analytically using the expression for synchrotron flux $f_x = f_{\nu_p}(1\text{keV}/\nu_i)^{-p/2}$, since $\nu_i \sim \nu_c \sim \nu_a$; f_x can also be expressed as $f_x \sim f_\gamma \tau^{-1} \gamma_i^{-p} (25)^{p/2} \nu_{\gamma_5}^{p/2}$, or in terms of observable parameters

$$f_x \sim \frac{9 \times 10^3}{17^p} \nu_{\gamma_5}^{\frac{p+2}{4}} f_\gamma^{\frac{34+p}{36}} t_\gamma^{\frac{2-p}{18}} t_a^{\frac{2-p}{9}} Y^{-\frac{16+p}{18}} (1+Y)^{\frac{2-p}{9}} d_{L28}^{\frac{p-2}{18}} (1+z)^{\frac{2-p}{9}} A_{2p}^{\frac{16+p}{18}} \eta_a^{\frac{(p-2)(p+18)}{36}} \text{ mJy}, \quad (94)$$

or $f_x \sim 9Y^{-\frac{16}{15}}(1+Y)^{-\frac{2}{15}} \text{ mJy}$ for *GRB- \dagger* with $\eta_a > 1$, $p = 3.2$ and $t_a \sim t_\gamma$; this is roughly consistent with the numerically calculated flux shown in fig. 10.

In the top right panel of Figure 10, the total 1 keV prompt flux is shown for a number of different values of ν_γ , f_γ , and t_γ . The dependence of the x-ray flux on these quantities agree with equation (94), which gives $f_x \propto \nu_\gamma^{\frac{13}{10}} f_\gamma^{\frac{31}{30}} t_\gamma^{-\frac{1}{15}}$ for $p = 3.2$: an increase in ν_γ or f_γ leads to an increase of f_x , and an increase in t_γ has little effect on the x-ray flux (fig. 10). The 1 keV flux for all of these cases ranges from 0.01 to 10^3 mJy during the burst; the flux at 100s, the time when the x-ray telescope aboard the *Swift* satellite starts looking at the burst, would be smaller by a factor of ~ 10 – 10^3 depending on GRB pulse duration. So, the x-ray flux accompanying the γ -ray radiation, for the SSC model of GRBs, is consistent with the observed data.

4.1.2b. Optical emission for $1/3 < \alpha \leq 1$ SSC solutions

The prompt optical flux accompanying γ -rays, in the SSC model, is shown in the bottom left panel of Figure 10. Analytically we find the prompt R-band flux due to the synchrotron component underlying the SSC model to be: $f_R \sim f_{\nu_p} \sim f_\gamma \tau^{-1}$, or

$$f_R \sim 9 \times 10^3 \nu_{\gamma_5}^{\frac{1}{2}} f_\gamma^{\frac{17}{18}} t_\gamma^{\frac{1}{9}} t_a^{\frac{2}{9}} Y^{-\frac{8}{9}} (1+Y)^{\frac{2}{9}} d_{L28}^{-\frac{1}{9}} (1+z)^{\frac{2}{9}} A_{2p}^{\frac{8}{9}} \eta_a^{\frac{17p-18}{18}} \text{ mJy} \quad (95)$$

which for *GRB- \dagger* reduces to $f_R \sim (8 \times 10^3 \text{ mJy}) Y^{-\frac{8}{9}} (1+Y)^{\frac{2}{9}}$. There are, however, many numerical solutions corresponding to $Y \gtrsim 10$ for which $f_R \sim 70$ mJy. It turns out that $\nu_a > 2$ eV for the low

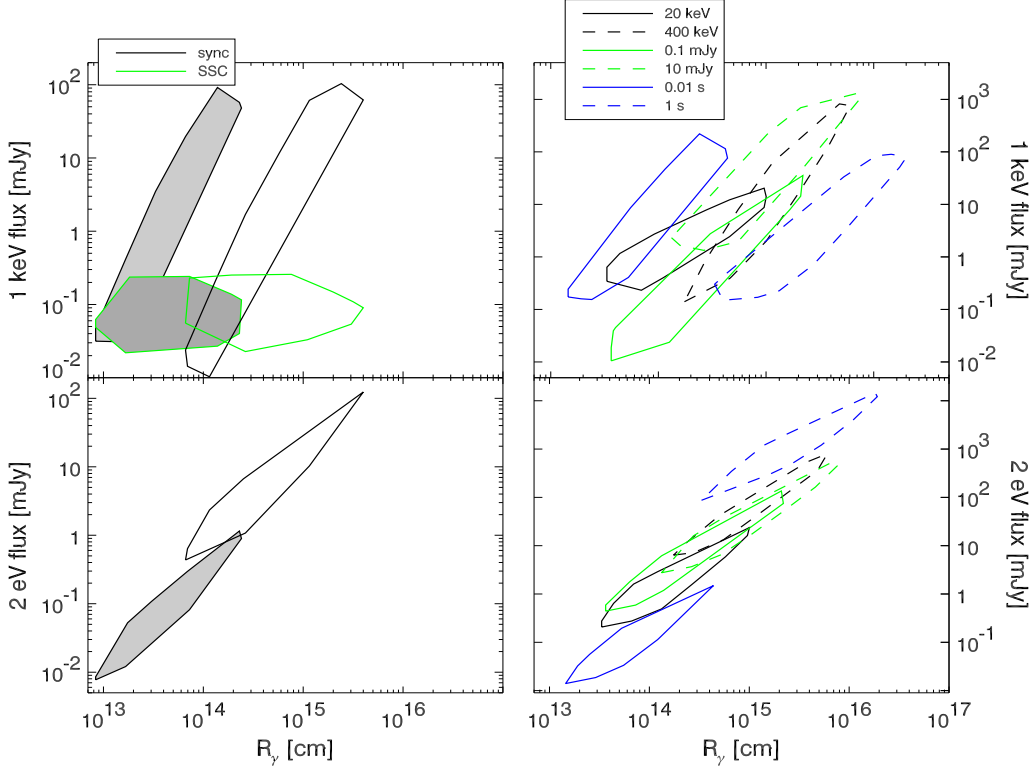


Fig. 10.— X-ray (1 keV) and optical (2eV) synchrotron and SSC flux accompanying the prompt GRB emission for SSC solutions with $1/3 < \alpha \leq 1$. **Right panels:** The sum of SSC and synchrotron contributions for several different sets of ν_γ , f_γ & t_γ as described in Figure 8. **Left two panels:** the areas shaded in gray are the x-ray and optical flux for *GRB-140806A* (a GRB that has $\nu_\gamma = 100\text{keV}$, $f_\gamma = 1\text{mJy}$ & $t_\gamma = 0.1\text{s}$) and with $t_a = t_\gamma/100$, and the unshaded areas are for *GRB-140806A* with $t_a = t_\gamma$.

radius solutions, by up to a factor of 3. If $\nu_i < 2\text{ eV} < \nu_a$, then the expression for optical flux is

$$f_R \sim 50\nu_{\gamma 5}^{-\frac{3}{4}} f_{\gamma 36}^{\frac{29}{36}} t_{\gamma 18}^{\frac{7}{9}} t_a^{\frac{7}{9}} Y^{-\frac{11}{18}} (1+Y)^{\frac{7}{9}} d_{L28}^{-\frac{7}{18}} (1+z)^{\frac{7}{9}} A_{2p}^{\frac{11}{18}} \eta_a^{-\frac{(7p+126)}{36}} \text{mJy} \quad (96)$$

giving $f_R \lesssim 7Y^{-\frac{11}{18}} (1+Y)^{\frac{7}{9}} \text{mJy}$ for *GRB-140806A*.

The optical flux, obtained by numerical calculations, is shown in the bottom right panel of Figure 10, for several sets of $(\nu_\gamma, f_\gamma, t_\gamma)$. The results are consistent with the dependences found in equations (95) or (96) when $\nu_a > 2\text{eV}$. The reason that the self absorbed f_R increases with ν_γ numerically while equation (96) shows a decrease is that $\eta_a \sim \nu_\gamma^{-1/2}$ (confirmed numerically), and the huge dependence of $f_R \propto \eta_a^{4.1}$ gives positive dependence of $f_R \sim \nu_\gamma^{1.3}$. The dependence of optical flux on the duration of the GRB pulse is due to the fact that longer pulses have larger R_γ and $\nu_a < 2\text{eV}$. The range of optical flux for SSC solutions is between 0.01 mJy to a few times 10^4 mJy (R magnitude from 21- to 6-mag). There is an approximately linear relationship between f_R and

R_γ . Solutions with R -magnitude of above 9-mag (1 Jy) are most likely ruled out. In particular, this rules out the 1 s pulse duration solutions that have $R_\gamma \gtrsim 2 \times 10^{15}$ cm. If the pulse width were 10 s, the SSC solutions would have prompt optical of between 1 and 4 Jy, or $R \sim 7$ mag, which is too bright to have been missed in optical follow up observations. We note that if GRB dissipation radius is $\sim 10^{16}$ cm as found in Kumar et al. (2007), then bright optical flux of $R > 9$ mag is expected in every GRB produced via SSC. Since this bright optical emission is not seen, this may pose major problems for the SSC process to produce GRBs with positive α .

If, however, electrons are accelerated multiple times during the course of a γ -ray pulse in the GRB light-curve, i.e. $t_a \ll t_\gamma$, the optical flux can be reduced significantly. The dependence $f_R \propto t_a^{2/9}$ (eq. 95) itself does not reduce f_R by much, but since $\nu_a \propto t_a^{-\frac{4(p+3)}{9(p+5)}} \sim t_a^{-0.3}$ as well, a smaller t_a gives a larger ν_a and that reduces the optical flux by an additional factor of $\sim t_a^{-0.6}$ and results in $f_R \propto t_a^{7/9}$; for $t_a = t_\gamma/100$, the optical flux is reduced by a factor of $\sim 10^2$ compared with the case where $t_a \sim t_\gamma$, in agreement with the numerical results found in the lower left hand panel of Figure 10. We've numerically searched the whole range of observable parameters and find that the scaling $f_R \propto t_a^{7/9}$ is valid through the entire solution space, and even the highest optical flux levels of 10 Jy (for the $t_\gamma \sim 1$ s case) is reduced below 0.1 Jy, or $R > 11$ mag, if $t_a \lesssim t_\gamma/10^2$. Multiple acceleration episodes for electrons is, therefore, a possible way of reducing the excessive optical flux that otherwise necessarily accompanies SSC solutions for γ -ray emission.

The optical flux should peak at the same time the GRB light curve peaks, since ν_c is on the order of 2 eV. The temporal decay of optical flux in this case is dictated by the curvature or the off-axis emission (Kumar & Panaitescu, 2000) — the optical light curve should fall off as $t^{-2-p/2} \sim t^{-3.6}$ as long as ν_a is below the R band. At first glance, it might seem that if $\nu_a > 2$ eV, and the synchrotron spectrum $\propto \nu^{5/2}$ or ν^2 in the optical band, the optical LC would be flat $\sim t^0$ or even rise as $t^{1/2}$. This behavior, however, lasts for a very short time since $(\nu_a/2\text{eV}) \lesssim$ a few, and $\nu_a \propto t^{-1}$ for off-axis emission; once ν_a drops below 2eV the optical flux would start falling off as $\sim t^{-3.6}$. The upper limit of $V \sim 18.5$ -mag (0.2 mJy) at 100s for many Swift detected bursts (e.g. Roming et al. 2006) is a lot smaller than the flux expected during the burst for the SSC model. If the pulse occurs at ~ 1 s post-trigger then the optical flux at 100s would be smaller than the prompt optical flux by a factor $\sim 10^7$ and that is quite consistent with observational upper limits for almost the entire solution space for the SSC-model.

We emphasize that a bright optical flash ($R \lesssim 14$ -mag) concurrent with γ -ray emission is a generic prediction of the SSC-model for GRBs with positive low energy index. Bright, prompt, optical radiation has been reported for a few bursts with positive α – e.g. 990123 (Akerlof et al. 1999; Briggs et al. 1999), 061007 (Golenetskii, S., et al. 2006; Yamaoka, K., et al. 2006), and the second emission episodes of 050401 (Golenetskii, S., et al. 2005) and 050820A (Cummings, J., et al. 2005) – however, if future observations fail to detect prompt optical with $R \lesssim 14$ -mag then that will suggest that one of the assumptions of the model developed in this work has to be abandoned – the most likely possibility, in our view, is to discard the assumption that $t_a \sim t_\gamma$ and that suggests that γ -rays are not generated in a shock heated medium.

4.2. SSC solutions for negative low energy spectral index

In this section we consider synchrotron-self-Compton solutions when the spectrum below ν_γ , the peak of νf_ν^{ic} , is $f_\nu^{ic} \propto \nu^\alpha$ with $\alpha < 0$. There are two different class of solutions in this case – those with the underlying seed synchrotron spectrum having $\nu_c < \nu_i$ and vice versa. We treat the two cases separately analytically, but plot the numerical solutions for both cases together in Figure 11. We use one vital piece of information gained from the numerical solutions to simplify our analytical calculations: the synchrotron self absorption frequency, ν_a , is larger than $\max(\nu_i, \nu_c)$, and therefore $\nu_\gamma \sim 4\nu_a \max(\gamma_i, \gamma_c)^2$; note that even though $\nu_a > \max(\nu_i, \nu_c)$, the spectral index below ν_γ is negative down to the frequency $\sim \nu_a \min(\gamma_i, \gamma_c)^2 < 10$ keV.

4.2.1. $\nu_c < \nu_i$ case

The equations that are solved for this case can be cast in a form very similar to the SSC $\alpha \approx 1/3$ case (considered in §4.1.1) by introducing two variables: $\eta_i \equiv \gamma_i/\gamma_c$ and $\eta_a \equiv \gamma_a/\gamma_i$. The equations for ν_c , ν_γ , f_γ , and Compton-Y expressed in terms of η_i & η_a are:

$$B^2 \Gamma \gamma_i \sim 7.7 \times 10^8 \eta_i (1+z) t_a^{-1} (1+Y)^{-1} \quad (97)$$

$$B \gamma_i^4 \Gamma \sim 2.3 \times 10^{12} \nu_{\gamma 5} (1+z) \eta_a^{-2} \quad (98)$$

$$B \Gamma^5 \tau^2 \sim 1.6 \times 10^6 f_\gamma t_\gamma^{-2} (1+z) d_{L28}^2 \eta_a^p \eta_i^2 \quad (99)$$

$$\tau \gamma_i^2 \sim 0.75 Y \left(\frac{p-1}{p-2} \right)^{-1} \eta_i. \quad (100)$$

These equations are solved the same way as outlined in the previous section, and we find the solutions to be:

$$\gamma_i \sim 84 \nu_{\gamma 5}^{1/4} f_\gamma^{-1/36} t_\gamma^{1/18} t_a^{1/9} Y^{1/18} (1+Y)^{1/9} d_{L28}^{-1/18} (1+z)^{1/9} A_{2p}^{-1/18} \eta_i^{-\frac{1}{9}} \eta_a^{-\frac{-(p+18)}{36}} \quad (101)$$

$$B \sim 200 \nu_{\gamma 5}^{-1/4} f_\gamma^{-1/12} t_\gamma^{1/6} t_a^{-2/3} Y^{1/6} (1+Y)^{-2/3} d_{L28}^{-1/6} (1+z)^{1/3} A_{2p}^{-1/6} \eta_i^{\frac{2}{3}} \eta_a^{\frac{6-p}{12}} \text{ Gauss} \quad (102)$$

$$\Gamma \sim 240 \nu_{\gamma 5}^{1/4} f_\gamma^{7/36} t_\gamma^{-7/18} t_a^{2/9} Y^{-7/18} (1+Y)^{2/9} d_{L28}^{7/18} (1+z)^{2/9} A_{2p}^{7/18} \eta_i^{-\frac{2}{9}} \eta_a^{\frac{7p-18}{36}} \quad (103)$$

$$\tau \sim 1.1 \times 10^{-4} \nu_{\gamma 5}^{-1/2} f_\gamma^{1/18} t_\gamma^{-1/9} t_a^{-2/9} Y^{8/9} (1+Y)^{-2/9} d_{L28}^{1/9} (1+z)^{-2/9} A_{2p}^{-8/9} \eta_i^{\frac{11}{9}} \eta_a^{\frac{p+18}{18}}. \quad (104)$$

The dependence of B , Γ , γ_i & τ on the observables is same as in equations 77-80 – the difference is in the dependence on η_a and η_1 . The distance of the γ -ray source from the center of the explosion is $R_\gamma \propto t_\gamma \Gamma^2 \propto \eta_i^{-\frac{4}{9}} \eta_a^{\frac{7p-18}{18}}$. We use the constraint that $\nu_a^{ic} \sim 4\nu_a \gamma_c^2 \sim 10^5 \nu_{\gamma 5} \eta_i^{-2} < 10$ keV to infer that $\eta_i \gtrsim 3.2$ for these solutions; we numerically find that $\eta_i \gtrsim 10$.

Numerical calculations of the allowed region in the 5-D parameter space for GRB - \dagger give $\gamma_i \lesssim 50$, $B \gtrsim 200$ Gauss, $\Gamma \lesssim 300$, and $\tau \gtrsim 3 \times 10^{-3}$. There is good agreement between the numerical and analytical γ_i and Γ solutions (see fig. 11), although analytical and numerical solutions for B , τ &

R_γ can differ by a factor of a few due to the difference of a factor of a few in the analytical and numerical value of η_i .

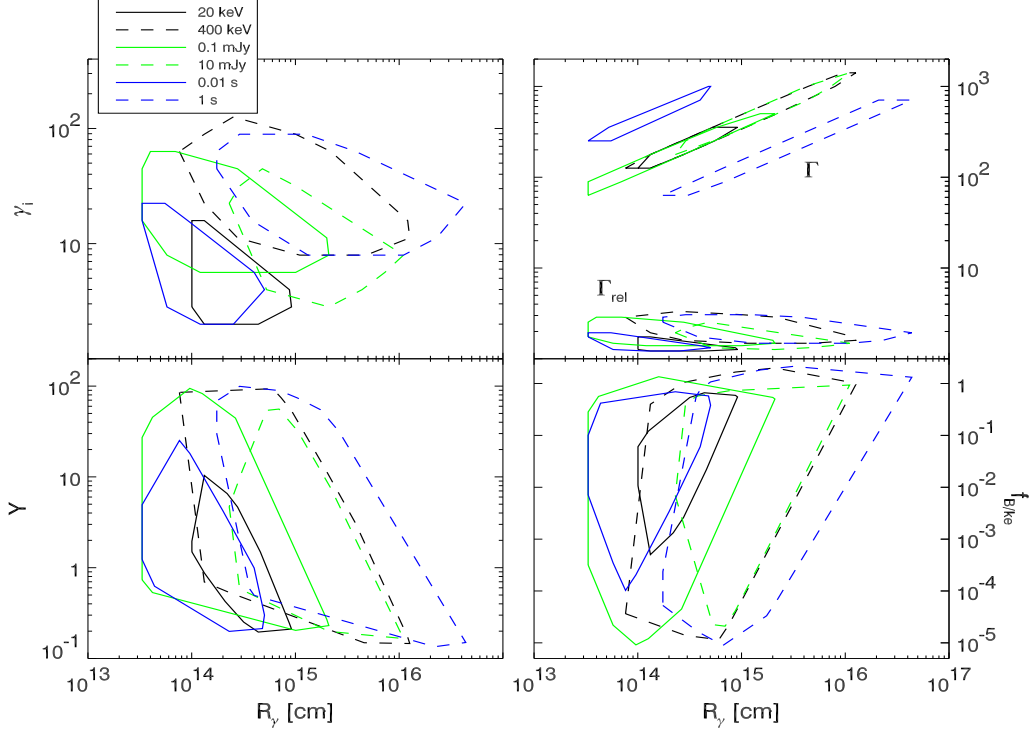


Fig. 11.— Synchrotron-Self-Compton solutions when the spectral index, α , below ν_γ (the peak of νf_ν^{ic}) is less than 0. There are two branches of the solutions both of which are shown in the figure. For one of these branches $\nu_c < \nu_i$, and for the other $\nu_c > \nu_i$; γ -ray sources corresponding to the $\nu_c < \nu_i$ branch lie at a smaller distance from the center of explosion (R_γ) than the other branch. Allowed regions for the 5-D parameter space is shown for a number of different sets of GRB observable parameters (see figure 2 caption for details). The top right panel shows the LF of the γ -ray source (one of the five basic parameters we use to describe the source) as well as the Γ_{rel} – the relative LF of collision of two shells obtained by mapping the 5-D parameter solution to internal shocks (see appendix A).

In figure 11, we show the numerical solutions for the allowed region in the 5-D space for the SSC-model for a wider range of observables. Note that results for both $\nu_i > \nu_c$ & $\nu_i < \nu_c$ (to be considered analytically in the next subsection) are plotted together in fig. 11. The allowed range for electron LF γ_i is 3–200 (fig. 11) which is characteristic of mildly relativistic shocks. If we cast the 5-D parameter solutions in terms of colliding shells as described in appendix A, we find the relative LF of collision between shells to be less than a few. For $\Gamma \sim 100$ & $\Gamma_{rel} \sim$ a few, there is little chance of an external forward-shock origin for these SSC photons. However, the 5-D solutions we find appear to be consistent with an internal shock; R_γ is smaller than the deceleration radius and $f_{B/ke} \lesssim 1$ for the entire SSC solution space.

The dependence of the solution space on ν_γ , f_γ , and t_γ is in agreement with analytical estimates; for example, we have verified the analytical dependence, $\gamma_i \propto \nu_\gamma^{\frac{1}{4}} f_\gamma^{-\frac{1}{36}} t_\gamma^{\frac{1}{6}}$ (for $t_a = t_\gamma$), given in equation (101), and $\Gamma \propto \nu_\gamma^{\frac{1}{4}} f_\gamma^{\frac{7}{36}} t_\gamma^{-\frac{1}{6}}$ (eq. 103). We find that SSC can produce a wide variety of GRBs with the low energy spectral index $\alpha \sim -1/2$ without requiring extreme parameter values.

In order for these solutions to remain viable, the prompt optical and x-ray flux needs to be in accord with observations and/or upper limits. We next look at the prompt x-ray and optical emission from these solutions.

4.2.1a. Prompt x-ray emission for SSC solutions with $\alpha \leq -1/2$

In the top two panels of Figure 12, we’ve plotted the synchrotron and SSC contributions to the x-ray (1 keV) flux accompanying the γ -ray emission during the burst. In the top left panel, we see that the 1 keV flux ranges from 0.1 to over 100 mJy for *GRB-130427A* and much of it is due to the underlying synchrotron emission.

There are at least a few solutions for each value of ν_γ , f_γ & t_γ we have considered with x-ray flux less than 10 mJy (fig. 12) with the exception of the $f_\gamma \sim 10$ mJy case. The high end of this range of x-ray flux is above the value typically observed by *Swift* at 100 seconds following the burst (10^{-4} to a few mJy); but we know from early x-ray observations that this flux is initially falling off very steeply, $\sim t^{-3}$, and therefore x-ray flux of $\sim 10^3$ mJy during the burst, $t_\gamma \lesssim 10$ s, would be less than 1 mJy at 100s, or within the observed flux range of the x-ray telescope aboard *Swift*.

We expect the x-ray flux to be

$$f_x = f_{\nu_p} \left(\frac{1\text{keV}}{\nu_i} \right)^{-\frac{p}{2}} \left(\frac{\nu_i}{\nu_c} \right)^{-\frac{1}{2}}, \quad (105)$$

(since synchrotron dominates). In terms of the observable quantities the flux is

$$f_x \approx \frac{9 \times 10^3}{17^p} \nu_{\gamma 5}^{\frac{p+2}{4}} f_\gamma^{\frac{34+p}{36}} t_\gamma^{\frac{2-p}{18}} t_a^{\frac{2-p}{9}} Y^{-\frac{16+p}{18}} (1+Y)^{\frac{2-p}{9}} d_{L28}^{\frac{p-2}{18}} (1+z)^{\frac{2-p}{9}} A_{2p}^{\frac{16+p}{18}} \eta_a^{\frac{(p-2)(p+18)}{36}} \eta_i^{\frac{p-2}{9}} \text{ mJy}, \quad (106)$$

so for $p = 2.5$ and $t_a \sim t_\gamma$, $f_x \propto \nu_\gamma^{\frac{9}{8}} f_\gamma^{\frac{73}{72}} t_\gamma^{-\frac{1}{12}}$. This analytical formula is in good agreement with numerical solutions shown in fig. 12.

The upper limit to the synchrotron flux can be understood from the limit we place on the synchrotron 10 keV flux. We restrict synchrotron flux at 10 keV to be less than the 10 keV SSC flux, in order that the GRB spectrum is SSC dominated. The 1 keV synchrotron flux is then $< f_\gamma (10\text{keV}/\nu_\gamma)^{(p-1)/2} \sim 55$ mJy for *GRB-130427A*, in agreement with Figure 12.

4.2.1b. Prompt optical emission for SSC solutions with $\alpha \leq -1/2$

In the bottom two panels of Figure 12, we plot the optical emission accompanying the γ -ray radiation for the SSC solutions. In the optical (2 eV), we look only at the synchrotron emission,

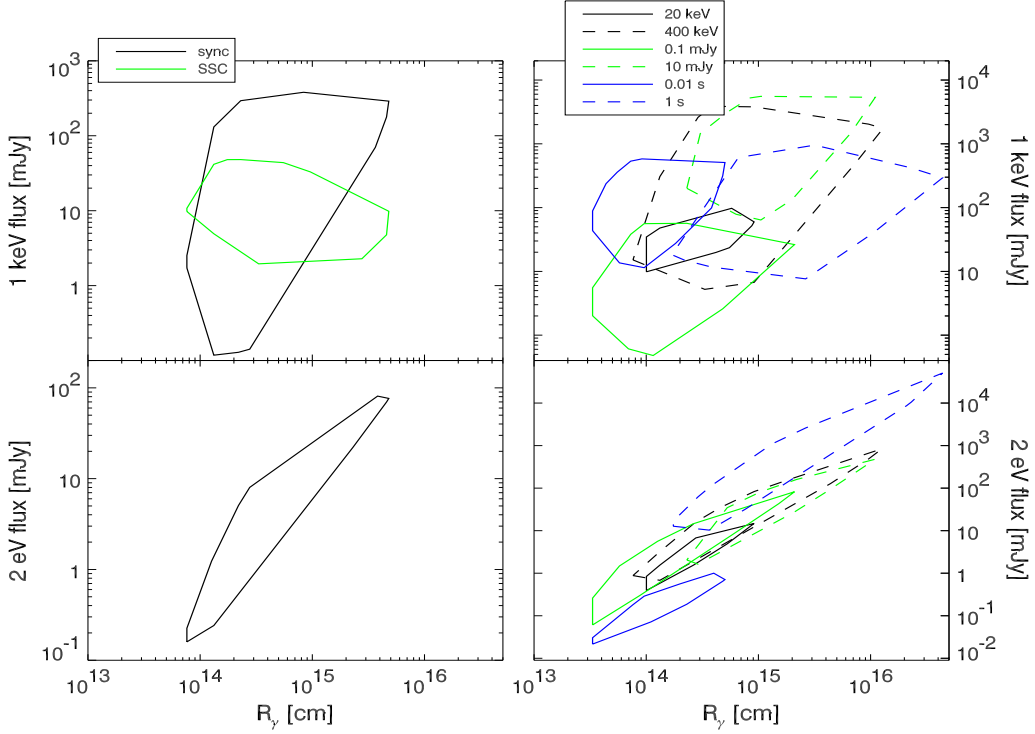


Fig. 12.— X-ray (1 keV) and optical flux simultaneous with the GRB emission for the SSC solutions with $\alpha < 0$ are plotted against the γ -ray emission radius. The top left panel shows the synchrotron & SSC contributions to the 1 keV flux for *GRB-120308A*, and the bottom left panel shows the optical (2 eV) flux associated with *GRB-120308A*-SSC solutions. The right panels show the 1 keV flux (top right) and 2 eV flux (bottom right) by summing up contributions of synchrotron and SSC for various sets of observed parameters for GRBs as described in the caption for fig. 2.

since the SSC flux is highly suppressed as $\nu_a^{ic} \gg 2\text{eV}$. The optical flux is between 0.2 and 100 mJy, or between $R \sim 18$ and 11 mags for *GRB-120308A* (fig. 12). For the range of ν_γ , f_γ , and t_γ we have considered, we find the optical flux to be between 0.02 mJy and 50 Jy, or $R \sim 20$ to 4 mags (bottom right panel of fig. 12). Observational limits on R band flux, 100s after the burst, are $\gtrsim 18.5$ mag, or $\lesssim 0.2$ mJy, for approximately half of Swift bursts (Roming et al. 2006). For small values of ν_γ , f_γ , and t_γ there is no problem satisfying this upper limit, but large ν_γ , f_γ , or t_γ might exceed the observed optical flux limit. Since the prompt optical flux falls off very rapidly with time as $t^{-(4+p)/2}$, for $t > t_\gamma$, SSC solutions with hundreds of mJy optical flux during the burst are consistent with the upper limit of $\sim 18\text{mag}$ at 100s. The solutions with optical flux greater than 100 mJy or so, however, can be ruled out, since prompt optical flux this bright is very rare.

Analytically, the R-band flux, dominated by synchrotron photons, is

$$f_R \approx \left(\frac{2\text{eV}}{\nu_a}\right)^{\frac{5}{2}} \left(\frac{\nu_a}{\nu_i}\right)^{-\frac{p}{2}} \left(\frac{\nu_i}{\nu_c}\right)^{-\frac{1}{2}} f_{\nu_p}, \quad (107)$$

provided that $\nu_a > 2\text{eV}$, and $\nu_c < \nu_i < \nu_a$. In terms of the observed quantities the flux is given by

$$f_R \sim 2 \times 10^3 \nu_{\gamma 5}^{-\frac{3}{4}} f_{\gamma}^{\frac{29}{36}} t_{\gamma}^{\frac{7}{18}} t_a^{\frac{7}{9}} Y^{-\frac{11}{18}} (1+Y)^{\frac{7}{9}} d_{L28}^{-\frac{7}{18}} (1+z)^{\frac{7}{9}} A_{2p}^{\frac{11}{18}} \eta_a^{-\frac{7(p+18)}{36}} \eta_i^{-\frac{7}{9}} \text{ mJy}. \quad (108)$$

If we assume that $t_a \sim t_{\gamma}$, we find $f_R \propto \nu_{\gamma}^{-\frac{3}{4}} f_{\gamma}^{\frac{29}{36}} t_{\gamma}^{\frac{7}{6}}$. This agrees with what we find numerically for f_{γ} and t_{γ} , but not ν_{γ} . Numerically, f_R increases with ν_{γ} , while this expression shows a decrease. This difference is caused by the sensitivity of $f_R \sim \eta_a^{-4}$ – numerically we find that $\eta_a \propto \nu_{\gamma}^{-1/2}$, changing the above dependence on ν_{γ} to be $f_R \sim \nu_{\gamma}^{\frac{5}{4}}$, in accord with results shown in Figure 12.

For *GRB-1*, $f_R \lesssim 120 Y^{-\frac{11}{18}} (1+Y)^{\frac{7}{9}} \text{ mJy}$. This estimation for f_R is larger by a factor ~ 10 than what we find numerically (see fig. 12). This factor of 10 difference is due to the fact that $\gamma_c \sim 1$ for many of these solutions. When $\gamma_c < 2$, we have a population of electrons that don't radiate synchrotron emission and we need to reduce the number of radiating particles. This is done by using $\nu_c \propto (\gamma_c - 1)^2$. Since $f_R \propto \nu_c^{\frac{1}{2}}$, the correct value of f_R , is a factor of $\gamma_c/(\gamma_c - 1)$ smaller than the crude analytical estimate above. The smallest value of γ_c that we find numerically is 1.08, and therefore the analytical expression for f_R overestimates the true flux, calculated numerically, by a factor of about ~ 14 . This indeed reconciles the analytical and numerical results.

The R-band flux increases with increasing t_{γ} . This is because increasing the pulse duration increases the radius at which the GRB emission is produced, and the synchrotron self absorption frequency is smaller at larger radii, and therefore brighter optical flux is observed. Thus, a prediction of the SSC model is that brighter optical flux accompanies wider GRB pulses — very spiky light curves (with short variability time scale) will have small optical flux that can escape detection, but those with wide pulses should have bright early optical afterglows. If a pulse duration were to be 10 s, we should expect prompt optical flux of 100 mJy or larger (R-band magnitude smaller than 11th). If this optical emission is not detected, it will point to one of the assumptions in our model for the SSC-emission being violated – most likely $t_a \not\sim t_{\gamma}$, i.e. electrons are not accelerated just once, but multiple times, during the course of a pulse duration of t_{γ} .

4.2.2. $\nu_i < \nu_c$ case

Analytically this case is very similar to the case of $\nu_c < \nu_i$ discussed in §4.2.1. We require this time that $\gamma_i/\gamma_c = \eta_i < 1$ and η_a is still > 1 . Since the ratio $\gamma_a/\gamma_c = \eta_a \eta_i$, we will see that some of the solutions can be expressed in terms of $\eta_a \eta_i$ instead of using η_i and η_a separately.

The equations that we are solving for, in this case are

$$B^2 \Gamma \gamma_i \sim 7.7 \times 10^8 \eta_i (1+z) t_a^{-1} (1+Y)^{-1} \quad (109)$$

$$B \gamma_i^4 \Gamma \sim 2.3 \times 10^{12} \nu_{\gamma 5} (1+z) \eta_a^{-2} \eta_i^2 \quad (110)$$

$$B \Gamma^5 \tau^2 \sim 1.6 \times 10^6 f_{\gamma} t_{\gamma}^{-2} (1+z) d_{L28}^2 \eta_a^p \eta_i^{2-p} \quad (111)$$

$$\tau\gamma_i^2 \sim 0.75Y \left(\frac{p-1}{(p-2)(3-p)} \right)^{-1} \eta_i^{3-p}. \quad (112)$$

These equations are almost identical to the SSC $\nu^{\frac{1}{3}}$ case of §4.1.1, with exception of the dependence on the variables η_i and η_a and a slight change in the Y expression with an additional factor of $(3-p)$. These equations are solved same way as outlined in §4.1.1. We find that the solutions have the same dependence on ν_γ , f_γ & t_γ as in equations 101–104. And the dependence on η_i and η_a are: $\gamma_i \propto \eta_a^{-\frac{(p+18)}{36}} \eta_i^{\frac{18-p}{36}}$, $B \propto (\eta_i\eta_a)^{\frac{6-p}{12}}$, $\Gamma \propto (\eta_i\eta_a)^{\frac{7p-18}{36}}$, and $\tau \propto \eta_i^{\frac{36-17p}{18}} \eta_a^{\frac{p+18}{18}}$. The distance of γ -ray source $R_\gamma \propto \Gamma^2 \propto (\eta_i\eta_a)^{\frac{7p-18}{18}}$. We constrain η_i by requiring $\nu_a^{ic} \sim 4\nu_a\gamma_i^2 \sim \nu_\gamma\eta_i^2 \lesssim 10$ keV, which suggests that $\eta_i \lesssim 0.3$, in accord with the numerical calculation.

Numerically, we find $\gamma_i \lesssim 20$, $B \lesssim 2 \times 10^3$ Gauss, $\Gamma \lesssim 10^3$, and $\tau \gtrsim 10^{-3}$ for *GRB-1* (fig. 11). The γ -ray source radius $R_\gamma \lesssim 2 \times 10^{15} Y^{-\frac{7}{9}} (1+Y)^{\frac{4}{9}}$ cm is in good agreement with $R_\gamma \lesssim 5 \times 10^{15}$ cm obtained by numerical calculations. Note that R_γ for this case is a factor of a few higher than the $\nu_c < \nu_i$ case discussed in §4.2.1.

The numerical results for the allowed region of 5-D space, for $\nu_c > \nu_i$, are also shown in Figure 11. The solutions corresponding to $\nu_i > \nu_c$ are those at larger radius – the right hand side of each solution contour, or bubble, shown in the figure. These solutions have smaller γ_i , larger Γ , smaller B & τ , and a little bit smaller Y . Since these solutions too seem viable for shock models, we explore below the x-ray and optical flux accompanying γ -ray emission.

4.2.2a. Prompt X-ray and optical flux

The analytical expression for the x-ray flux is almost identical to that found for the $\nu_c < \nu_i$ case (eq. 106) – the only difference is in the dependence on η_a and η_i . We find that –

$$f_x \propto (\eta_i\eta_a)^{\frac{(p-2)(p+18)}{36}}, \quad (113)$$

and the lower limit on the x-ray flux is $\sim 50Y^{-\frac{37}{36}}(1+Y)^{-\frac{1}{18}}$ mJy; this is in agreement with numerical results shown in fig. (12).

The R-band flux, dominated by synchrotron emission, is

$$f_R \sim \left(\frac{2\text{eV}}{\nu_a} \right)^2 \left(\frac{\nu_a}{\nu_c} \right)^{-\frac{p}{2}} \left(\frac{\nu_c}{\nu_i} \right)^{-\frac{p-1}{2}} f_{\nu_p} \quad (114)$$

which is, in terms of the observed quantities, given by

$$f_R \sim 3 \times 10^3 \nu_{\gamma 5}^{-\frac{1}{2}} f_\gamma^{-\frac{5}{6}} t_\gamma^{\frac{1}{3}} t_a^{\frac{2}{3}} Y^{-\frac{2}{3}} (1+Y)^{\frac{2}{3}} d_{28}^{-\frac{1}{3}} (1+z)^{\frac{2}{3}} A_{1p}^{\frac{2}{3}} (\eta_a\eta_i)^{-\frac{p+18}{6}} \text{ mJy} \quad (115)$$

with the value of $f_R \lesssim 1700$ mJy for *GRB-1*. This is higher than the numerical results that give $f_R \lesssim 200$ due to the sensitivity of f_R on $\eta_a\eta_i \gtrsim 2$. If we assume that $t_a \sim t_\gamma$, as has been done numerically, we find $f_R \propto \nu_\gamma^{-\frac{1}{2}} f_\gamma^{\frac{5}{6}} t_\gamma$. Numerically we find that f_R increases with ν_γ , f_γ , and t_γ ,

and is most sensitive to t_γ . The increase of f_R with ν_γ is again due to the high sensitivity on $\eta_a\eta_i$ which numerically we find is $\propto \nu_\gamma^{-1/2}$.

We note that the optical flux for this case ($\nu_i < \nu_c$) is larger than when $\nu_c < \nu_i - 10^2 - 10^3 \text{ mJy}$ – since R_γ is larger for these solutions. For $t_a/t_\gamma = 10^{-2}$ f_R is reduced by a factor of ~ 50 . This brings the highest flux for the $t_\gamma \sim 1 \text{ s}$ solutions down to about 140 mJy – still a bit bright, but there are many other solutions for this case that have flux smaller than about 10 mJy, and probably in accord with observations and upper limits. Thus, bright optical flux is a generic prediction of the SSC model for γ -ray generation whether the low energy spectral index is positive or negative; the optical is particularly bright for $\alpha > 0$. This is a problem for the SSC model if $R_\gamma \sim 10^{16} \text{ cm}$, as found in Kumar et al. (2007), as the brightest optical flux is produced at the larger R_γ . One of the, possibly only, ways to avoid bright, prompt, optical emission is if $t_a \ll t_\gamma$.

5. GeV photon signal for synchrotron and SSC solutions

Detection of GeV photons by the Gamma Ray Large Area Space Telescope (GLAST) (McEnery & GLAST Mission 2006) will be a useful piece of evidence to use to determine if GRBs are produced by synchrotron or SSC emission mechanisms. The IC scattering of γ -ray photons produced by synchrotron will peak above the GLAST band, $\gg 100 \text{ GeV}$, while the second IC scattered SSC photons will peak at $\sim 1 \text{ GeV}$.

For the synchrotron cases $\alpha = 1/3$ and $-(p-1)/2$, $\max(\gamma_i, \gamma_c) \sim 10^4$ and $\tau \lesssim 10^{-6}$, giving the peak of IC scattered flux νf_ν at $\nu_G \sim \min[\nu_\gamma \max(\gamma_i, \gamma_c)^2, \max(\gamma_i, \gamma_c) \Gamma m_e c^2 / (1+z)] \sim 10^4 \text{ GeV}$ and flux $\nu f_\nu \sim \tau f_\gamma \nu_G \sim 10^{-7} \text{ erg s}^{-1} \text{ cm}^{-2}$. We need to ensure that such high energy photons can escape the source region and are not converted to electron-positron pairs. This effect is incorporated in our numerical calculations and is discussed below. Moreover, photons of energy larger than $\sim 1 \text{ TeV}$ are converted to e^\pm by collision with infrared photons and therefore we would not see $\gtrsim 1 \text{ TeV}$ photons from GRBs at cosmological distances.

The SSC $\alpha > 0$ solutions have $\gamma_i \sim \gamma_c \lesssim 10^2$ and $\tau \gtrsim 10^{-4}$ giving the second scattering peak of $\nu_G \sim 4\nu_\gamma \gamma_i^2 \sim 1 \text{ GeV}$ and the flux $\nu f_\nu \sim 10^{-7} \text{ erg s}^{-1} \text{ cm}^{-2}$. The SSC $\alpha < 0$ solutions have very similar ν_G and νf_ν . The SSC signals are well above the GLAST threshold so we expect to see a GeV signal from GRBs produced by the SSC process. For synchrotron solutions, however, the IC flux might be below the GLAST threshold. The spectral shape will also be different – ν_G is well above the GLAST band for the synchrotron case, while SSC should peak at the low end of the GLAST band.

Using analytical results for the synchrotron $\alpha = 1/3$ case (Equations 45–48), we find that the IC scattered signal peaks at

$$\nu_G^s \sim \gamma_i \Gamma m_e c^2 / (1+z) \sim 2 \times 10^4 \nu_{\gamma 5}^{\frac{1}{4}} f_{\gamma 5}^{\frac{1}{8}} t_\gamma^{-\frac{1}{4}} t_a^{\frac{1}{2}} Y^{-\frac{1}{8}} (1+Y)^{\frac{1}{2}} d_{L28}^{\frac{1}{4}} (1+z)^{-\frac{1}{2}} \left[\frac{p}{p-2} \right]^{\frac{1}{8}} \text{ GeV}; \quad (116)$$

This is due to the Klein-Nishina reduction to cross-section above electron rest frame photon energy of $m_e c^2$.

The frequency above which the high energy spectrum is attenuated due to $\gamma\gamma \rightarrow e^-e^+$ within the GRB source is $\nu_{\pm} \sim (\Gamma m_e c^2)^2 / \nu_{\tau \sim 1}$, where $\nu_{\tau \sim 1}$ is the frequency of the synchrotron photon at which the optical depth to pair production with ν_{\pm} photons is 1. The optical depth to pair production is $\tau_{\gamma\gamma} \sim \sigma_T n'_{\nu'} R_{\gamma} / \Gamma$, where $n'_{\nu'} \sim L_{iso}(\nu) / 4\pi \Gamma c R_{\gamma}^2$ is the comoving number density of photons between ν' and $2\nu'$, R_{γ} / Γ is the comoving shell width, and $L_{iso}(\nu)$ is the observed isotropic luminosity per unit frequency. To find $\nu_{\tau \sim 1}$, we set $\tau_{\gamma\gamma} \sim 1$ and solve the equation using the observed γ -ray spectrum; ν_{\pm} is calculated from Γ & $\nu_{\tau \sim 1}$. In terms of the observable parameters for the synchrotron $\alpha = 1/3$ case, we find

$$\nu_{\pm} \sim 4 \times 10^3 \nu_{\gamma 5}^{\frac{1}{4}} f_{\gamma}^{\frac{1}{4}} t_{\gamma}^{-1} t_a Y^{-\frac{3}{4}} (1+Y) d_{L28}^{\frac{1}{2}} (1+z)^{\frac{1}{2}} \left[\frac{p}{p-2} \right]^{\frac{3}{4}} \text{ GeV} \quad (117)$$

where we have assumed that the synchrotron GRB spectrum is $L_{iso}(\nu) \propto \nu^{-2}$ for $\nu > \nu_{\gamma}$. Since $\nu_{\pm} < \nu_G^s$ (calculated above), and the spectrum falls off very steeply above ν_{\pm} , the IC spectrum will peak at ν_{\pm} for many of the synchrotron solutions.

The flux at ν_G^s , with appropriate Klein-Nishina cross section, is

$$[\nu f_{\nu}]^s \sim 8 \times 10^{-10} \nu_{\gamma 5}^{-\frac{3}{2}} f_{\gamma}^{\frac{3}{2}} t_{\gamma}^{-1} Y^{\frac{1}{2}} d_{L28} (1+z)^{-2} \left[\frac{p}{p-2} \right]^{-\frac{1}{2}} \text{ erg s}^{-1} \text{ cm}^{-2}. \quad (118)$$

This flux is probably just at the GLAST threshold for detection. If $\nu_{\pm} < \nu_G^s$, the νf_{ν} spectrum peaks at ν_{\pm} , and the flux at this frequency will be smaller than that in equation (118); the attenuation of $\gtrsim \text{TeV}$ photons as they propagate through the inter-galactic medium would further reduce the observed flux. The results are very similar for the $\alpha = -(p-1)/2$ case, since the $\alpha = 1/3$ case is a subset of the $\alpha = -(p-1)/2$ solutions with $\gamma_i \sim \gamma_c$.

For the SSC case, using the $\alpha > 0$ analytical results in Equations 90 – 93, the 2^{nd} IC peak is

$$\nu_G^{ic} \sim 3 \nu_{\gamma 5}^{\frac{3}{2}} f_{\gamma}^{-\frac{1}{18}} t_{\gamma}^{\frac{1}{9}} t_a^{\frac{2}{9}} Y^{\frac{1}{9}} (1+Y)^{\frac{2}{9}} d_{L28}^{-\frac{1}{9}} (1+z)^{\frac{2}{9}} A_{2p}^{-\frac{1}{9}} \eta_a^{-\frac{p+18}{18}} \text{ GeV} \quad (119)$$

and the flux at this peak is

$$[\nu f_{\nu}]^{ic} \sim 7 \times 10^{-7} \nu_{\gamma 5} f_{\gamma} Y A_{2p}^{-1} \text{ erg s}^{-1} \text{ cm}^{-2}. \quad (120)$$

ν_G is smaller than ν_{\pm} for the majority of the SSC solution space, so the 2nd inverse Compton scattering spectrum will indeed peak at ν_G . For the SSC $\alpha < 0$ case, the expressions are very similar – the only difference is the dependence on η_a , η_i , and p :

$$\nu_G^{ic} \sim 3 \nu_{\gamma 5}^{\frac{3}{2}} f_{\gamma}^{-\frac{1}{18}} t_{\gamma}^{\frac{1}{9}} t_a^{\frac{2}{9}} Y^{\frac{1}{9}} (1+Y)^{\frac{2}{9}} d_{L28}^{-\frac{1}{9}} (1+z)^{\frac{2}{9}} A_{1p}^{-\frac{1}{9}} \eta_a^{-\frac{p+18}{18}} \eta_i^{\frac{18-p}{18}} \text{ GeV} \quad (121)$$

and the flux at this peak is

$$[\nu f_{\nu}]^{ic} \sim 7 \times 10^{-7} \nu_{\gamma 5} f_{\gamma} Y \eta_i^{3-p} A_{1p}^{-1} \text{ erg s}^{-1} \text{ cm}^{-2}. \quad (122)$$

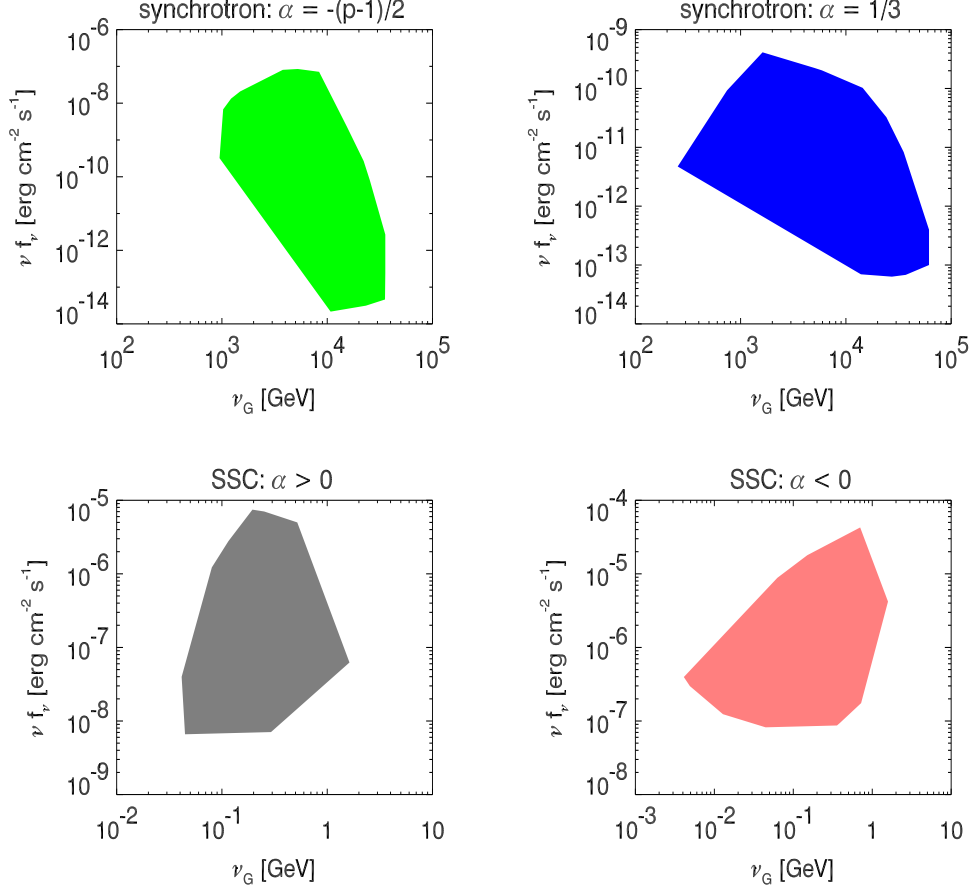


Fig. 13.— Numerical results for the IC scattering of prompt γ -ray photons in the source. The four panels show the peak of IC spectrum (ν_G) and the flux (νf_ν) at the peak when the γ -ray emission is produced via the synchrotron process (top two panels) and via the SSC process (bottom two panels) for $\alpha > 0$ & $\alpha < 0$ cases; for all of these cases we took the underlying γ -ray spectrum with $\nu_\gamma = 100\text{keV}$ & $f_\gamma = 0.1\text{mJy}$. The IC signal for many of the synchrotron solutions are affected by photon-photon pair production within the GRB source, and that is included in these numerical calculations; however the conversion of $\gtrsim 1\text{TeV}$ photons to e^\pm due to collision with infrared photons in the inter-galactic medium is not shown in the figure (no photon above 1 TeV can reach us from a GRB source at cosmological distances). The effect of pair production is very small in the SSC cases. The Klein-Nishina cross-section has been used in these calculations, and it significantly affects the IC peak flux when γ -rays are generated via the synchrotron process.

We show numerical results for ν_G and νf_ν for 4 cases in Figure 13 – the two synchrotron cases of $\alpha = -(p-1)/2$ and $1/3$ and the SSC cases of $\alpha < 0$ and > 0 . These numerical results are in rough agreement with our analytical estimates.

In summary, IC scattering of prompt γ -ray photons, when the GRB emission is produced via

the synchrotron process, gives rise to a spectrum that peaks at $\sim \text{TeV}$, the flux is of order $10^{-9} \text{ erg cm}^{-2} \text{ s}^{-1}$ (fig. 13), the spectrum below the peak is between $\nu^{1/3}$ or $\nu^{-(p-1)/2}$, and the spectrum above the peak is expected to be sharply cutoff due to pair production. On the other hand, if the GRB emission is produced via the SSC process then the spectrum of 2^{nd} IC scattered photons should peak at $\sim 1 \text{ GeV}$, with a flux of $\sim 10^{-6} \text{ erg cm}^{-2} \text{ s}^{-1}$ (fig. 13), and the spectrum above the peak should be $f_\nu \propto \nu^{-1.5}$. This signal should be detected by GLAST. If GRBs are not detected in the GLAST band, that would suggest that GRB prompt emission is not generated via the SSC process. We note that the GLAST band flux cannot be reduced in the case of repeated acceleration of electrons during a single GRB pulse.

6. Comparison with prior work on γ -ray generation mechanism

We provide a brief comparison with published work on γ -ray generation in the internal shock model (Rees & Meszaros 1994; Paczynski & Xu 1994; Papathanassiou & Meszaros 1996; Meszaros & Rees 1997; Sari & Piran 1997b) and the formalism/results of this paper. There is a fairly extensive literature on this topic and this is not the place to provide a general review. What we wish to do is to describe the main difference between previous approaches and the work presented here.

We should note that γ -ray generation in the external shock model has also been looked at by a number of people eg. Rees & Meszaros (1992), Meszaros & Rees (1993), Piran et al. (1993), Dermer et al. (1999), Dermer & Mitman (1999), McMahon et al. (2004), Ramirez-Ruiz & Granot (2006); the issue of variability in external shocks is discussed in Sari & Piran (1997a), Dermer & Mitman (1999), Nakar & Granot (2006). We don't have anything particularly enlightening to say regarding the external shock model that has not already been mentioned by one of these authors; the general problem with shocks is discussed in §3 & §4.

The main difference between previous works and our approach is that previous works considered the forward problem i.e., starting with a parameterization of the properties of colliding shells and resulting shocks the emergent radiation field was calculated, whereas our approach is to start with the minimum number of physical parameters needed (five) to calculate the observed flux and spectrum – at one instant in time or for one pulse in a multi-pulse GRB lightcurve – and determine these using the observed data. For synchrotron & IC radiations the parameters needed are γ_i, Γ, B, N , and τ , which are determined by the observational data $\nu_\gamma, f_\gamma, t_\gamma$, and α for a pulse in GRB LC. The 5 parameters in turn are used to provide constraint on the nature of GRB source. The *old forward approach* is wedded to a particular model – either internal or external shock – whereas the method used in this work is relatively model independent.

The parameters of the internal shock model can be mapped into the five parameters ($\gamma_i, \Gamma, B, N, \tau$) in a straightforward manner – this in fact is done implicitly in all the *forward approach* papers in order to calculate the emergent radiation. The converse of this is not true, however, since the internal shock model has more than 5 independent parameters (appendix A describes how to

go from the five parameters to providing a limit on some of the internal shock parameters such as the initial LFs of colliding shells and their comoving densities).

Papathanassiou & Meszaros (1996) and Sari & Piran (1997b) carried out a fairly detailed analysis of prompt emission in the internal shock model. These authors addressed a set of questions such as the ability of synchrotron/SSC in internal shocks to produce a spectral peak near 100 keV, the observed flux in the γ -ray band, and short time scale variability. Papathanassiou & Meszaros (1996) and Sari & Piran (1997b) realized that the cooling time scale for electrons (compared to the dynamical time) for internal shocks is short and although Sari & Piran (1997b) don’t explicitly say, their work applies to GRBs with $\alpha = -1/2$. Papathanassiou & Meszaros (1996) look at composite synchrotron/SSC spectra, however there are many free parameters and little comparison to observed properties of GRBs. Had these authors investigated the self-consistency of synchrotron internal-shock model for the case of $\alpha = 1/3$, they would have discovered the problem reported in this paper using their *forward modeling* approach.

Ghisellini et al. (2000) did in fact worry about synchrotron solutions when $\alpha > 0$ and concluded that it is impossible to account for it in shock based models (this is paraphrasing their actual wordings). They pointed out that electron cooling time, during prompt emission, is much smaller than the dynamical time [as was reported in Papathanassiou & Meszaros (1996) and Sari & Piran (1997b)] and therefore the GRB spectrum below the peak should be always $\nu^{-1/2}$ if the radiation is produced via synchrotron process. Ghisellini et al. (2000) considered the possibility that a lower strength magnetic field would avoid the excessive cooling of electrons, and rejected it based on the argument that IC emission would dominate in this case i.e., $Y \gg 1$, and that IC spectrum too would be falling off as $\nu^{-1/2}$ or steeper due to IC cooling. We find that a smaller magnetic field can avoid excessive cooling, so that $\alpha = 1/3$, and at the same time Compton $Y \sim 1$. The reason for these different conclusions is that we don’t impose any restriction on the source distance that *forward calculations* based on internal shocks do. The most serious problem with synchrotron $\alpha = 1/3$ case is that $R_\gamma > R_d$ unless $n_0 \ll 1 \text{ cm}^{-3}$ (see §3.2).

Ghisellini et al. (2000) correctly pointed out that re-acceleration of electrons, in shock based models, would not work because it requires too much energy; one has a continuous stream of electrons crossing the shock front – and to accelerate all of these electrons to their original energy distribution, so that $\alpha = 1/3$, while they are rapidly losing energy to radiation will indeed require much more energy than is available in the shock. The re-acceleration invoked in this work is not shock based. It in fact requires abandoning shock models and considering a scenario where particles are NOT being added to the “system” – the source for γ -ray photons – continuously (as in shock based models) but where the source has a fixed number of particles that are being continuously accelerated; there is no excessive energy problem in this scenario.

7. Discussion

In this paper we have investigated the generation of γ -rays in gamma-ray bursts via synchrotron or synchrotron-self-inverse-Compton (SSC) emissions in a relativistic outflow. The SSC radiation from a relativistic source can be fully described by a set of 5 parameters (γ_i , Γ , B , N , τ); see table 1 for definition of symbols used in the paper. For each possible low energy spectral index, we have analytically and numerically determined the region of the 5-D parameter space that is consistent with a set of GRB observations – ν_γ , f_γ , & t_γ . For these allowed regions – or *solution* sub-space – we calculate the x-ray and optical fluxes that should be seen concurrent with the γ -ray radiation to further narrow down the properties of γ -ray sources. The set of five parameters also allows us to determine the distance of the source from the center of explosion (R_γ).

We find that if γ -ray emission were to be produced via the synchrotron process, the required set of parameters and burst radius have extreme values that are not internally consistent and are in conflict with afterglow data. In particular, when the low energy spectrum is $f_\nu \propto \nu^{1/3}$ or $\nu^{-\frac{p-1}{2}}$, the Lorentz factor of the source is required to be larger than $\sim 10^3$, in disagreement with afterglow modeling, and the source distance (R_γ) is larger than the deceleration radius even when the density of the medium is as small as $\sim 0.1 \text{ cm}^{-3}$. The requirement on the magnetic field strength is also very stringent; the comoving field strength is required to lie in a very narrow range of about $\sim 10\text{--}30$ Gauss in order to explain the radiation for a typical burst as synchrotron emission. Allowing for the possibility of multiple electron acceleration episodes, i.e. $t_a \ll t_\gamma$, alleviates the problem of large R_γ & Γ ; in this scenario the synchrotron process could account for the prompt γ -ray radiation for GRBs (see §3.1 & 3.2) although R_γ is still larger than the source distance determined for a subset of bursts detected by Swift (Kumar et al. 2007).

The reason that synchrotron solutions with $\alpha = -(p-1)/2$ & $1/3$ require large R_γ & Γ is easy to understand. The number of electrons needed to produce the observed flux via the synchrotron process is $\sim 10^{53} f_\gamma / (B\Gamma)$. And in order to keep the Compton-Y parameter ($Y \sim \tau \gamma_i \gamma_c$) less than ~ 10 — otherwise most of the energy will come out in IC-scattered photons at $\nu \gg 1 \text{ GeV}$ — the source must have small τ or large R_γ . Moreover, since $t_\gamma \sim R_\gamma / (4c\Gamma^2)$, large R_γ solutions also have large Γ for a given GRB pulse width of t_γ . The reason that $t_a \ll t_\gamma$ offers a way out of this problem is also easy to understand. Frequent re-acceleration of charge particles makes it possible to have larger magnetic field while keeping $\nu_c \gtrsim 100 \text{ keV}$. This decreases the number of particles required to produce the observed flux (f_γ), and that in turn makes it possible to have a smaller R_γ .

For $f_\nu \propto \nu^{-1/2}$, the allowed region of the 5-D parameter space for the synchrotron process is quite reasonable. However, interpreting these solutions in terms of the internal shock model requires the ratio of LFs of the two colliding shells to be rather large ($\gtrsim 10 - 20$) when the ratio of magnetic energy to electron energy is $\lesssim 10$, i.e. if we want the energy fraction in electrons to be not too small — otherwise γ -ray production would be very inefficient (see §3.3).

The SSC process provides viable solutions for the prompt emission of a large fraction of GRBs. We have considered almost all different possibilities of the low energy spectrum for GRBs: $f_\nu^{ic} \propto \nu^\alpha$

below the peak of νf_ν^{ic} with $-1 \lesssim \alpha \leq 1$. The solution space (a hypersurface in the 5-D parameter space) is quite large for $\alpha < 0$ and $0.5 \lesssim \alpha \leq 1$. However, there are no SSC solutions when $\alpha \sim 1/3$; the reason is that the synchrotron characteristic and cooling frequencies should be equal ($\nu_i \sim \nu_c$) in order that $\alpha = 1/3$, and in that case the synchrotron-self-absorption frequency is shown to be roughly equal to ν_i as well (see §4.1.1), and therefore the low energy spectral index is ~ 1 and NOT $\sim 1/3$ as desired.

The SSC solution space for $\alpha < 0$ and $0.5 \lesssim \alpha \leq 1$ has source LF of order 100, the minimum electron energy $\lesssim 10^2 m_e c^2$ (characteristic of mildly relativistic shocks), and $10^{14} \lesssim R_\gamma \lesssim 10^{16}$ cm is smaller than the deceleration radius. These solutions are accompanied by bright optical synchrotron flux of ~ 10 mJy (14th mag) to several hundred mJy for bursts at $z \sim 2$ – brightest for bursts with $\alpha \sim 1$ and those bursts with pulse duration on the order of $\gtrsim 1$ s. Moreover, the optical flux is correlated with R_γ – the flux is larger for larger R_γ – and for $R_\gamma \gtrsim 2 \times 10^{15}$ (cf. Kumar et al. 2007), the optical flux is $\gtrsim 100$ mJy ($< 12^{\text{th}}$ mag). Bright optical flux contemporaneous with γ -rays is a prediction of the SSC model that is in conflict with prompt optical follow up observations of a large number of bursts detected by Swift (Roming et al. 2006).⁶ We note that the large optical flux accompanying γ -rays can be reduced only if each radiating electron is accelerated numerous times ($\gtrsim 100$) in time period of order the duration of a pulse in the GRB lightcurve, i.e. $t_a \lesssim t_\gamma/10^2$. GRB models based on converting kinetic energy to radiation via shocks have $t_a \sim t_\gamma$, where particles are accelerated at the shock-front and not down-stream, but continuous particle acceleration might work for some alternate scenarios such as magnetic field reconnection/dissipation. Magnetic outflow model for GRBs has been proposed/investigated by a number of people cf. Usov (1992, 1994), Thompson (1994), Katz (1997), Meszaros & Rees (1997), Wheeler et al. (2000 & 2002), Vlahakis & Konigl (2001), Spruit et al. (2001), Lyutikov & Blandford (2003), Thompson (2006). However, the model has not been developed to the extend where it can be tested with GRB observations.

The data from the upcoming high-energy mission GLAST should be able to settle the question whether GRBs are produced via synchrotron or the SSC process (see §5); see Gupta & Zhang (2007), Granot et al. 2007 (and references therein) for recent work on how GLAST would help our understanding of GRBs.

To summarize our main conclusions, we find that the synchrotron process has serious difficulty accounting for the prompt emission in GRBs. The SSC offers reasonable solutions for all GRBs except those with spectral index of $\sim 1/3$ below the peak. SSC solutions predict very bright optical emission (> 10 mJy or 14-mag for $z \sim 2$) accompanying γ -ray lightcurves which is in conflict with a number of well observed bursts. A possible solution to this problem might be to drop the assumption

⁶The simultaneous optical and γ -ray observations for a few bursts show bright optical flares. For example, GRB 041219a was observed in optical and IR simultaneously with γ -rays (Vestrand et al. 2005; Blake et al. 2005); the optical flux peaked at 13.7 magnitude at approximately the same time as the first main pulse of the GRB lightcurve (as expected for the SSC model), and IR measurements Blake et al. (2005) show evidence of rapid variability with the last spikes in the GRB light curve. GRB 990123, with a positive α , had a peak optical flux during the burst of ~ 1 Jy (Akerlof et al. 1999), however the optical lightcurve was not correlated with the γ -ray lightcurve.

that $t_a \sim t_\gamma$. The assumption of one shot acceleration of electrons i.e., $t_a \sim t_\gamma$, is motivated by shock based physics for GRBs and it may have to be replaced with an alternate scenario in which all electrons that radiate in the γ -ray band are accelerated continuously throughout the duration of a γ -ray pulse. In that scenario there are viable synchrotron solutions when $\alpha \sim 1/3$ – a case that otherwise cannot be explained by the SSC mechanism.

Acknowledgments

PK dedicates this work to Bohdan Paczynski, a mentor, a friend and an excellent scientist from whom he has learned much about GRBs. This paper is the culmination of work over a long period of time and the authors are much indebted to Tsvi Piran for many enlightening discussions during this period, and Craig Wheeler for discussions about magnetic outflows and for his encouragement. We thank Savannah Kumar and Monica Kidd for help with fig. 1, and Alin Panaitescu & Bing Zhang for useful comments on the paper. This work is supported in part by grants from NSF (AST-0406878) and NASA Swift-GI-program.

REFERENCES

- Akerlof, C., et al. 1999, *Nature*, 398, 400
- Berger, E., et al. 2005, *Nature*, 438, 988
- Blake, C. H., et al. 2005, *Nature*, 435, 181
- Briggs, M. S., et al. 1999, *ApJ*, 524, 82
- Broderick, A. 2005, *MNRAS* 361, 955
- Cummings, J., et al. 2005, *GCN* 3858
- De Pasquale, M., et al. 2006, *MNRAS*, 365, 1031
- Della Valle, M., et al. 2003, *A&A*, 406, L33
- Della Valle, M., et al. 2006, *ApJ*, 642, L103
- Dermer, C.D., Chiang, J., and Botcher, M., 1999, *ApJ*, 513, 656
- Dermer, C.D., and Mitman, K.E. 1999, *ApJ*, 513, L5
- Fox, D. B., et al. 2005, *Nature*, 437, 845
- Frail, D.A., et al. 2001, *ApJ*, 562, L55
- Galama, T. J., et al. 1998, *Nature*, 395, 670

- Gehrels, N., et al. 2005, *Nature*, 437, 851
- Ghisellini, G., Celotti, A. & Lazzati, D., *MNRAS*, 313, L1
- Golenetskii, S., et al. 2005, *GCN* 3179
- Golenetskii, S., et al. 2006, *GCN* 5722
- Gorosabel, J., et al. 2006, *A&A*, 450, 87
- Gupta, J., & Zhang, B. 2007, *arXiv:0708.2763*
- Granot, J., Cohen-Tanugi, J. and do Couto e Silva, E., 2007, *arXiv:0708.4228*
- Hjorth, J., et al. 2003, *Nature*, 423, 847
- Katz, J. I. 1997, *ApJ*, 490, 633
- Kawabata, K. S., et al. 2003, *ApJ*, 593, L19
- Kumar, P. 1999, *ApJ*, 523, L113
- Kumar, P., & Panaitescu, A. 2000, *ApJ*, 541, L51
- Kumar, P., McMahon, E., Barthelmy, S. D., Burrows, D., Gehrels, N., Goad, M., Nousek, J., & Tagliaferri, G. 2006, *MNRAS*, 367, L52
- Kumar, P., et al. 2007, *MNRAS*, 376, L57
- Landau, L.D., & Lifshitz, E.M. 1982, *Fluid Mechanics*, Pergamon Press
- Lazzati, D., Ghisellini, G., Celotti, A. & Rees, M.J. 2000, *ApJ*, 529, L17
- Lithwick, Y. & Sari, R. 2001, *ApJ*, 555, 540
- Lyutikov, M. & Blandford, R.D. 2003, *astro-ph/0312347*
- Malesani, D., et al. 2004, *ApJ*, 609, L5
- McEnergy, J., & GLAST Mission Team 2006, *Gamma-Ray Bursts in the Swift Era*, 836, 660
- McMahon, E., Kumar, P., and Panaitescu, A. 2004, *MNRAS*, 354, 915
- McMahon, E., Kumar, P., & Piran, T. 2006, *MNRAS*, 366, 575
- Medvedev, M. V. 2000, *ApJ*, 540, 704
- Meszáros, P., & Rees, M. J. 1993, *ApJ*, 405, 278
- Meszáros, P. and Rees, M. 1997, *ApJ* 482, L29

- Mészáros, P. 2002, *ARA&A*, 40, 137
- Mészáros, P., & Rees, M. J. 1997, *ApJ*, 476, 232
- Nakar, E. 2007, *ArXiv Astrophysics e-prints*, arXiv:astro-ph/0701748
- Nakar, E. and Granot, J. 2006, *ArXiv Astrophysics e-prints*, arXiv:astro-ph/0606011
- Narayan, R., Paczynski, B., & Piran, T. 1992, *ApJ*, 395, L83
- Nousek, J. A., et al. 2006, *ApJ*, 642, 389
- O’Brien, P. T., et al. 2006, *ArXiv Astrophysics e-prints*, arXiv:astro-ph/0601125
- Paczynski, B. 1991, *Acta Astronomica*, 41, 257
- Paczynski, B. 1998, *ApJ*, 494, L45
- Paczynski, B., & Xu, G. 1994, *ApJ*, 427, 708
- Panaitescu, A., & Kumar, P. 2001, *ApJ*, 560, L49
- Panaitescu, A., & Kumar, P. 2002, *ApJ*, 571, 779
- Panaitescu, A., & Kumar, P. 2004, *MNRAS*, 353, 511
- Papathanassiou, H., & Mészáros, P. 1996, *ApJ*, 471, L91
- Pian, E., et al. 2006, *Nature*, 442, 1011
- Piran, T. 1992, *ApJ*, 389, L45
- Piran, T. 1999, *Phys. Rep.*, 314, 575
- Piran, T. 2005, *Reviews of Modern Physics*, 76, 1143
- Piran, T., Shemi, A., and Narayan, R. 1993, *MNRAS*, 263, 861
- Ramirez-Ruiz, E., and Granot, J. 2006, *ArXiv Astrophysics e-prints*, arXiv:astro-ph/0608379
- Rees, M.J. & Mészáros, P. 1992, *MNRAS*, 258, 41p
- Rees, M.J. & Mészáros, P. 1994, *ApJ*, 430, L93
- Rhoads, J.E. 1999, *ApJ*, 525, 737
- Roming, P. W. A., et al. 2006, *ApJ*, 652, 1416
- Rybicki, G.B. and Lightman, A.P., 1979, *Radiative Processes in Astrophysics*, John Wiley & Sons (New York)

- Rykoff, E. S., et al. 2005, ApJ, 631, L121
- Sari, R., & Piran, T. 1995, ApJ, 455, L143
- Sari, R. & Piran, T., 1997a, ApJ, 485, 270
- Sari, R. & Piran, T., 1997b, MNRAS, 287, 110
- Sari, R. & Piran, T., 1999, ApJ, 517, L109
- Sari, R., Piran, T. & Halpern, J.P., 1999, ApJ, 519, L17
- Sari, R., Piran, T. & Narayan, R. 1998, ApJ, 497, L17
- Schady, P., et al. 2005, GCN 3039
- Spruit, H.C., Daigne, F. & Drenkhahn, G. 2001, AA 369, 694
- Stanek, K. Z., et al. 2003, ApJ, 591, L17
- Thompson, C. 1994, MNRAS, 270, 480
- Thompson, C. 2006, ApJ, 651, 333
- Usov, V. V. 1992, Nature, 357, 472
- Usov, V. V. 1994, MNRAS, 267, 1035
- Vestrand, W. T., et al. 2005, Nature, 435, 178
- Vlahakis, N. & Konigl, A. 2001, ApJ 563, L129
- Wheeler, J.C., Yi, I., Hoflich, P., and Wang, L., 2000, ApJ 537, 810
- Wheeler, J.C., Meier, D.L., and Wilson, J.R., 2002, ApJ 568, 807
- Wijers, R. A. M. J., & Galama, T. J. 1999, ApJ, 523, 177
- Woosley, S. E. 1993, ApJ, 405, 273
- Woosley, S. E., & Bloom, J. S. 2006, ARA&A, 44, 507
- Yamaoka, K., et al. 2006, GCN 5724
- Zhang, B. 2007, Chinese Journal of Astronomy and Astrophysics, 7, 1

A. Determination of the relative Lorentz factor of colliding shells

We can relate solutions $(\gamma_i, \Gamma, B, N, \tau)$ we find for a set of observables to parameters for any model for GRBs. In this appendix we relate our solutions to the parameters for the internal shock model where γ -rays are produced by collision of two shells, as shown in Figure 14. Internal shocks are produced by a collision between fast ejecta catching up with slower ejecta (Rees & Meszaros 1994; Paczynski & Xu 1994) which in the discrete version is modeled as the collision between two homogeneous shells moving with LFs Γ_1 and Γ_2 (Γ_1 is LF of the faster, inner shell). [The external shock can be thought of as a special case of internal shocks which results from collision between a stationary circum-stellar medium ($\Gamma_2 = 1$) and the ejecta from the burst.]

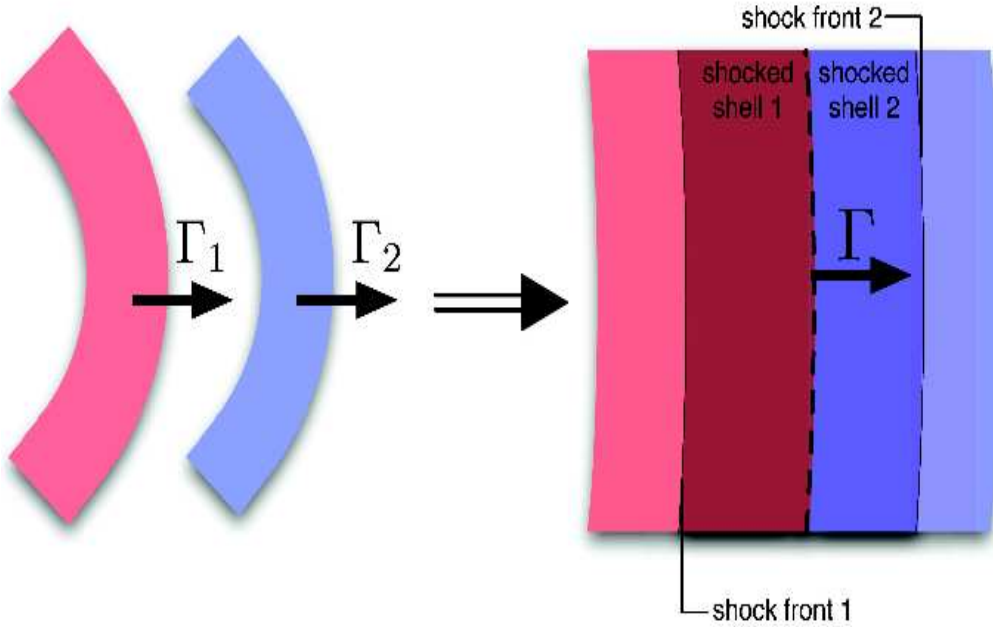


Fig. 14.— Pictorial representation of two colliding shells — internal shock model.

This appendix is devoted to describing the method we use to place a lower limit to the relative LF of the colliding shells from Γ_{sh} , the LF of the shock front in the γ -ray producing shell, which is directly related to γ_i (one of the 5 parameters) via equation (11), and by varying the ratio of densities in the inner and outer shells (n_1/n_2) subject to the condition that the efficiency for γ -ray production is not less than $\sim 10\%$; as a by product we find the comoving density ratio for the shells.

The LF of unshocked inner shell, which is moving faster and lies a bit closer to the center of

explosion than the outer shell, can be determined from the addition of LFs Γ_{sh} and Γ –

$$\Gamma_1 = \Gamma_{sh}\Gamma(1 + v_{sh}v), \quad (\text{A1})$$

provided that the γ -ray emission we observe is produced in the inner shell when it is shock heated (v & v_{sh} are speeds corresponding to LFs Γ – the LF of the γ -ray source – & Γ_{sh}). On the other hand if it is the outer shell that produces the observed γ -ray emission then its LF factor, before it was shocked, is given by

$$\Gamma_2 = \Gamma_{sh}\Gamma(1 - v_{sh}v). \quad (\text{A2})$$

The LF of the shell that does not contribute significantly to the observed γ -ray emission cannot be determined uniquely. The problem is that in the absence of any observed emission that can be identified with this shell we cannot say anything directly about the LF of the shock front moving into this shell. However, we can still constrain its LF by requiring that the comoving density of this shell is such that the efficiency for thermal energy produced in the collision is no less than $\sim 10\%$ (most GRBs for which we have good afterglow data and we can determine the kinetic energy of the ejecta show that the efficiency for converting kinetic energy to γ -rays is about 10% or more).

The efficiency of γ -ray production is used to constrain n_1/n_2 , and that in turn provides a lower limit for the relative LF Γ_{rel} . The fraction of kinetic energy converted to thermal energy when two shells of mass m_1 and m_2 collide with a relative LF of Γ_{rel} is (Kumar, 1999; Piran, 1999)

$$f_r = 1 - \left[1 + \frac{2(m_2/m_1)(\Gamma_{rel} - 1)}{[1 + m_2/m_1]^2} \right]^{-1/2} \quad (\text{A3})$$

For equal mass shells a $\Gamma_{rel} = 1.5$ collision converts 10% of the kinetic energy of shells to thermal energy, and for $\Gamma_{rel} > 5$ the conversion efficiency is more than 40%. We need, however, to figure out the fraction of energy produced in a collision that is radiated in the typical γ -ray observing band of 15–400 keV during the time interval t_γ , in two shells that are not of equal mass.

The ratio of the mass of the two shells is the mass swept up by the two shocks in the time equal to the shock transit time for the shell that produces the observed γ -ray emission. This is given by

$$\frac{m_1}{m_2} = \frac{n_1(4\Gamma_{s1} + 3)v_{ss1}}{n_2(4\Gamma_{s2} + 3)v_{ss2}}. \quad (\text{A4})$$

where n_1 and n_2 are the densities of shell 1 & 2, Γ_{s1} and Γ_{s2} are the shock LFs in the frame of each unshocked shell (if the GRB emission is predominantly from shell 1, then $\Gamma_{s1} = \Gamma_{sh}$), and v_{ss1} and v_{ss2} are the speeds of the shock fronts with respect to each unshocked shell.

The shock front speeds are determined from the following cubic equation obtained from the continuity of energy, momentum and particle number fluxes across the shock front (Landau & Lifshitz, 1980):

$$\Gamma_{ss}^3 + \left(1 - \frac{2}{\alpha}\right) \Gamma_{su} \Gamma_{ss}^2 - \left(1 - \frac{1}{\alpha^2}\right) \Gamma_{ss} - \Gamma_{su} \left(1 - \frac{1}{\alpha}\right)^2 = 0. \quad (\text{A5})$$

where Γ_{su} & Γ_{ss} are the LF of the shock front wrt to the unshocked and shocked fluid respectively, and α depends on the equation of state of the shocked gas and is approximated by

$$\alpha = \frac{4\Gamma_0 + 1}{\Gamma_0 + 1}, \quad (\text{A6})$$

which provides a smooth interpolation between the sub-relativistic value for $\alpha = 5/2$ and the highly relativistic value of 4.

The shock LF wrt the unshocked fluid in the shell not dominating the GRB emission (Γ_{s_2} , if we assume that the GRB is being produced in shell 1) can be determined from the condition of pressure balance across the surface of discontinuity separating the shocked fluids in the two shells-

$$n_1(4\Gamma_{s_1} + 3)(\Gamma_{s_1} - 1) = n_2(4\Gamma_{s_2} + 3)(\Gamma_{s_2} - 1). \quad (\text{A7})$$

For a given density ratio n_1/n_2 and Γ_{s_1} we can solve the above equation to determine Γ_{s_2} , which in turn is used to determine shock front speed wrt the unshocked fluid for the outer/inner shell using

$$\Gamma_{s_2} = \Gamma_{ss_2}\Gamma_{su_2} [1 - v_{ss_2}v_{su_2}], \quad (\text{A8})$$

and the cubic equation A5 for Γ_{ss_2} . These pieces together give us m_1/m_2 and Γ_{rel} , which are used to calculate f_r – the fraction of the kinetic energy of the two shells converted to thermal energy in shell collision (eq. A3).

The ratio of the internal energy of the shocked gas in these two shells is

$$\frac{E_1}{E_2} = \frac{n_1(4\Gamma_{s_1} + 3)(\Gamma_{s_1} - 1)v_{ss_1}}{n_2(4\Gamma_{s_2} + 3)(\Gamma_{s_2} - 1)v_{ss_2}}. \quad (\text{A9})$$

The fraction of the total internal energy of the shocked gas in shell ‘1’ is then $f_1 = \frac{E_1}{E_2} / \left(\frac{E_1}{E_2} + 1 \right)$. We assume that the majority of this energy is indeed being radiated in the GRB band. For shell ‘2’, $f_2 = 1 - f_1$, and we find the fraction of the total radiation contributing to the GRB band, f_{GRB} ; f_{GRB} is found from the ratio $\nu_{i_1}f_{\nu_2}(\nu_{i_1})/\nu_{i_2}f_{\nu_2}(\nu_{i_2})$, where $\nu_{i_1}/\nu_{i_2} = (\gamma_{i_1}/\gamma_{i_2})^2$ (assuming that the magnetic field is equal in both shells). The radiation efficiency in the GRB band for the shell collision is then $f_R(f_1 + f_2f_{GRB})$.

When considering synchrotron radiation as the primary source of emission in the γ -ray band we need to take into account the energy fraction that is lost to very high energy photons ($\nu \gg 200$ keV) produced via the inverse-Compton process. The fraction of energy radiated via the synchrotron emission is $1/(1+Y)$, therefore, the total efficiency for energy production in shell collisions must be larger than the desired 10% by a factor of $1+Y$ – this effectively restricts solutions to $Y \lesssim 10$. $Y \gtrsim 0.1$ if inverse-Compton emission is the main source for the observed γ -ray emission and also Y must not be greater than $\sim 10^3$ otherwise most of the radiative energy will be in the 2nd inverse-Compton photons of much higher energy. In the same sense, we need to make sure the ratio of magnetic energy to that in electrons is $\lesssim 1$, in order for the electrons to radiate efficiently.

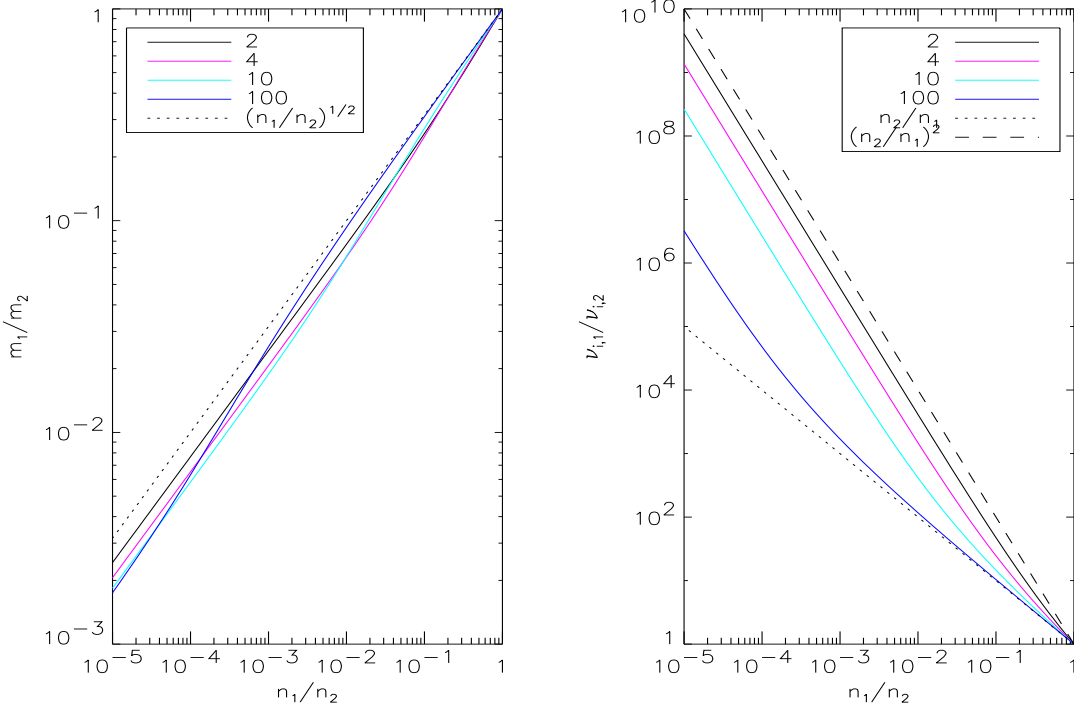


Fig. 15.— Left panel: Dependence of the ratio of the two shell masses, m_1/m_2 , on the ratio of densities, n_1/n_2 . The colored lines show the relation for different relative Lorentz factor, Γ_{rel} , as shown in the legends. The dotted and dashed lines show the applicable dependence on the density ratio. For high Γ_{rel} and $n_1/n_2 > 0.01$, $m_1/m_2 \propto (n_1/n_2)^{1/2}$, however the deviation from this relation for small Γ_{rel} and n_1/n_2 is small – about a factor of 2. Right panel: Dependence of the ratio of synchrotron injection frequencies (ν_i) in the two shells on n_1/n_2 . For high Γ_{rel} and $n_1/n_2 > 0.01$, $\nu_{i,1}/\nu_{i,2} \propto n_2/n_1$. At low Γ_{rel} and small n_1/n_2 , the ratio of injection frequencies in the two shells significantly deviates from this, and for mildly relativistic Γ_{rel} , can be better approximated by $\nu_{i,1}/\nu_{i,2} \propto (n_2/n_1)^2$, shown by the the dashed line.

For highly relativistic forward and reverse shocks $v_{ss1} \approx v_{ss2} \approx 1/3$, $\Gamma_{s2} \approx \Gamma_{s1}(n_1/n_2)^{1/2}$, $\Gamma_{rel} \approx \Gamma_{s1}\Gamma_{s2}$, $m_1/m_2 \approx (n_1/n_2)^{1/2}$, and the ratio of the characteristic synchrotron frequency in shell 1 to shell 2 (assuming the same magnetic field strength) is $\sim n_2/n_1$. We note that the assumption of highly relativistic shocks is not valid for many solutions we find for the prompt γ -ray emissions, and that all the results reported in paper are obtained by numerically solving the appropriate equations. The numerically solved relationships of the ratio of the masses and injection frequencies in the two shells are shown in Figure 15, and compared to the analytical estimates for highly relativistic shocks.

In summary, for a given $\Gamma_{sh}(\gamma_i)$ we vary n_1/n_2 and determine the mass ratio and the relative LF of the shell collision (Γ_{rel}) so that the gamma-ray production efficiency is above a certain desired value (10%). All of the numerical results we show for Γ_{rel} were calculated using these steps. Using

our upper limit on Γ_2 , we also calculate the expected emission from the shell 2 in the x-ray and optical bands, and include this in our analysis.

B. Jitter radiation process and GRBs

A radiation mechanism, called jitter radiation, has been suggested by Medvedev (2000) as the process for γ -ray emission for those cases where the low energy spectrum rises more steeply than $\nu^{1/3}$ expected of the synchrotron radiation (such spectra are said to lie “above the line of death” because a non-self-absorbed synchrotron spectrum cannot have this steep of a rise). The jitter radiation is produced when the coherence length scale for magnetic field is short and electron trajectory is perturbed before it has traveled a distance of a Larmor radius. This is an attractive idea for explaining a class of GRBs lying above the line of death, and we explore its applicability to GRBs in this appendix.

The peak jitter frequency in lab frame (as seen by an observer at rest in the host galaxy) is:

$$\nu_j = \sqrt{16\pi q^2 \Gamma_{sh} n_e / (m_e \bar{\gamma}_e) \gamma_p^2 \Gamma}, \quad (\text{B1})$$

where q is electron charge, Γ is the bulk Lorentz factor (LF) of the source, $\gamma_p = \min\{\gamma_i, \gamma_c\}$, γ_c is the thermal LF of electrons that cool on a dynamical time, γ_i is the minimum thermal LF of electrons behind the shock front (note that $\gamma_i = \epsilon_e(m_p/m_e)\Gamma_{sh}(p-2)/(p-1)$; where Γ_{sh} is the LF of the shock front wrt the unshocked shell), n_e is the comoving electron density in the unshocked shell, and $\bar{\gamma}_e \sim 3 - 4$ is the initial effective thermal Lorentz factor of the streaming electrons.

In order to get the gamma-ray burst spectrum below the peak to be proportional to $\sim \nu^1$, we want $\nu_j \sim 10^5$ eV (the peak of the GRB spectrum is of order 100 keV). Therefore, from the above equation we find the following condition on comoving electron density in the unshocked shell:

$$n_e \approx \frac{4 \times 10^{28}}{\Gamma^2 \gamma_p^4} (\bar{\gamma}_e / \Gamma_{sh}) \quad (\text{B2})$$

or the optical depth of the source to Thomson scattering is:

$$\tau \approx 4n_e \Gamma_{sh} R_\gamma \sigma_T / \Gamma \approx \frac{10^{16} \bar{\gamma}_e t_\gamma}{\Gamma \gamma_p^4} \quad (\text{B3})$$

where R_γ is the distance of the source from the center of the explosion, and $t_\gamma \approx R_\gamma / (4\Gamma^2 c)$ is the GRB variability time scale.

For internal shock Γ_{sh} is of order a few, and therefore, $\gamma_i \approx 10^3$. In this case we find the optical depth of the source to be

$$\tau \approx \frac{10^4 \bar{\gamma}_e t_\gamma}{\Gamma}. \quad (\text{B4})$$

Or $\tau \sim 1$ for $t_\gamma \sim 10^{-2}$ sec, and $\Gamma \sim 10^3$. The next step is to estimate the LF of cooling electrons (γ_c), which can be shown to be:

$$\gamma_c \approx \frac{6\pi m_e c(1+z)}{\sigma_T B^2 t_\gamma \Gamma(1+Y)}, \quad (\text{B5})$$

where B is the magnetic field in the source co-moving frame, and Y is the Compton- Y -parameter; $Y \approx \tau \gamma_c \gamma_i$ (for $p \approx 2$).

If γ_c is not much less than γ_i then Y is very large (of order a million), and most of the radiation energy will come out as SSC photons at $> 10^2$ GeV. And moreover, electrons cool very rapidly resulting in the synchrotron cooling frequency (ν_c) to be much less than 100 keV, and therefore the spectrum below the peak will be $\nu^{-1/2}$ and not $\propto \nu^1$. Even if we take γ_c to be order unity, we still run into similar problems.

We, therefore, do not include the jitter process in our analysis of GRB prompt radiation mechanism.